

**Olfactory coding in vertebrates:
a novel tuning mechanism for receptor affinity and
evolution of the olfactory receptor repertoire**

Inaugural-Dissertation

zur

Erlangung des Doktorgrades

der Mathematisch-Naturwissenschaftlichen Fakultät

der Universität zu Köln

vorgelegt von

Kanika Sharma

aus Jalandhar, India

Köln, 2018

Berichtersteller: Prof. Dr. Sigrun I. Korsching
Prof. Dr. Arnd Baumann

Tag der mündlichen Prüfung: 26.10.2018

ABSTRACT

Information about our environment is to a large extent carried by the chemical senses, and in particular the olfactory sense. Vertebrates perceive thousands of diverse odor molecules with a supply of a wide range of essential information ranging from localising prey or food, avoiding predators, mating behaviour, to social communication. Because olfactory receptor proteins play such an essential role in the specific recognition of diverse stimuli, understanding how they interact with and transduce their cognate ligands is a high priority. This constitutes one of the most complex ligand/receptor binding problems in biology due to the sheer quantity of potential odor molecules facing a limited albeit huge number of different olfactory receptors.

Most olfactory receptors are G-protein coupled receptors and form large gene families. One type of olfactory receptors is the trace amine-associated receptor family (TAAR). TAARs generally recognize amines and one particular member of the zebrafish TAAR family, TAAR13c, is a high affinity receptor for the death-associated odor cadaverine, which induces aversive behavior.

Here we have modeled the cadaverine/TAAR13c interaction by multistep docking. By exchanging predicted binding residues via site-directed mutagenesis, and measuring the activity of the mutant receptors, we confirmed a binding site for cadaverine at the external surface of the receptor, in addition to an internal binding site, whose mutation resulted in complete loss of activity. Elimination of the external binding site generated supersensitive receptors which suggests this site to act as a gate, limiting access of the ligand to the internal binding site and thereby downregulating the affinity of the native receptor. Potentially related mechanisms have been described for non-olfactory G-protein coupled receptors.

The topology of TAAR-expressing neurons in the teleost olfactory epithelium has not been described yet. We have investigated representative *taar* genes from three classes to test the principle of partial spatial segregation known from other olfactory receptor families for the TAAR family. We report that expression of *taar* genes is intermingled with expression zones of odorant receptor genes, which in fish share a single sensory surface with TAARs. Individual *taar* genes show distinct, albeit broadly overlapping expression zones.

In the third part of my thesis I investigated the genome of a cartilaginous fish, *Scyliorhinus canicula*, commonly known as small spotted catshark in order to delineate its chemosensory receptor repertoire: OR, V1R/V2R, TAAR, and T1R/T2R. This is the first repertoire described for a true shark, an important intermediate in the evolution of vertebrates. In contrast to bony vertebrates, but very similar to a chimera (elephant shark), the olfactory receptor repertoire of catshark is dominated by the V2R family.

Zusammenfassung

Informationen über unsere Umwelt werden zu einem großen Teil von den chemischen Sinnen getragen, insbesondere vom Geruchssinn. Wirbeltiere nehmen tausende verschiedene Geruchsmoleküle wahr, die eine breite Palette von essentiellen Informationen liefern, die von der Lokalisierung von Beutetieren, der Vermeidung von Raubtieren, dem Paarungsverhalten bis hin zur innerartlichen Kommunikation reichen. Da olfaktorische Rezeptorproteine eine so wichtige Rolle bei der spezifischen Erkennung verschiedener Stimuli spielen, hat das Verständnis, wie sie mit ihren verwandten Liganden interagieren eine hohe Priorität. Dies stellt eines der komplexesten Ligand / Rezeptor-Bindungsprobleme in der Biologie dar, und zwar aufgrund der schier unendlichen Menge potentieller Geruchsmoleküle, die einer begrenzten, wenn auch sehr großen Anzahl verschiedener Geruchsrezeptoren gegenüberstehen.

Die meisten Geruchsrezeptoren sind G-Protein-gekoppelte Rezeptoren und bilden große Genfamilien. Eine Art von Geruchsrezeptoren sind die Trace-Amin-assoziierten Rezeptoren (TAAR). TAARs erkennen im Allgemeinen Amine und ein spezielles Mitglied der Zebrafisch-TAAR-Familie, TAAR13c, ist ein hochaffiner Rezeptor für den Verwesungsgeruch Cadaverin, der ein aversives Verhalten hervorruft.

Hier haben wir die Cadaverin / TAAR13c-Interaktion durch mehrstufiges Docking modelliert. Durch zielgerichtete Mutagenese der vorhergesagten Bindungsstellen und Aktivitätsmessung der mutierten Rezeptoren bestätigten wir eine Bindungsstelle für Cadaverin an der äußeren Oberfläche des Rezeptors, zusätzlich zu einer internen Bindungsstelle, deren Mutation zu einem vollständigen Verlust der Aktivität führte. Die Eliminierung der externen Bindungsstelle erzeugte supersensitive Rezeptoren, was darauf hindeutet, dass diese Stelle als ein Gate wirkt, welches den Zugang des Liganden zur inneren Bindungsstelle einschränkt und dadurch die Affinität des nativen Rezeptors herabreguliert. Potentiell ähnliche Mechanismen sind für nicht-olfaktorische G Protein-gekoppelte Rezeptoren beschrieben worden.

Die Topologie der TAAR-exprimierenden Neuronen im olfaktorischen Epithel des Zebrafisches wurde bisher nicht beschrieben. Wir haben repräsentative *taar* Gene aus 3 Klassen untersucht, um das von anderen olfaktorischen Genfamilien bekannte Prinzip der räumlichen Segregierung für die TAAR-Familie zu überprüfen. Verschiedene *taar* Gene werden in breiten, aber klar voneinander verschiedenen Expressionszonen exprimiert, wobei die Taar-exprimierenden Neurone integriert sind in die Expressionszonen anderer Duftstoffrezeptorgene, da bei Fischen im Gegensatz zu Tetrapoden eine einzige sensorische Oberfläche vorliegt.

In einem dritten Teil meiner Arbeit untersuchte ich das Genom eines Knorpelfisches, *Scyliorhinus canicula*, gemeinhin als Kleingefleckter Katzenhai bekannt, um das Repertoire an chemosensorischen Rezeptoren (OR, V1R / V2R, TAAR und T1R / T2R) zu identifizieren. Dies ist die erste derartige Untersuchung für einen echten Hai, eine wichtige Zwischenstufe in der Evolution der Wirbeltiere. Im Gegensatz zu Knochenfischen, aber ähnlich der Situation bei einer Chimäre (elephant shark) wird das chemosensorische Genrepertoire der Haifische durch die V2R Familie dominiert.

Contents

1. Acknowledgement	7
2. Introduction	9
2.1 General anatomy and function of the olfactory organ is conserved from fish to mammals.....	9
2.1.1 The rodent olfactory system.....	10
2.1.2 The teleost fish olfactory system.....	11
2.1.3 Insect olfactory system.....	11
2.2 Olfactory receptor gene family repertoire	12
2.2.1 Odorant Receptors (ORs).....	12
2.2.2 Trace Amine-Associated Receptor Family (TAARs).....	13
2.2.3 Vomeronasal Receptors	14
2.2.4 Other receptor types.....	15
2.3 Olfactory receptor structure prediction	15
3. Aims of the study	17
4. Publications of the Dissertation	18
4.1. Elimination of a ligand gating site generates a supersensitive olfactory receptor	19
4.2. Full rescue of an inactive olfactory receptor mutant by elimination of an allosteric ligand-gating site	32
4.3. The Chemosensory Receptor Repertoire of a True Shark Is Dominated by a Single Olfactory Receptor Family	44
4.4. Manuscript in preparation	66
Spatial topology of zebrafish TAAR expressing neurons is broadly overlapping but distinct	67
4.4.1 Abstract	68
4.4.2 Background.....	68
4.4.3 Results and discussion.....	68
4.4.3.1 Relative Radius	70
4.4.3.2 Relative Height	72
4.4.4 Materials and Methods	74
5. Discussion	76
Evolution of olfactory receptors: from phylogeny to function	76
6. References	81
7. Summary	87
8. APPENDIX	89
9. AUTHOR CONTRIBUTIONS	90
10. ERKLÄRUNG (DECLARATION)	91
11. Curriculum vitae	92

For the love of science
and
My parents, who tried

1. Acknowledgement

At the beginning of the thesis, I would like to take some time to thank all the people without whom these projects would never have been possible. Although it is just my name on the cover, many people have contributed to the research in their own particular way and for that I want to give them special thanks.

First of all, I am deeply indebted to my adviser Prof. Dr. Sigrun Korsching for her fundamental role in my doctoral work. Thank you for believing in my abilities and being such a big inspiration. Sigrun provided me with every bit of guidance, assistance, and expertise that I needed during my first few months; then, when I felt ready to venture into research on my own and branch out into new research areas, she gave me the freedom to do whatever I wanted, at the same time continuing to contribute valuable feedback, advice, and encouragement. I cannot express enough gratitude towards her for having confidence in my abilities as someone from computational background wanting to learn wet biology. In addition to our academic collaboration, I greatly value the close personal rapport that Sigrun and I have developed over the years. I am always going to remember her “don’t do as I do, do as I say” phrase and all the examples of logical fallacies. I am also thankful for the excellent example she has provided as a successful woman biologist, an incredible professor and a great mentor. I quite simply cannot imagine a better adviser.

I would also like to thank Prof. Dr. Arnd Baumann for all the guidance and successful collaborations. Many thanks to Prof. Dr. Kay Hofmann and Prof. Dr. Arnd Baumann for accepting to be in my thesis committee, and for the interest in my work. Many thanks to Sabine for carrying out the work that required a lot of patience and skills. Being a part of graduate school has been an incredible experience. I would like to extend a big thanks to Dr. Isabel for showing me the right way when I need to see and being an excellent advisor during the tough times. Also, Kathy for taking such good care of me during all these years. You were the first person I would run to for all complications I faced in Germany, and still do.

Because of the research environment sustained by Sigrun, I have crossed paths with many graduate students and postdocs who have influenced and enhanced my research. I am indebted to all the present and former Olfis for providing a wonderful working environment. Thank you Ivan and Gaurav for introducing me to molecular biology. It was endearing experience working with you both. Vladimir (soldier) who was a great friend to share stories and experiences. Daniel has been a great co-worker to talk to. Thank you for all the short and long conversations we had during this time. You have always been keen to extend your help in whichever way possible keeping the sense of humour intact. Thanks Milan for your scientific feedback during our talks. Manish has been a great friend throughout this time in the lab and probably the only one who listened to all my journal clubs with full attention. Thank you Mehmet for always ordering equipment, kits and taking out time to look out for all the solutions, chargers, screens and whatever I asked you for. Adnan has led me to the current state of my entire work. He provided me the benefits of his own work experience and during the most difficult times when writing this thesis and papers, he gave me the moral support and the freedom I needed to move on. He has been my

support system throughout. I would also like to thank Venkatesh and Shahrzad for being great lab members. I had a great scientific group in PhD and I want to thank all of you for being incredible folks outside lab. Discussing science on lab retreats, learning skiing (thanks Daniel), cooking together and not to forget, theist vs. atheist conversations during retreats were incredible fun.

As long as I'm writing names down, I cannot neglect that of Heena, my best, most constant friend since high school. She's provided me a lot of support and encouragement over the years; a great girl and I don't want to miss an opportunity to get that in the permanent record.

All this has been possible because of my parents, who stood against everything to see me here. Thank you ma for your unconditional love and support. Thank you papa for being such a great role model. I can't thank you enough for going through all the hardships just to see us in better schools. I can't even begin to thank you both for all of your sacrifices as parents. Finally my sister, Kritika, who is everything to me, apart from being a very annoying sibling.

2. Introduction

Chemoreception - the ability to perceive chemicals through adequate receptor molecules or mechanisms – enables a motile organism to move towards an energy source and is present from bacteria to higher eukaryotes. The ability to find and utilize energy sources is crucial for all living organisms. In humans, many times a given smell redirects us to a certain episode of our childhood. In the animal world the olfactory sense is one of the primary tools used to make sense of the environment. Animals in their natural environment are surrounded by odors which are a rich source of information for mate choice, mother–infant recognition and signalling between members of a group. Potentially millions of structurally diverse odor molecules are perceived and discriminated by vertebrates which supply them with a wide range of information, ranging from predator and prey localization to mating behaviour, underlining the importance of the olfactory sense to the survival of the species.

The molecular understanding of olfaction reached a breakthrough in 1991 with the significant discovery of a large, multigene family of olfactory receptors in rat by Linda Buck and Richard Axel (Buck and Axel 1991) which was recognized in 2004 by the award of Nobel Prize in Physiology or Medicine. One of the major questions currently under investigation in the field concerns the evolution of olfactory receptors and their function. Novel techniques like next generation sequencing led to the publication of hundreds of genomes allowing large-scale studying of receptor evolution covering entire branches of the tree of life, including early-derived as well as evolutionary young species. This could lead us to understanding the evolutionary origin of olfaction as a specialized chemosensory sense.

2.1 *General anatomy and function of the olfactory organ is conserved from fish to mammals*

Chemosensory systems develop very early in evolution, as even bacteria can respond to chemical change. This type of reception is universal and found universally. Most olfactory stimuli do not consist of a single compound, but are complex mixtures of different active compounds. The smell of a rose for example is made up by a mixture of 275 different components (Ohloff, 1994). Considering the vast array of different chemicals, it is not surprising that different organisms use a large repertoire of distinct receptors, signalling pathways and anatomically segregated subsystems to sample their environment (Fig 1).

In both mammals as well as fish, the olfactory system harbours specialized sensory neurons located in epithelial sensory surfaces. These neurons, referred to as olfactory sensory neurons (OSNs), choose to express a single olfactory receptor, from a variety of olfactory receptor families. The “one neuron - one receptor” rule represents the first principle of organization in olfactory systems (Serizawa, Miyamichi et al. 2004). This rule seems to be valid for mature OSNs of mouse (Serizawa, Ishii et al. 2000, Serizawa, Miyamichi et al. 2004) as well as zebrafish (Barth, Dugas et al. 1997) although there are reported exceptions (Mombaerts 2004, Sato, Miyasaka et al. 2007, Hanchate, Kondoh et al. 2015). The total number of different olfactory receptors expressed in an animal’s OSNs constitutes their receptor

repertoire. The axons of olfactory sensory neurons project to the olfactory bulb (OB), where axons from neurons expressing the same receptor converge onto glomeruli. The principle of axonal convergence, “one receptor - one glomerulus”, represents the second principle of olfactory system organization. It has been described in the mammalian olfactory system (Takeuchi and Sakano 2014) as well as in fish (Ahuja, Ivandic et al. 2013, Ahuja and Korsching 2014). Odorants bind to their respective receptors, creating an action potential that is carried to the olfactory bulb glomeruli. The glomeruli are innervated by specialized interneurons, i.e. mitral cells, and the signal is transported to higher brain areas, where odor evaluation takes place and adequate behavioral responses are generated.

The principal structure of the olfactory system with the basic building blocks (receptors, OSNs, glomeruli, and central nervous system) is conserved from insects to mammals. In mammals, reptiles, and amphibians the olfactory system underwent a segregation and comprises an additional olfactory surface, the vomeronasal organ (VNO). Sensory neurons in the VNO have different properties and primarily express receptors for the detection of pheromones (Karlson and Luscher 1959, Dulac and Axel 1995). The ontogenetic development of the additional olfactory subsystem has been described in an metamorphic amphibian (*Xenopus laevis*), whose olfactory receptor repertoires in the different subsystems also allow implications on the transition of the olfactory system from water to land living animals (Gliem, Syed et al. 2013, Syed, Sansone et al. 2017). In fish, which only have one olfactory organ, the olfactory epithelium, a partial segregation within the sensory surface can be observed. Pheromone and amino acid-sensing OSNs are present in the apical layer, while the OSNs harbouring the classical olfactory receptors and a family of amine sensing receptors are present in the basal layer of the epithelium. These cell populations also have distinct projection targets in the olfactory bulb (Sato, Miyasaka et al. 2005, Braubach, Fine et al. 2012).

2.1.1 The rodent olfactory system

The olfactory system functions as an elaborate molecular and cellular machinery for detection and discrimination of a vast number of chemical compounds in the environment (Dulac and Axel 1995). To manage these complex and diverse varieties of functions, rodents and tetrapods in general have a bipartite anatomically segregated olfactory system divided into a main olfactory epithelium (MOE) and a vomeronasal organ (VNO). Apart from these, rodents also possess two other subsystems i.e. the septal organ (SO) and the Grueneberg ganglion (GG) (Figure 1A) (Fleischer, Schwarzenbacher et al. 2006).

The MOE consists of ciliated neurons expressing an enormous repertoire of olfactory receptors (odorant receptors, ORs) (Mombaerts, Wang et al. 1996). MOE also expresses other receptors called trace amine-associated receptors (TAARs) (Zou and Buck 2006), and membrane guanylyl cyclase receptor (GC-D) (Fulle, Vassar et al. 1995, Lindemann, Ebeling et al. 2005). The VNO contains microvillous neurons expressing two families of vomeronasal receptors (V1Rs and V2Rs) and formyl peptide receptors (FPRs) believed to detect pheromones (Buck 2000, Riviere, Challet et al. 2009) although it does not have a monopoly in this regard. The main olfactory

system can also mediate pheromone responses, for instance in the rabbit (Hudson and Distel 1986), pig (Dorries, Adkins-Regan et al. 1997) and mice (Keller, Douhard et al. 2006). Information from the VNO is transmitted to the accessory olfactory bulb (AOB), which further projects towards amygdala and hypothalamus that are involved in aggression and mating behavior (Hasen and Gammie 2009).

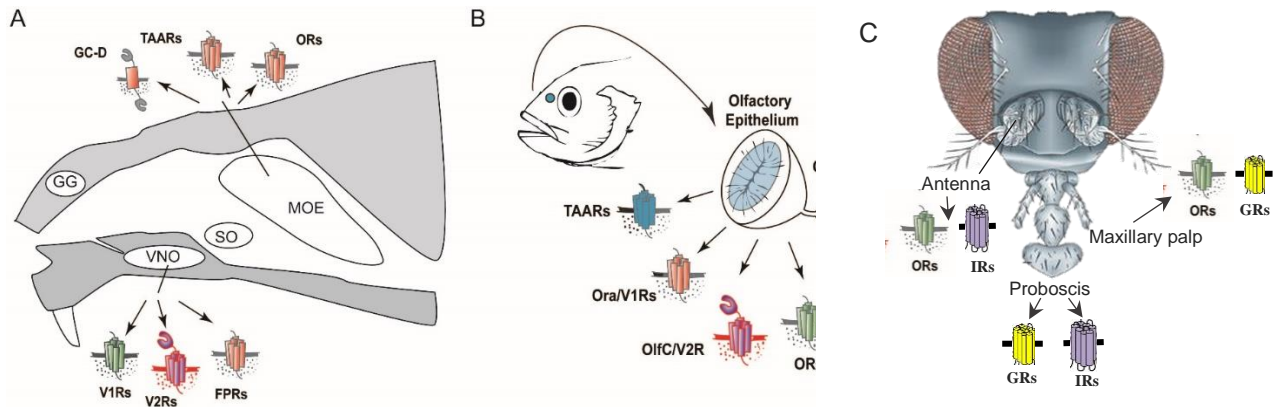


Figure 1: Schematic diagram of olfactory systems in mouse, zebrafish and drosophila (A): Main olfactory epithelium (MOE) showing TAARs, Guanylyl cyclase-D and ORs receptors, Grueneberg ganglion (GG), vomeronasal organ (VNO) expressing V2Rs, V1Rs, and FPRs, septal organ of masera (SO). (B): Zebrafish olfactory system. Scheme showing olfactory epithelium expressing TAARs, ORA/V1Rs, OlfC/V2Rs and ORs. (A) (B) Modified from (Luis Saraiva doctoral thesis (Saraiva & Korsching 2007) (C) Modified from (Kaupp 2010)

2.1.2 The teleost fish olfactory system

In contrast to the mammalian olfactory system, teleosts have single sensory surface which called OE for olfactory epithelium (Figure 1B). In many teleost fish species, the OE is rosette-shaped, with an inner region containing sensory surface and non-sensory region on the periphery (Figure 1B). There are four types of OSNs present in the sensory region of the OE. These OSNs (ciliated, microvillous, crypt and kappe (only shown in zebrafish so far)) project their axons in the olfactory bulb (OB) (Traynelis, Wollmuth et al. 2010) (Hansen and Zielinski 2005) (Ahuja and Korsching 2014) labelled with their specific markers, OMP, S100, TRPC2 and Go respectively (Germana, Montalbano et al. 2004, Sato, Miyasaka et al. 2005). Microvillous neurons express V2R/OlfC receptors, ciliated neurons express large families of OR and TAAR genes, and crypt neurons express a single V1R-related ORA receptor (Hansen and Zielinski 2005, Alioto and Ngai 2006, Hussain, Saraiva et al. 2009, Oka, Saraiva et al. 2012).

2.1.3 Insect olfactory system

Olfaction is the most important of the senses for insects, critical for feeding, mate recognition and predator avoidance (Hansson and Stensmyr 2011, Gadenne,

Barrozo et al. 2016). Insects possess antennal structures, the functional equivalents of the human nose, for receiving odours. Apart from antennae, insects also detect odours with their maxillary palps and/or labial palps (Hansson and Stensmyr 2011). The distal segment of the antennae is covered with olfactory sensilla which encapsulate and protect the sensitive dendrites of the olfactory sensory neurons (OSNs) (Zacharuk, 1980) (Figure 1C). Odor molecules diffuse through pores in the sensilla walls, enter the sensillum lymph where they interact with odorant-binding proteins (OBPs) and are then transferred through the aqueous medium towards the dendrites of OSNs (Leal 2013). To recognize olfactory signals, insects use several families of receptor proteins, the ionotropic receptors (IRs) which are ligand-gated ion channels sensitive to acid and amine odours, carbon dioxide-sensing gustatory receptors (GRs) and, large class of odorant receptors (ORs) which are also ligand-gated ion channels and are related to GRs (Suh, Bohbot et al. 2014, Wicher 2015).

2.2 Olfactory receptor gene family repertoire

The molecular identity of the olfactory receptors came to light in 1991 with the pioneer work of Linda buck and Richard Axel leading to discovery of large and diverse family of G protein coupled receptors (GPCRs) proposed to function as olfactory receptors (Buck and Axel 1991). The repertoire of vertebrate olfactory receptors currently consists of 6 gene families the odorant receptors (ORS), vomeronasal receptors (V1R/ORA and V2R/OlfC), trace amine-associated receptors (TAAR), guanylate cyclase (GC-D), recently identified non-GPCR receptor family MS4A, which is coexpressed with the guanylate cyclase GC-D, and the recently characterised formyl peptide-like receptors (FPR) (Buck 2004, Fleischer, Schwarzenbacher et al. 2006). Insects also possess several dedicated families of olfactory receptors ORs, IRs, and GRs. Where vertebrate ORs are seven transmembrane helix (TMH) G protein-coupled receptors (GPCRs) (Kato and Touhara 2009), the insect ORs are also seven TMH proteins; however, membrane topology analysis of the insect OR subunits both *in vivo* and expressed in cell lines revealed that they have the opposite orientation in the membrane, with an intracellular N-terminus and an extracellular C-terminus (Benton, Sachse et al. 2006, Lundin, Kall et al. 2007, Tsitoura, Andronopoulou et al. 2010). Also, insect OR-mediated olfaction requires the co-expression of two OR genes in each OSN: a co-receptor *Orco*, previously known as *Or83b* (Vosshall and Hansson 2011) which is broadly expressed across OSNs (Larsson, Domingos et al. 2004), and an odorant-binding subunit (*OrX*) that is expressed in a specific subset of OSNs (Carey, Wang et al. 2010).

2.2.1 Odorant Receptors (ORs)

Vertebrate ORs are G protein-coupled receptors (GPCRs) having seven transmembrane α -helical regions and can be classified into five groups by sequence similarities (Fredriksson, Lagerstrom et al. 2003), and ORs belong to the largest group of them, the rhodopsin-like class A GPCR superfamily. Insects also have OR

genes in their genomes, but insect and vertebrate OR genes share no sequence similarity (Hansson and Stensmyr 2011). Repertoires of ORs studied in humans (Glusman, Yanai et al. 2001), mice (Young, Friedman et al. 2002), dogs (Olender, Fuchs et al. 2004), and other mammals (Niimura and Nei 2007) revealed that the number of ORs in mammals varies from <400 in higher primates to around 1200 in rats or opossums (Niimura and Nei 2007). Despite a significant fraction of the genome dedicated to ORs, humans (and higher primates) have undergone extensive pseudogenisation (Niimura, Matsui et al. 2018), possibly reflecting the relatively reduced importance of olfaction in those species. The teleost fishes have a much smaller number of ORs than mammals (Alioto and Ngai 2005, Niimura and Nei 2005). ORs are present in clusters in vertebrate genomes (Niimura and Nei 2003). The evolutionary dynamic nature of this family is characterized by rapid expansion, gene duplication, extensive gene loss via pseudogenization, and diversifying selection (Young and Trask 2002, Alioto and Ngai 2005). Vertebrates can detect and discriminate higher number of different volatile chemicals than the number of ORs encoded in the genome. This perception is possibly achieved through a mechanism called 'combinatorial receptor code' i.e. an odour molecule can be recognized by more than one ORs, and one olfactory receptor can recognize several odour molecules (Friedrich and Korsching 1997) (Malnic, Hirono et al. 1999). The evolutionary origin of OR gene family was elucidated by comparing teleosts, amphibian, and mammalian ORs and appears that they were already present in the common ancestor of all teleosts and tetrapods (Alioto and Ngai 2005, Niimura and Nei 2005). Some of the OR genes even go back to the common ancestor of jawed and jawless fish (Freitag et al., 1999) (Grus and Zhang 2009). OR gene family in zebrafish contains about 150 genes (Alioto and Ngai 2005, Korsching 2009) as compared to up to two thousand genes in mammals (Fleischer, Breer et al. 2009, Korsching 2009).

2.2.2 Trace Amine-Associated Receptor Family (TAARs)

TAARs belong to the class A (rhodopsin-like) GPCRs and share homology with other biogenic amine receptors such as dopamine and serotonin receptors which recognize amines through a key salt bridge involving three conserved transmembrane aspartic acid residues (Shi and Javitch 2002). Initially, TAARs were considered as neurotransmitter receptors as well, however, recently in mammals, they were reported to be expressed in olfactory sensory neurons (Liberles and Buck 2006). Thus, TAARs joined GPCR family that serve as olfactory receptors. TAARs are an important class mediating fear and/or aversive responses in mammals and fish (Dewan, Pacifico et al. 2013) (Hussain, Saraiva et al. 2013, Takahashi 2014). Among the structurally diverse ligands for mammalian TAARs are predator odors, as well as biogenic amines and amines of other sources (Ferrero, Lemon et al. 2011, Ferrero, Wacker et al. 2012, Pacifico, Dewan et al. 2012). The zebrafish TAAR gene repertoire is the only family which is much larger than the mammalian repertoire with 112 TAARs in zebrafish and only 15 characterized TAARs in mice (Hussain, Saraiva et al. 2009). TAAR genes can be classified into 3 classes, with the third and youngest class emerging in teleost fish (Hussain, Saraiva et al. 2009). This class is also characterized by the complete loss of the aminergic ligand-binding motif

which is stringently conserved in the other 2 classes (Hussain, Saraiva et al. 2009), however may still be able to detect amines by non-classical monoamine recognition (Li, Tachie-Baffour et al. 2015). The third class is the largest clade in teleost fish TAARs forming three-fourths of all teleost TAAR genes (Hussain, Saraiva et al. 2009). Except TAAR1 which is not expressed in zebrafish OE, all other TAARs are assumed to function as olfactory receptors, based on studies in rodent, primate, and fish where they are involved primarily in detecting social or alarm cues using volatile amines as ligands (Hussain, Saraiva et al. 2009, Pacifico, Dewan et al. 2012, Li, Tachie-Baffour et al. 2015). OSNs expressing TAARs co-express Golf, the G protein to which also odorant receptors couple (Liberles and Buck 2006). Luik ORs, TAAR repertoire has very dynamic evolution and has undergone expansion, contraction, and mutations across the phylogeny allowing recognition of diverse sets of amines (Hussain, Saraiva et al. 2009, Li, Tachie-Baffour et al. 2015).

Recently the first teleost TAAR, TAAR13c was orphanised in Korsching lab (Hussain, Saraiva et al. 2013). In zebrafish, TAAR13c was shown to give high-affinity response to its natural ligand, cadaverine (1, 5-diaminopentane, a major product of fish tissue decay) and other related aliphatic diamines with odd carbon chain lengths (Hussain, Saraiva et al. 2013). Most mammalian TAARs, and some from teleosts retain the negatively charged Asp3.32, which participates in volatile amine recognition (Li, Tachie-Baffour et al. 2015). Among these, a small group of TAARs contain a second aspartate at position 5.42 participating in ligand recognition. In my PhD time I explored the impact of these two negative charges in the binding of ligands using computational bioinformatics and confirmed the results with calcium imaging.

2.2.3 Vomeronasal Receptors

Tetrapod vomeronasal receptors type 2 (V2Rs) were independently described as putative pheromone receptors by three different groups only two years after the discovery of V1Rs (Herrada and Dulac, 1997, Matsunami and Buck, 1997, Ryba and Tirindelli, 1997). V2Rs belong to the class C of GPCRs, and are closely related to the mammalian metabotropic glutamate receptors. This is also the reason why the teleost V2R-corresponding receptor gene family has been termed OlfC. In rodents, there are 3 families of GPCR, vomeronasal receptor type1 and type 2 (V1R, V2R) and formyl-peptide receptors (FPRs), all of which are expressed in the sensory neurons of the accessory olfactory organ named vomeronasal epithelium (VNO) (Herrada and Dulac 1997, Matsunami and Buck 1997, Dulac 2000, Riviere, Challet et al. 2009). The teleost odorant receptors A (ORA) family is related to V1R family in mammals (Pfister and Rodriguez 2005, Saraiva and Korsching 2007, Behrens, Frank et al. 2014). ORA receptors exhibit high sequence diversity and in teleost ORA receptor family is relatively small with typically 6 members, compared to over 100 genes in the rodent rodents. Moreover there are very few gene birth and death events in the ORA family, compared to the rapidly evolving V1R family (Zapilko and Korsching 2016). In contrast to all other olfactory receptors of the GPCR type, the teleost OlfC is related to mammalian V2R family and belongs to class C GPCRs. They have a large (70 kDa) N-terminal extracellular domain (Pin, Galvez et al. 2003). Zebrafish has about 60 V2R genes (Ahuja, Reichel et al. 2018) while no intact V2R

genes are present in humans (Shi and Zhang 2009) and have been proposed to recognize mainly amino acids (Luu, Acher et al. 2004). Mammalian V2Rs may also recognize small peptides that serve as ligands for major histocompatibility complex (MHC) molecules (Leinders-Zufall, Brennan et al. 2004, Leinders-Zufall, Ishii et al. 2014).

2.2.4 Other receptor types

In recent work an adenosine-sensing GPCR has been identified in zebrafish (Wakisaka et al., 2017). This receptor, termed A2c, is expressed in a specialized type of OSNs and seems to be involved in food-finding behaviour. MS4A receptors have been identified as a non-GPCR family of olfactory receptors in mice, which recognize pheromones and fatty acids (Greer et al., 2016). In mice MS4As are expressed in a special type of OSNs projecting to the necklace glomeruli. These four transmembrane spanning receptors, which are also present in the zebrafish genome (Zuccolo et al., 2010), are coexpressed with guanylate cyclase-D and, as they do not define as GPCRs, rely on an alternative signal transduction pathway using cGMP. Interestingly, several MS4A receptors are co-expressed in single OSNs, indicating a novel mechanism for olfactory detection and encoding.

2.3 Olfactory receptor structure prediction

The interaction of odors with their receptors is one of the most complex ligand-receptor binding problems in biology due to the large quantity of potential odor molecules facing a limited albeit huge number of different olfactory receptors. Because olfactory receptor proteins play such an essential role in the specific recognition of diverse stimuli, understanding how they interact with and transduce their cognate ligands is a high priority. However, only in very few cases we possess a molecular understanding of the binding interaction between a receptor and its odorant. Until now crystal structures are not available for any olfactory receptor, and therefore the prediction of olfactory receptor structures has relied on computational studies using established templates such as the beta-adrenergic receptor (β -AR)₁ (Cherezov, Rosenbaum et al. 2007) and rhodopsin (Palczewski, Kumasaka et al. 2000). Molecular dynamics techniques have been used to study ligand-GPCR interactions in opsins (Lemaitre, Yeagle et al. 2005), cholecystokinin-1 receptor (Henin, Maigret et al. 2006), β_2 -adrenergic receptor (Huber, Menon et al. 2008, Niesen, Bhattacharya et al. 2011), and opioid receptor models (Zhang, Sham et al. 2005).

In my PhD studies, I aimed to understand the interaction of TAAR13c with its native ligand cadaverine i.e. the molecular basis at the very beginning of this neural circuit. I chose TAAR13c because there is a good evidence that activation of this single receptor can result in generating a behaviour response in zebrafish therefore constitutes a molecular basis of this particular neuronal circuit. Also, TAAR13s is specifically activated by diamines, with pronounced selectivity for odd chains of medium length. We modelled the cadaverine/TAAR13c interaction, exchanged predicted binding residues by site-directed mutagenesis, and measured the activity of

the mutant receptors. We observed two binding sites for cadaverine; one at the external surface, and an internal binding site, whose mutation resulted in complete loss of activity. In stark contrast, elimination of the external binding site generated supersensitive receptors. Receptor modeling suggested this site to act as a gate, limiting access of the ligand to the internal binding site and thereby downregulating the affinity of the native receptor. This constitutes a novel mechanism to fine-tune physiological sensitivity to socially relevant odors. We used a multistep docking algorithm which suggested a plausible path for cadaverine from the external to the internal binding site. Furthermore we combined a gain-of-function gating site mutation and a loss-of-function internal binding site mutation in one recombinant receptor. This receptor had almost wildtype ligand affinities, consistent with modeling results that showed localized effects for each mutation.

2.4 Topology for zebrafish TAAR expressing OSNs

Olfaction is different from the majority of the other senses in that the sensory surface does not map the parameter to be represented. Instead, neurons expressing the same sensory receptor, are scattered within the sensory surface (Ressler, Sullivan et al. 1993, Weth, Nadler et al. 1996). However, analysis of expression patterns of zebrafish and rodent odorant receptors has shown that different ORs segregate into distinct spatial subdomains within a common sensory surface and the expression is not completely random (Miyamichi, Serizawa et al. 2005). The borders between subdomains in some cases appear to be sharp, e.g. between zone I and II in the mammalian OE (Ressler, Sullivan et al. 1993, Vassar, Ngai et al. 1993, Strotmann, Wanner et al. 1994), but in many cases the expression zones of different genes overlap widely (Weth, Nadler et al. 1996, Miyamichi, Serizawa et al. 2005).

In the fish olfactory system, a single sensory surface holds all four olfactory receptor gene families. Zebrafish Ors are found in distinct if broadly overlapping expression zones that seem to cover the entire sensory region of the OE (Weth, Nadler et al. 1996). Recently, our group showed that the expression of a major olfactory receptor family, the V2R-related OlfCs follows a similar patterns and is intermingled with OR-representing OSNs (Ahuja, Reichel et al. 2018). However, nothing was known about the topology of TAAR-expressing neurons in the zebrafish OE.

During my thesis, I investigated the expression pattern of five representative *taar* genes (TAAR10 from class 1, TAAR12f and TAAR13c from class 2, TAAR15a and TAAR19l from class 3) in olfactory epithelia of adult zebrafish. The results show that *taar* genes follow the same expression logic as the OR family, expression is scattered and non-random with broad expression zones.

3. Aims of the study

Chemical senses are essential in enabling organisms to detect food, predators, find suitable mates and analyse food quality. Their importance can be gleaned from the continuous presence of a large receptor repertoire, which comes at considerable metabolic cost. Due to a large number of cognate olfactory receptors and even larger multitude of odor molecules, olfaction poses one of the most complex ligand-receptor matching problems in biology. Moreover, investigating receptor/ligand interaction in selected cases will generate a deeper understanding of olfactory receptor function.

In this study I have modelled the TAAR13c and predicted the interaction with its natural ligand, cadaverine, followed by exchanging predicted binding residues by site-directed mutagenesis, and measured the activity of the mutant receptors. In the course of this study, I identified an external binding site of cadaverine which acts as a gate. This constitutes a novel molecular mechanism for regulating ligand access to the activating binding site described for the first time in an olfactory receptor of any species so far.

I have also investigated representative *taar* genes from 3 classes to test whether the principle of spatial segregation observed for odorant receptors and *OffC* genes extends to TAAR family. Furthermore I thought to examine, how expression of *taar* genes is integrated into expression zones of odorant receptor genes, which in fish share a single sensory surface with *TAARs*.

In my third, part I have delineated the chemosensory receptor repertoire OR, V1R/V2R, TAAR, and T1R/T2R of a cartilaginous fish, *Scyliorhinus canicula* commonly known as small spotted catshark. This is the first repertoire described for a true shark, an important intermediate in the evolution of vertebrates.

4. Publications of the Dissertation

4.1. Publication 1

Kanika Sharma, Gaurav Ahuja, Ashiq Hussain, Sabine Balfanz, Arnd Baumann and Sigrun I. Korsching "**Elimination of a ligand gating site generates a supersensitive olfactory receptor.**" *Sci Rep* **6**, 28359 (2016).

doi: 10.1038/srep28359

<https://www.nature.com/articles/srep28359>

SCIENTIFIC REPORTS



OPEN

Elimination of a ligand gating site generates a supersensitive olfactory receptor

Kanika Sharma¹, Gaurav Ahuja^{1,*}, Ashiq Hussain^{1,†,*}, Sabine Balfanz^{2,*}, Arnd Baumann² & Sigrun I. Korsching¹

Received: 05 April 2016

Accepted: 01 June 2016

Published: 21 June 2016

Olfaction poses one of the most complex ligand-receptor matching problems in biology due to the unparalleled multitude of odor molecules facing a large number of cognate olfactory receptors. We have recently deorphanized an olfactory receptor, TAAR13c, as a specific receptor for the death-associated odor cadaverine. Here we have modeled the cadaverine/TAA13c interaction, exchanged predicted binding residues by site-directed mutagenesis, and measured the activity of the mutant receptors. Unexpectedly we observed a binding site for cadaverine at the external surface of the receptor, in addition to an internal binding site, whose mutation resulted in complete loss of activity. In stark contrast, elimination of the external binding site generated supersensitive receptors. Modeling suggests this site to act as a gate, limiting access of the ligand to the internal binding site and thereby downregulating the affinity of the native receptor. This constitutes a novel mechanism to fine-tune physiological sensitivity to socially relevant odors.

The interaction of odors with their cognate receptors constitutes one of the most complex ligand/receptor binding problems in biology due to the sheer quantity of potential odor molecules facing a limited albeit huge number of different olfactory receptors which in some species comprise close to 10% of all proteins^{1,2}. The tuning width of these receptors is extremely variable, with odor spectra ranging from exceedingly broad^{3,4} to monospecific⁵. In some cases a single functional group of the ligand dominates the specificity of the ligand/receptor interaction, in other cases an ensemble of chemical features is recognized^{6–8}. However, only in very few cases do we possess a molecular understanding of the binding interaction between an odorant and its receptor⁹. So far crystal structures are not available for any olfactory receptor, and thus prediction of olfactory receptor structures has relied on modeling studies using established templates such as the beta-adrenergic receptor (β -AR)¹⁰ and rhodopsin¹¹, further supported by site-directed mutagenesis and subsequent functional analysis of mutant receptors¹².

We have used a similar approach to unravel the ligand interaction of a zebrafish olfactory receptor specific for aliphatic diamines, TAAR13c⁶. The trace amine associated receptor (TAAR) family is the only olfactory receptor family that is much larger in teleost fish compared to tetrapods, suggesting an essential role for TAARs in fish¹³. Zebrafish possess 112 *taar* genes, compared to only 15 in mouse and even less in the amphibian and avian lineages⁶. Since zebrafish serve as a model system for vertebrates, and their olfactory system is qualitatively similar to that of vertebrates including mammals¹⁴, zebrafish are well suited to gain deeper insight into vertebrate olfactory receptor properties.

We have recently shown TAAR13c to be a highly sensitive and specific receptor for the death-associated odor cadaverine⁶, which emanates from carrion *via* bacterial decarboxylation of lysine. Cadaverine is strongly repulsive for humans and, interestingly, it also elicits strong innate aversive behavior in zebrafish⁶. At low concentrations of cadaverine mostly TAAR13c-expressing neurons get activated suggesting that a single olfactory receptor might suffice to generate a powerful odor-driven behavior⁶. Here we aimed to understand the molecular basis at the very beginning of this neural circuit, i.e. the interaction of TAAR13c with its native ligand cadaverine.

We have performed thorough modeling of the TAAR13c receptor to identify potential binding site residues, and found all of them clustering in the upper third of the transmembrane domains of TAAR13c. We mutated several of these candidate residues and compared the activation of mutant to wildtype receptors in a heterologous

¹Institute of Genetics, Biocenter, University at Cologne, Zùlpicherstrasse 47a, 50674 Cologne, Germany. ²Institute of Complex Systems (ICS-4), Research Center Jùlich, 52428 Jùlich, Germany. [†]Present address: Max Planck Institute for Neurobiology, Am Klopferspitz 18A, 82152 Martinsried, Germany. ^{*}These authors contributed equally to this work. Correspondence and requests for materials should be addressed to S.I.K. (email: sigrun.korsching@uni-koeln.de)

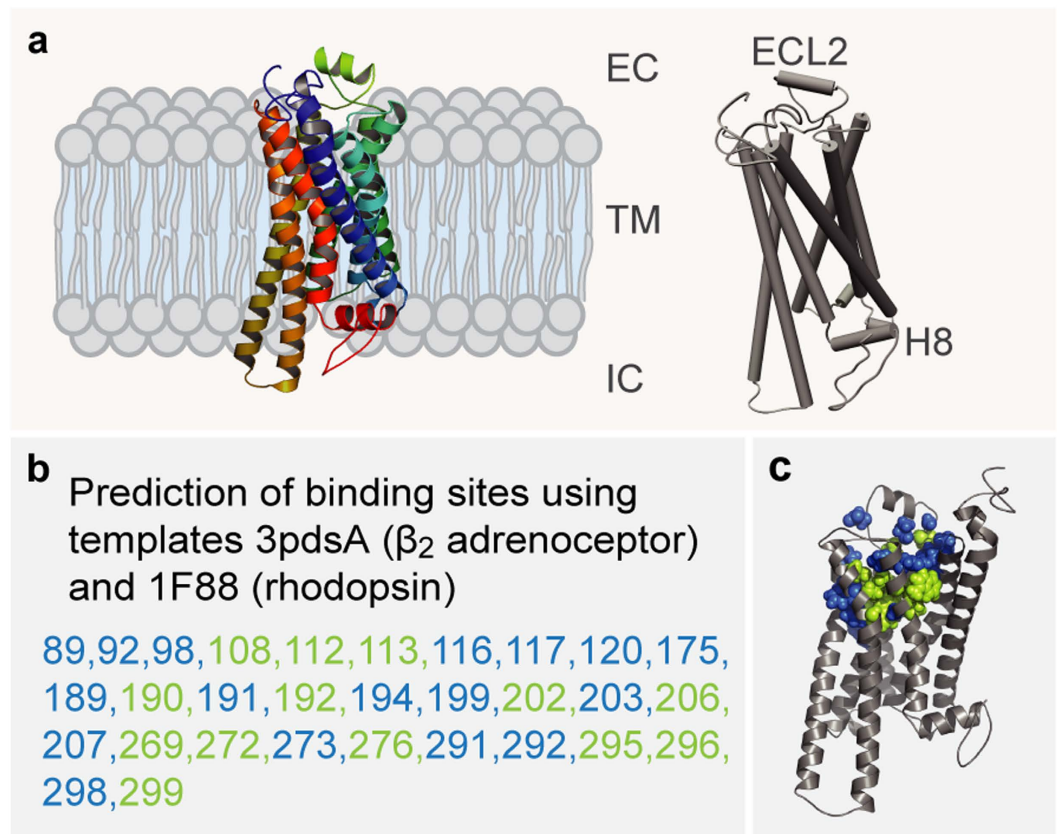


Figure 1. Homology modeling of TAAR13c predicts 7 TM, two additional short helices, and potential binding residues clustered in the upper third of the TM region. (a) Cartoon representation of the TAAR13c model based on comparison with six crystal structures shows the expected seven transmembrane domains and two short extra helices. The planks representation to the right shows a short α -helix to be located in ECL2 and an intracellular eighth helix, H8 located parallel to the membrane plane. (b) Ligand binding residues (given as residue number in TAAR13c) as predicted by sequence profile comparison with binding sites of PDB templates 3pdsA (FAUC-50- β_2 adrenoceptor complex) and 1F88 (bovine rhodopsin); blue, residues only reported in one of the models; green, residues predicted in both models. (c) Predicted binding residues listed in panel (b) shown as spheres in the TAAR13c structure, color code as before. Note the presence of two 'green' columns.

cell expression system. Two aspartates, Asp112^{3,32} and Asp202^{5,42}, buried in the plane of the membrane, were identified as essential components of an internal binding site for cadaverine. Another aspartate, Asp279^{6,58}, was found to constitute an essential residue of a second binding site located at the extracellular surface of the receptor. Both conservative and non-conservative substitutions of Asp279^{6,58} generated supersensitive receptors. Based on our modeling data we suggest the external binding site to act as a gate, which cadaverine has to pass on its way to the internal binding site. As long as the external binding site is occupied, the gate is closed, and thus limits the free access of cadaverine to the internal binding site. This constitutes a novel molecular mechanism for regulating ligand access to the activating binding site. To the best of our knowledge, such a gating mechanism has not been suggested for any olfactory receptor of any species so far.

Results

Modeling of TAAR13c predicts the expected 7TM structure and two additional small helices in ECL2 and C-terminus. We have modeled the TAAR13c structure as a prerequisite to gain structural insights into the molecular architecture and functional constraints of its binding pocket. The homology model of TAAR13c was based on X-ray crystal structures of six templates (see Mat. & Meth and Supplementary Data 2). The TAAR13c primary structure shares a maximal identity of 33% to its closest homolog, the β_1 adrenergic receptor (β_1 AR; Protein Data Bank Entry 4AMJ)¹⁵.

The homology model of TAAR13c (Fig. 1a) revealed the canonical bundle of seven transmembrane (TM) α -helices followed by an eighth intracellular helix (H8) running parallel to the membrane axis. In rhodopsin, an interaction between H8 and TM7 keeps the receptor in a prereceptive state¹⁶, but no such interaction was seen in the TAAR13c model. Interestingly, in the model based on β_1 AR we also observed a short α -helix in extracellular loop 2 (ECL2) of TAAR13c, which is absent in most class A GPCRs, but present in the β -adrenergic receptors¹⁷. Furthermore, a disulfide bridge is predicted between Cys105^{3,25} at the extracellular end of TM3 and Cys190 in ECL2. This disulphide bond provides conformational restraint and is important for effectively tethering ECL2 to the helical bundle¹⁸. The highly conserved landmark motif DRH/Y, here DRH, is located at the cytoplasmic end

of TM3 as expected¹⁷. This motif stabilizes the inactive state in some receptors, and governs G-protein coupling in other receptors¹⁹. We also observed the ‘ionic lock’ between the DRH motif and a glutamate residue at the cytosolic surface of TM6. Due to a salt bridge that is formed between Arg130^{3,50} of the DRH motif and Glu251^{6,34} in TM6, the third and sixth TM helices are connected, a feature which is conserved among all family A GPCRs¹⁷.

Docking of cadaverine validates a binding pocket in the outer-third of the TM domain. We then used COACH²⁰ to predict putative cadaverine binding residues by sequence profile comparison of TAAR13c with binding sites of several PDB structures, with best fits found for 3pdsA (FAUC50/ β_2 adrenoceptor complex) and 1F88 (bovine rhodopsin) in the TAAR13c homology model (Fig. 1b). COACH is a meta-server approach to generate complementary ligand binding site predictions using comparative methods, which recognize ligand-binding templates from BioLiP protein function database by binding-specific substructure and sequence profile comparisons²¹. Initially 30 such residues were found. They all clustered in the upper third of the TM domain suggesting that the putative binding pocket is located within this region (Fig. 1c). The classical amine-binding motif of aminergic receptors consists of Asp112^{3,32} and Trp296^{7,40}, both of which were also predicted as binding partners of cadaverine²². In close proximity to these residues and at the same plane of the membrane another aspartate residue, Asp202^{5,42}, was predicted as a binding partner. We hypothesized that this residue might be involved in binding to the second amino group of cadaverine and examined the region surrounding Asp112^{3,32}, Asp202^{5,42} and Trp296^{7,40} (i.e. the upper one-third of TM3, 5, and 6) by computational docking of cadaverine.

The docking results confirmed the involvement of Asp112^{3,32} and Asp202^{5,42} in ligand binding. Our results suggest that one amino group of cadaverine (protonated at physiological pH) forms a salt bridge with Asp112^{3,32} at a distance of 2.7 Å (Fig. 2c, Table 1), well within the range given for salt bridges 1.75–4.0 Å²³. This Asp112^{3,32} is stabilized by a hydrogen bond to the hydroxyl group of Tyr299. A similar salt bridge has been described for β_1 - and β_2 ARs²⁴. The second protonated amino group of cadaverine was docked 3.2 Å away from Asp202^{5,42} allowing formation of another salt bridge (Fig. 2c). This particular residue is known to undergo binding interactions with ligands in many other GPCRs, forming hydrogen bonds, van der Waals interactions and salt bridges²⁵. Further binding residues validated by docking were Leu113^{3,33}, Thr203^{5,43}, Trp269^{6,48}, and Phe272^{6,51}, all situated within 5 Å distance from cadaverine and thus well within the range of van der Waals interactions (3–6 Å²⁶) (Supplementary Table 1). Thus, these residues are likely candidates for stabilizing the hydrophobic backbone of cadaverine. In addition to cadaverine, diaminoheptane, which has a very similar affinity to TAAR13c⁶, forms the same two salt bridges as cadaverine (2.9 Å distance to Asp112^{3,32} and 2.4 Å to Asp202^{5,42}).

Docking did not confirm Trp296^{7,40} as a binding residue in TAAR13c. Notably, Trp296^{7,40} is 11.5 Å away from the docked cadaverine, and furthermore the residue is located on the distal side of TM7 relative to cadaverine, excluding a van der Waals interaction (Fig. 2f). This was unexpected, because in class A GPCRs this tryptophan is highly conserved, and serves to stabilize the hydrophobic backbone of amines as part of the amine-binding motif²².

In addition to cadaverine, TAAR13c is activated by putrescine, a smaller diamine, albeit with much lower affinity⁶. Docking of putrescine into the TAAR13c model revealed the same salt bridge with Asp112^{3,32} as for cadaverine, albeit at a slightly larger distance of 3.0 Å (Table 1). However, Asp202^{5,42} is not able to form the second salt bridge, because the distance of 5.5 Å between the amino group of putrescine and the carboxylic group of Asp202^{5,42} (Table 1) is too large for a typical salt bridge and only allows a rather weak binding interaction²⁷. This finding would explain the decrease in affinity of TAAR13c for putrescine compared to cadaverine. Nevertheless the weak interaction between Asp202^{5,42} and the second amino group of putrescine seems to be relevant because the corresponding monoamine (butylamine) is not able to activate TAAR13c at all⁶.

Taken together, these data strongly suggest that TAAR13c activation relies on the interaction of two amino groups provided by the ligand with two negatively charged residues in the binding cavity of the receptor, and that stabilization of the ligand backbone is not achieved by the canonical tryptophan, here Trp296^{7,40}, in TM7 of the DW motif.

Docking of cadaverine suggests a second binding site for diamines. In addition to the above-mentioned residues, we identified another docking site on the extracellular surface of the receptor (Fig. 2g,h). The main binding residue of this second site is Asp279^{6,58}, which forms a salt bridge with one amino group of cadaverine (Fig. 2i) and putrescine, each at a distance of 3.1 Å (Table 1). Surrounding apolar residues Phe194 in ECL2 and Phe291^{7,35} in TM7 are also predicted as interaction partners, and presumably serve to stabilize the ligand’s apolar backbone (Supplementary Table 1). No residue coordinating the second amino group was detected in this docking site, suggesting that it might not discriminate for chain length. Thus, this site differs in two properties from the internal docking site: (i) it does not noticeably distinguish between cadaverine and putrescine, and (ii) it does not require a second amino group to bind the ligand. Since TAAR13c activation strongly depends on the ligand’s chain length and absolutely requires the second positive charge of the ligand⁶, this second docking site containing Asp279^{6,58} is rather unlikely to serve as the ligand binding site that activates the receptor. In order to provide independent experimental proof for the predicted docking residues, we generated a series of receptor mutants by site-directed mutagenesis and studied receptor activity after heterologous expression in mammalian cells.

Mutation of the aminergic DW motif shows only the aspartate as required for ligand binding.

As described above, docking predicted only the Asp112^{3,32} but not the Trp296^{7,40} residue of the conserved DW motif to interact with cadaverine (Fig. 2) and putrescine. A series of substitutions were generated for both residues to examine their effects on receptor activity. For the aspartate we chose D112E as a conservative exchange, since the charge is kept and only its position is slightly changed due to the longer side chain in glutamate. Other mutations employed were D112N, which eliminates the charge, but keeps the polarity, and finally D112A, which

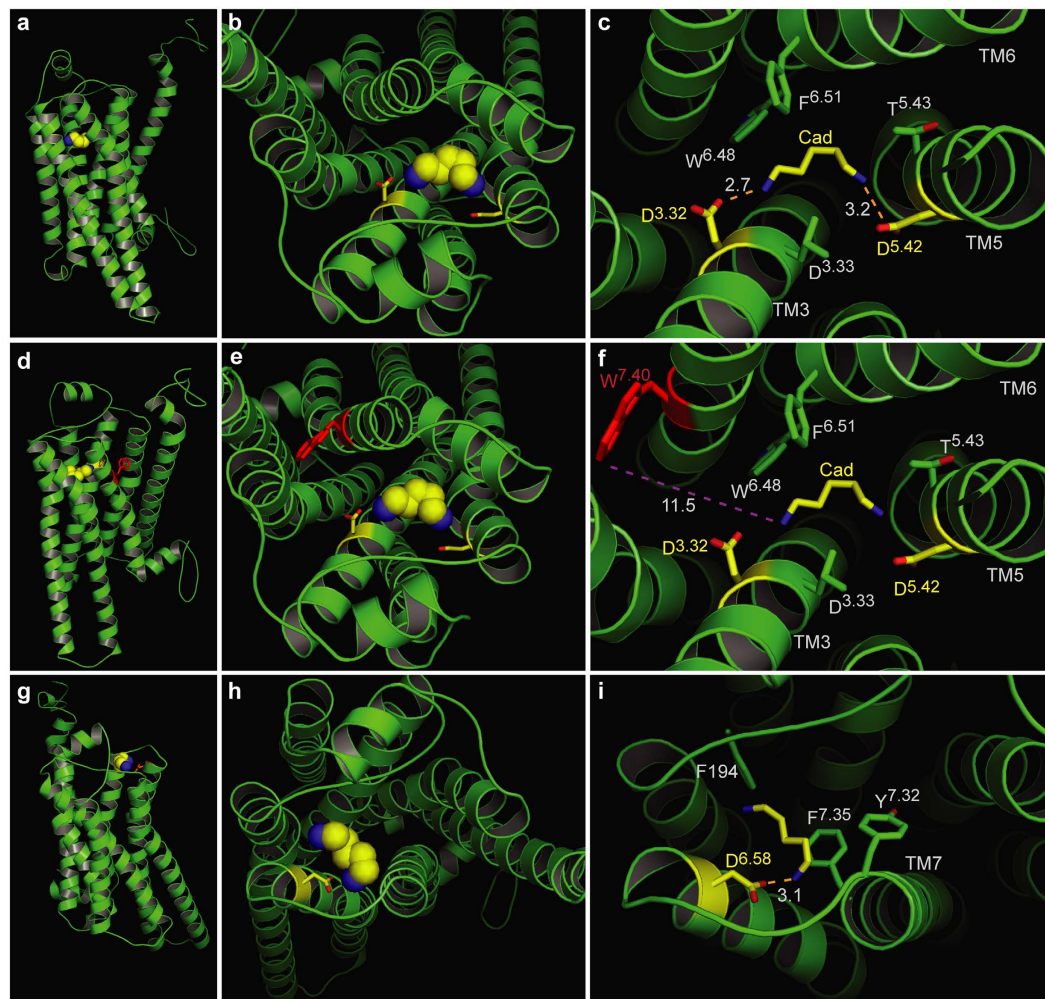


Figure 2. Two binding sites for cadaverine predicted by docking to wildtype TAAR13c. TAAR13c structure (green) is shown with cadaverine (cad; yellow, backbone; blue, amino groups) and coordinating aspartate residues (yellow, backbone; red, carboxyl group). (a) Sideview of TAAR13c shows spatial position of cadaverine docked to the internal binding site, located in the external third of the TM region. (b) Enlarged view from the extracellular surface onto the same binding site shown in panel (a). (c) Enlargement from panel (b) (same view) showing cadaverine, the major interacting residues and the distances in Å from the carboxyl groups of aspartates D^{3.32} and D^{5.42} to the amino groups of cadaverine. Salt bridges are visualized as orange dashed lines. (d) Side view (turned about 90° compared to panel (a)) shows the side chain of W^{7.40} located away from the predicted binding site. (e) View from the extracellular surface, enlarged, same orientation as panel (b). W^{7.40} is positioned on the distal side of its TM relative to the binding site. (f) Enlargement from panel (e) (same view) showing cadaverine, the two interacting aspartate residues and the large distance to the side chain of W^{7.40} (purple dashed line), which is thus unlikely to participate in binding interactions. (g) Side view (turned about 90° compared to panel (a)) showing cadaverine bound at an additional binding site on the external surface. (h) View onto the extracellular surface, enlarged, orientation turned 180° relative to panel (b). A single aspartate (D^{6.58}) coordinates cadaverine. (i) Enlargement from panel (h) (similar view) showing cadaverine, the major interacting residues and the distance from the carboxyl group of D^{6.58} to the amino group of cadaverine. The salt bridge is visualized as orange dashed line.

removes both the charge and polarity. Mutant receptors were stably transfected into HEK293 cells that constitutively express the A2 subunit of an olfactory cyclic nucleotide-gated (CNG) ion channel (see Mat. & Meth.). Activation of TAAR receptors and subsequent cAMP production could be monitored in these cell lines as elevated Ca²⁺ levels due to Ca²⁺ influx through cAMP-dependent opening of the CNG channels. We observed that even the most conservative exchange, D112E, reduced TAAR13c activation drastically, and shifted the dose response curve for cadaverine more than two orders of magnitude to higher concentrations (Fig. 3a, Table 1). Mutation to either asparagine or alanine completely abolished cadaverine-evoked activity. Consistent with these experimental results, docking simulations with cadaverine showed the absence of the wildtype salt bridge in all three mutants (Table 1). Taken together we conclude that Asp112^{3.32} is a pivotal part of the binding site leading to activation of the TAAR13c receptor by cadaverine.

Wildtype/Mutant	EC50 (μM , mean \pm SEM)		Distance to Cad-NH ₂		Distance to Put-NH ₂	
	cad	put	pos112	pos202	pos112	pos202
TAAR13c	15.2 \pm 2.2	>1000	2.7	3.2	3.0	5.5
D112A	loss	loss	2.4	10.8	10.7	4.9
D112E	\gg 1000	loss	9.2	3.2	9.8	5.0
D112N	loss	loss	12.0	3.1	12.0	3.1
D202A	loss	loss	2.4	10.8	10.7	4.9
D202E	loss	loss	9.2	3.2	9.8	5.0
D202N	loss	loss	3.0	9.5	2.5	10.6
D279A	2.1 \pm 1.0	31 \pm 13	3.0	3.7	3.0	6.4
D279E	0.72 \pm 0.24	10 \pm 4	2.9	3.5	3.0	5.6
D279N	1.1 \pm 0.8	7.3 \pm 3.6	2.9	3.5	3.0	5.6
W296F	42 \pm 6	>1000	-	-	-	-
W296G	55 \pm 48	loss	-	-	-	-
W296Y	28 \pm 8	>1000	-	-	-	-
D78E	64 \pm 28	>1000	-	-	-	-

Table 1. EC50 and contact distances for cadaverine and putrescine amino groups with Asp112^{3,32} and Asp202^{5,42} for mutant and wildtype TAAR13c.

Similar effects were observed for the mutant receptors when putrescine was applied as a ligand (Fig. 3a, Table 1), and again, even the D112E variant displayed a drastic reduction of the putrescine response. These results confirm the involvement of Asp112^{3,32} also for the predicted interaction with putrescine. We were intrigued that binding to putrescine, which is one methylene group shorter than cadaverine, could not be improved by the longer side chain of glutamate²⁸, and therefore performed docking simulations with the D112E mutant and putrescine. Indeed, the distance between the charged glutamate side chain and the amino group of putrescine was predicted as 9.8 Å (Table 1), well beyond the range of a salt bridge²⁷, and thus consistent with the drastic reduction in affinity observed for the D112E receptor mutant. In fact, docking of putrescine showed for all three mutants that at most one amino group is able to form a typical salt bridge, whereas the other amino group is too far away for a binding interaction (Table 1). Taken together, experimental and modeling results obtained with Asp112^{3,32} mutants and putrescine again confirmed the involvement of Asp112^{3,32} in ligand binding as predicted by modeling and docking the wildtype receptor (see above).

The tryptophan residue Trp296^{7,40} of the DW motif¹³ was not predicted to be part of the binding site (Fig. 2f). We therefore examined whether replacement of this residue might affect receptor activity. Three mutants were generated, either exchanging the tryptophan for phenylalanine (less bulky), tyrosine (switch to polar residue) or glycine (no side chain interaction possible). Stably transfected cell lines were established with all mutants, and receptor activity was examined with a series of cadaverine and putrescine concentrations (Fig. 3b).

Cadaverine and putrescine were able to activate all three mutants, with similar affinity as wildtype, even for the drastic W296G exchange (Fig. 3b, Table 1), in sharp contrast to the almost complete loss of activity in all Asp112^{3,32} mutants. Furthermore, the efficacy of W296F was similar to wildtype TAAR13c. A slight reduction of efficacy was observed for the W296Y mutant, which might be caused by a different interaction of the more hydrophilic tyrosine with neighboring side chains compared to the tryptophan in wildtype TAAR13c. Efficacy was strongly reduced in the W296G mutant, conceivably due to a loss of structural stability by insertion of the highly flexible glycine into a transmembrane domain. Taken together, binding experiments for all three mutants, W296F, W296Y, and W296G, show little loss in affinity and (with one exception) efficacy, confirming that Trp296^{7,40} is irrelevant for the binding interaction to cadaverine and putrescine, as predicted by the theoretical model.

A second aspartate, Asp202^{5,42} in TM5 is required for activation of TAAR13c by cadaverine and putrescine.

Docking studies suggested an interaction of Asp202^{5,42} with the second amino group of cadaverine (Fig. 2c). We followed a similar strategy as before and generated cell lines expressing the following receptor mutants: D202E, D202N, and D202A. Functional testing with cadaverine revealed that even the most subtle replacement, the D202E substitution, eliminated the activity of the receptor completely (Fig. 3c). The same results were obtained for the other substitutions of D202 to either asparagine or alanine (Fig. 3c). Docking simulations for cadaverine with the mutants showed a large distance of about 10 Å between the mutated residues and the second amino group of cadaverine, consistent with a loss of the second salt bridge present in the wildtype receptor (Table 1). Hence we conclude that Asp202^{5,42} is another pivotal residue in the cadaverine binding site and participates in the activation of the TAAR13c receptor.

As observed for cadaverine, all three receptor variants remained quiescent when cell lines were treated with putrescine (Fig. 3, Table 1). Docking data showed that the distance between the glutamate and the second amino group of putrescine was about twice as large as in the wildtype receptor (Table 1), consistent with the inability of putrescine to activate the D202E mutant receptor. A similar result was obtained for the other two mutations (Table 1). Thus, all experiments performed with Asp202^{5,42} mutants are consistent with docking results for these mutants, and confirm the prediction of Asp202^{5,42} as an essential component of the diamine binding site that can activate TAAR13c.

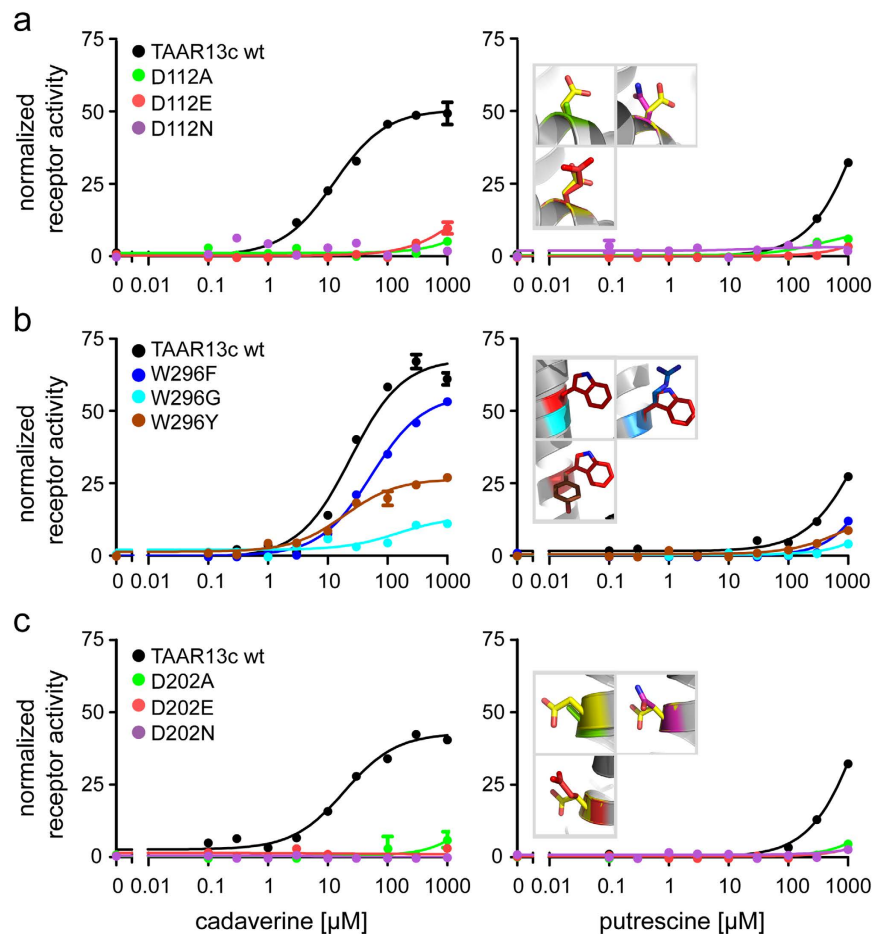


Figure 3. Concentration-response curves of TAAR13c mutated in the internal binding site and Trp296^{7,40}. HEK293 cell lines constitutively expressing CNG channels and either wildtype or TAAR13c mutants were incubated with concentration series of cadaverine or putrescine (10 nM to 1 mM). Changes in intracellular Ca^{2+} were detected by Fluo-4 and calculated as $\Delta F/F$. Values were normalized to the fluorescence ratio obtained with NKH477, an agonist of membrane-bound adenylyl cyclases. Representative binding curves are shown color-coded for mutation (green, A; red, E; magenta, N; blue, F; cyan, G; brown, Y), error bars (SD, $n = 4$) are shown if exceeding symbol size. Left column, responses to cadaverine; right column, responses to putrescine. Insets in right panels show the positions of the mutant side chains (same color as for the respective binding curves) overlaid over the wildtype residue (D, yellow and W, red, respectively). (a) Mutation of the D112 residue to D112E, D112N and D112A results in almost complete loss of activation by cadaverine, with small residual activity only at the highest concentration tested, 1mM. Activation by putrescine is abolished in all D112 mutants. (b) Mutants W296F, W296Y and even W296G were activated by both cadaverine and putrescine, at similar EC_{50} 's as wildtype TAAR13c. Efficacy for W296F is very similar to wildtype TAAR13c but reduced for W296Y and W296G. (c) Mutation of the D202 residue to D202E, D202N, and D202A results in complete loss of activation by cadaverine and putrescine.

Elimination of the external binding site for diamines generates a supersensitive receptor. To examine the relevance of the potential binding site on the extracellular face of TAAR13c predicted by docking, we generated three variants of Asp279^{6,58}, i.e. D279E, D279N, and D279A, and expressed them stably in cell lines. All three receptor variants displayed a massive increase in affinity and efficacy (Fig. 4a). The most pronounced effect was observed for D279E, whose apparent affinity (EC_{50}) to cadaverine increased over twentyfold (Table 1). For the D279N and the D279A mutant receptors we observed a 14fold and a 7fold increase of EC_{50} , respectively (Table 1). The efficacy for all three mutants increased as well, with the most pronounced effect seen for the D279N mutant - about twice the value of wildtype TAAR13c (Fig. 4a). Hence modifications of Asp279^{6,58} result in supersensitive receptors. A similar increase in affinity and efficacy of these three receptor variants was measured when cell lines were treated with putrescine (Fig. 4a, Table 1). Notably, EC_{50} 's of the mutants for putrescine reached values of 7–30 μM , very similar to those determined for cadaverine on wildtype TAAR13c.

When we performed docking simulations, no external binding site was predicted for all three mutants, i.e. the modification of Asp279^{6,58} eliminated this binding site. The internal binding site, however, remained intact, with distances to the ligand amino groups in the range of those observed for wildtype TAAR13c (Table 1), and similar subsets of additional contact sites (Supplementary Table 1).

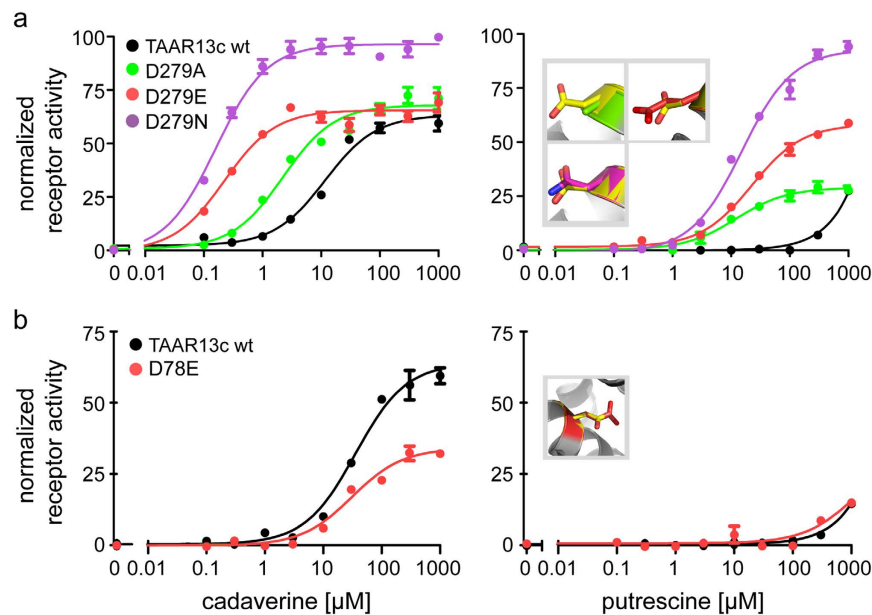


Figure 4. Concentration-response curves of TAAR13c mutated in the external binding site and a control site. HEK293 cell lines constitutively expressing CNG channels and either wildtype or TAAR13c mutants were incubated with concentration series of cadaverine or putrescine (10 nM to 1 mM). Changes in intracellular Ca^{2+} were detected by Fluo-4 and calculated as $\Delta F/F$. Values were normalized to the fluorescence ratio obtained with NKH477, an agonist of membrane-bound adenylyl cyclases. Representative binding curves are shown color-coded for mutation (green, A; red, E; magenta, N; blue, F; cyan, G; brown, Y), error bars (SD, $n = 4$) are shown if exceeding symbol size. Left column, responses to cadaverine; right column, responses to putrescine. Insets in right panels show the positions of the mutant side chains (same color as for the respective binding curves) overlaid over the wildtype residue (D, yellow and W, red, respectively). (a) For mutant D279E the apparent affinity to cadaverine and putrescine as estimated by EC_{50} increased about twenty and hundredfold, respectively, compared to wildtype. EC_{50} values for binding of cadaverine to D279N and D279A mutants increased 14fold and 7fold, respectively. Notably, the EC_{50} values for binding of putrescine to D279N and D279A mutants were as low as those observed for wildtype TAAR13c binding to cadaverine. (b) Mutant D78E bound cadaverine and putrescine similarly well compared to wildtype. Since this aspartate residue is located in the TM region, but outside of the ligand binding site, this result shows that an exchange of aspartate to glutamate in the TM region *per se* does not impair receptor activity.

These observations are consistent with the hypothesis that a ligand-occupied external binding site blocks access to the internal binding site. Elimination of the external binding site relieves this block, leading to an increase in effective ligand concentration in the vicinity of the internal binding site, thus generating a supersensitive receptor.

Discussion

It is a complex but fascinating challenge to gain deeper understanding how the binding of a multitude of different odor molecules to a large cohort of olfactory receptors evokes specific cellular responses. In recent years ligands have been reported for many olfactory receptors^{4,6,29,30}. However, only in very few cases do we possess a molecular understanding of the binding interaction between an odorant and its receptor⁹. So far crystal structures are not available for any olfactory receptor, and thus prediction of olfactory receptor structures has relied on modeling studies. Here we used modeling and docking to predict binding interactions of a receptor linked to a robust innate avoidance behavior. This receptor is a member of the TAAR family of olfactory receptors, TAAR13c, which is activated by the death-associated odor cadaverine in the micromolar range, and, much less efficiently, by the closely related diamine putrescine⁶.

We applied a two-pronged approach to elucidate the mechanism of TAAR13c activation: (i) receptor modeling and docking to uncover residues participating in ligand binding and receptor activation; (ii) site-directed mutagenesis of predicted binding residues followed by functional analysis in an heterologous expression system. For wildtype TAAR13c and all mutants we performed docking simulations with cadaverine and putrescine, and determined bond length between pivotal binding residues of the receptor and ligand amino groups as an estimate of binding strength. In all cases predicted alterations in bond lengths of the mutant receptors were consistent with the experimentally observed changes in activity profiles.

Our results identified Asp112^{3,32} and Asp202^{5,42}, but not Trp296^{7,40} as essential elements of a binding site for cadaverine and putrescine in the upper third of the TM region (internal binding site). The results for the mutation of the two aspartates to alanine reaffirm a recent independent study³¹. Our broader approach to the mutational analyses including the conservative exchanges from aspartate to glutamate and asparagine allows us to confidently state that the observed loss of receptor activation is not due to general conformational changes caused by

the rather drastic aspartate to alanine exchange. Furthermore, we also examined whether an aspartate to glutamate transition as such could impair receptor function. We mutated an aspartate residue within the TM region of the receptor, but outside of the predicted binding site (D78^{2,50}) to glutamate. This mutation did not impair the receptor's properties, strongly suggesting that the exchange of an aspartate to glutamate in the TM region as such is not sufficient to generate coarse conformational changes resulting in a loss of receptor function (Fig. 4b). Similarly, mutations of Trp296^{7,40} did not alter the receptor's activation profile by cadaverine and putrescine. Thus, the drastic changes in TAAR13c affinity seen even for the conservative D112E and D202E exchanges most likely are due to the structural change within the binding pocket. The requirement for binding residues for two functional groups we reported here is fully consistent with the ligand profile of TAAR13c⁶.

Asp112^{3,32} and Trp296^{7,40} together constitute the so-called DW motif, which is highly conserved in aminergic receptors^{25,32}. Asp112^{3,32} is assumed to coordinate the amino group of amine-containing ligands, and Trp296^{7,40} is supposed to interact with the apolar or aromatic backbone. However, the orientation of the diamines cadaverine and putrescine in the binding pocket necessitated by coordination of the second amino group to Asp202^{5,42} precludes coordination of the backbone by Trp296^{7,40}, in accordance with the experimental results.

Interestingly, a second binding site for cadaverine and putrescine was predicted at the external surface of TAAR13c, right above the internal binding site discussed in the preceding paragraph. Mutation of the pivotal element of this binding site, Asp279^{6,58}, resulted in a supersensitive receptor, which displayed an increase in apparent affinity (EC₅₀) for cadaverine and putrescine of up to two orders of magnitude. This rather unexpected result prompted us to examine the predicted structure of TAAR13c for possible mechanistic explanations. Both the internal and the external binding site were predicted by modeling and confirmed by mutational analysis as discussed above. However, whereas the internal binding site (Asp112^{3,32}, Asp202^{5,42}) is necessary for receptor activation, the external binding site (Asp279^{6,58}) is not, and in fact impairs receptor activation.

We hypothesized that the external binding site, when occupied, might block access of the ligand to the internal binding site. There are only two conceivable access points to the internal binding site, highlighted in the surface view of the docking model (Fig. 5a,b). One of these sites is flanked by a positively charged residue, Arg92^{2,64}. This constraint makes it unlikely to allow passage of positively charged diamine compounds into the receptor's internal binding pocket.

The second access point has no such restrictions and thus appears suitable to allow access of the ligand to the internal binding site (Fig. 5b,h). This access point is located directly below the external binding site and thus can be expected to be blocked as long as the external binding site is occupied by ligand (Fig. 5b,c). Only after dissociation of the ligand from the external binding site there is a chance for it to travel towards the internal binding site (Fig. 5h). Thus the external binding site acts as a gate that may be closed (binding site occupied by ligand) or open (binding site not occupied). Elimination of the external binding site by exchanging Asp279^{6,58} destroys the gate and ligand access to the internal binding site is no longer impeded by the intermediary step of binding to the external site. Thus, a supersensitive receptor is generated. In the wildtype TAAR13c, the external binding site serves to downregulate the affinity to diamines, conceivably to adjust it to a physiologically meaningful range. This phenomenon constitutes a novel mechanism in olfactory receptor function.

Some recent reports in the literature describe increases in affinity for mutations of the ligand binding site that leads to receptor activation^{33,34}. These effects are generally small (often two fold, in rare cases up to tenfold). In contrast, here we report a considerably stronger effect on receptor affinity - up to two orders of magnitude - by introducing mutations far away from the activating binding site, and also far away from the intracellular signal transducing regions. Downregulation of a receptor's activity by occupation of an external ligand binding site constitutes a distinct, novel mechanism, by which odorant access to the internal ligand binding site that leads to receptor activation is impaired. Future studies will be required to elucidate, whether such a mechanism might occur in perception of other socially relevant odors, and how widespread it might be in olfactory receptor activation.

During evolution, the affinity of olfactory receptors had to be constantly tuned to physiologically relevant odor concentrations. Sometimes this may have amounted to downtuning the affinity, either directly at the activating binding site, or indirectly *via* a ligand-regulated gating mechanism such as described here for TAAR13c. Gating mechanisms to regulate open/closed states of ion channels and transmitter receptors are well known. Here we show for the first time that gating also plays a role in olfactory perception.

Materials and Methods

Heterologous expression of TAAR13c receptor mutants. Cell lines that constitutively expressed either the wildtype TAAR13c receptor or a receptor mutant were generated using a previously established protocol³⁵. We used a cell line that had been stably transfected with a gene encoding a variant of the A2-subunit of the olfactory cyclic nucleotide-gated (CNG) ion channel^{36,37}. Approximately 8 μg of the respective TAAR13c expression vectors were introduced into ~4 × 10⁵ cells by a modified calcium-phosphate method³⁸. Stably transfected cells were selected in the presence of the antibiotic G418 (0.8 mg/ml). Expression of TAAR13c was monitored by Western blotting (Supplementary Data 1) with specific anti-TAAR13c antibodies⁶ and anti-Rhodopsin antibodies (Sigma Aldrich, Taufkirchen, Germany).

Monitoring functional TAAR13c receptor activity in cell lines. Activation of TAAR13c by cadaverine and putrescine evoked a rise in intracellular cAMP concentration that activates the CNG channels³⁵ and thereby causes an influx of Ca²⁺ through the open channels. Changes in [Ca²⁺]_i were monitored with the Ca²⁺-sensitive fluorescent dye Fluo-4. Cells were grown in 96-well dishes to a density of approximately 2 × 10⁴ cells per well. Cells were loaded at room temperature with Fluo-4 AM as described previously³⁷. After 90 min, the loading solution was substituted for dye-free ECS (extracellular solution; 120 mM NaCl, 5 mM KCl, 2 mM MgCl₂, 2 mM CaCl₂, 10 mM HEPES, and 10 mM glucose, pH 7.4 [NaOH]) containing 100 μM IBMX. The plate was transferred

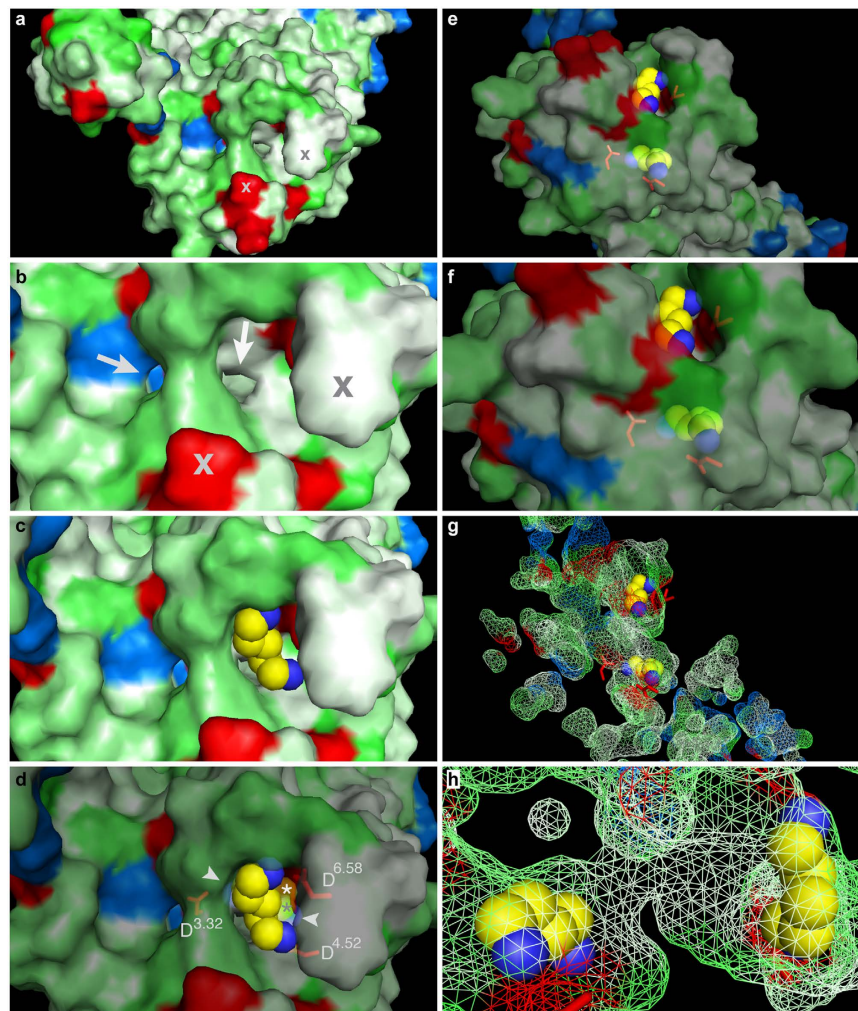


Figure 5. Occupied external binding site blocks access of cadaverine to the interior binding and activation site. Surface view (panels a–f) and mesh view (panels g,h) of the TAAR13c model docked with cadaverine visualizes a potential access path for cadaverine. (a) View from the extracellular surface; red, acidic residues; blue, basic residues; green, polar residues; white, hydrophobic residues; cross, same protrusions as marked in panel (b). (b) Enlarged detail of panel a; arrows point to two potential access paths for passage of cadaverine to the internal binding site. Note that the positively charged Arg92^{2,64} precludes access via left route. (c) Cadaverine docked into the external binding site, same view as in panel b. Note that the access to the internal binding site is blocked. (d) Same view as panel (b,c), but partly transparent; aspartates of external (D^{6.58}) and internal (D^{3.32} and D^{4.52}) binding sites are shown in stick mode; asterisks mark cadaverine bound to the internal binding site; arrowheads point to the amino groups of cadaverine docked into the internal binding site, which lies right below the external binding site shown in top view. (e) Slightly tilted view onto the external surface to display both binding sites at once, external binding site is up. Partial transparency visualizes cadaverine docked into the internal binding site, down; aspartates of external and internal binding sites are shown in stick mode, red. (f) Enlargement of panel (e). (g) Same orientation and magnification as in panel e; mesh view of all predicted cavities, with cadaverine docked into the external and internal binding site. (h) Enlarged view turned 90° counter clockwise and 90° front-to-back compared to panel (g). Note the tunnel connecting the external (left) and internal (right) binding site.

into a fluorescence reader (FLUOstar Omega, BMG Labtech, Offenburg, Germany) to monitor Fluo-4 fluorescence. The excitation wavelength was 485 nm. Fluorescence emission was detected at 520 nm. A concentration series of cadaverine or putrescine (10^{-7} to 10^{-3} M) as well as 10^{-5} M NKH477 (positive control) was added once Fluo-4 fluorescence had reached a stable value in each well. The changes in Fluo-4 fluorescence were recorded automatically. The fluorescence signal generated by the adenylyl cyclase activator NKH477 was set to 100% as an internal standard. Concentration–response curves were established from at least three independent experiments with quadruplicate measurements in each experiment.

Data were analyzed and displayed using Prism 5.04 software (GraphPad, San Diego, CA, USA).

Wildtype/Mutant	Forward Primer, 5'-3' orientation	Reverse Primer, 5'-3' orientation
TAAR13c	atggattatcatcacaagaa	tcaaaccgtaataaattgat
D112A	ccggttttgcctgtttctcac	gtgagaacagggaaccgg
D112N	acaccggtttaacctgtttctcac	gtgagaacagggttaaaccgggtg
D112E	ccggttttgaactgtttctcac	gtgagaacaggttcaaacggg
D202A	tggtcagtttagccacattacta	tagtaatgtggctaaactgacca
D202N	tggtcagtttaaacacattacta	tagtaatgtgtttaaactgacca
D202E	tggtcagtttagagacattacta	tagtaatgtctaaactgacca
D279A	actctctggggcctacattaac	gttaatgtagggagccaccagagagt
D279N	actctctgggtaacacattaac	gttaatgtagggattcaccagagagt
D279E	actctctggggagcctacattaac	gttaatgtagggctccaccagagagt
W296G	tgatcatttggtgtaggctacac	gtgtagcctaaccaccaaatgcatca
W296Y	tgatcatttggttacttaggctacac	gtgtagcctaagtaaccaaatgcatca
W296F	tgatcatttggttcttaggctacac	gtgtagcctaagaaccaaatgcatca
D78E	ctggctctggcgaactgctgg	ccagcagttcccgagaccag

Table 2. Sequences of mutagenic primers used.

Introduction of mutations into TAAR13c. As starting point for mutagenesis we used a full length TAAR13c cDNA construct that harbored an N-terminal extension encoding the first 20 amino acids of bovine rhodopsin in pcDNA3.1 (–) expression vector⁶. Point mutations were introduced using the QuikChange Site-directed mutagenesis kit (Agilent Technologies, Santa Clara, USA). In brief, PCR reactions were performed using *PfuUltra* High-Fidelity DNA Polymerase with the above described plasmid as a template, and mutagenic primers listed in Table 2. Parental strands, which are methylated in contrast to the PCR products, were selectively digested with DpnI enzyme and the resulting product was transformed into XL-1 blue supercompetent *E. coli* cells by electroporation. Screening of recombinants was done by colony PCR using wild type TAAR13c primers. Colonies positive for the desired mutation were grown under standard conditions in LB broth and the plasmids were isolated using a plasmid DNA purification kit from Zymo research (California, USA). All mutations were verified by DNA sequencing.

Homology modeling and ligand docking of TAAR13c. Homology models of TAAR13c were generated using GPCR-I-TASSER³⁹ based on the crystal structure of six homologous templates and sequence alignments of these templates with TAAR13c (Supplementary Data 2). The sequence alignments were verified by inspection for proper aligning of conserved motifs and disulfide bridges. The model with the highest C-score (–0.36), which is well within the confidence range⁴⁰, was chosen as the final structure. In initial experiments the mutant structure was generated with the above protocol and compared to a mutant model generated using side chain substitution in the wildtype structure using Chimera⁴¹. We observed no detectable RMSD difference (<0.05) between models generated by these two methods. Thus, subsequently homology models for mutants were generated by side chain substitution in the wildtype homology model. The receptor model was prepared for docking by adding protons and charges were assigned to ionizable side chains using the DockPrep function in Chimera. The model was then subjected to minimization using ModRefiner⁴². The final model backbone conformation was inspected by Ramachandran plot using Rampage⁴³ (Supplementary Fig. 1). The ligand was used with flexible, rotatable bonds and was docked into the binding site using Autodock Vina⁴⁴ with default parameter setting (iterated local search global optimizer)⁴⁴. The resulting conformations were analyzed using AutoDock Tools⁴⁵. PyMol⁴⁶ was used for visualization of various ligand conformations and for preparing figures.

References

- Strotmann, J., Levai, O., Fleischer, J., Schwarzenbacher, K. & Breer, H. Olfactory receptor proteins in axonal processes of chemosensory neurons. *The Journal of neuroscience: the official journal of the Society for Neuroscience* **24**, 7754–7761, doi: 10.1523/JNEUROSCI.2588-04.2004 (2004).
- Young, J. M. & Trask, B. J. The sense of smell: genomics of vertebrate odorant receptors. *Hum Mol Genet* **11**, 1153–1160 (2002).
- Grosmaître, X. *et al.* SR1, a mouse odorant receptor with an unusually broad response profile. *The Journal of neuroscience: the official journal of the Society for Neuroscience* **29**, 14545–14552, doi: 10.1523/JNEUROSCI.2752-09.2009 (2009).
- Saito, H., Chi, Q., Zhuang, H. & Matsunami, H. & Mainland, J. D. Odor coding by a mammalian receptor repertoire. *Sci Signal* **2**, ra9, doi: 10.1126/scisignal.2000016 (2009).
- Zhang, J. & Webb, D. M. Evolutionary deterioration of the vomeronasal pheromone transduction pathway in catarrhine primates. *Proc Natl Acad Sci USA* **100**, 8337–8341, doi: 10.1073/pnas.1331721100 (2003).
- Hussain, A. *et al.* High-affinity olfactory receptor for the death-associated odor cadaverine. *Proc Natl Acad Sci USA* **110**, 19579–19584, doi: 10.1073/pnas.1318596110 (2013).
- Zhang, J., Pacifico, R., Cawley, D., Feinstein, P. & Bozza, T. Ultrasensitive detection of amines by a trace amine-associated receptor. *The Journal of neuroscience: the official journal of the Society for Neuroscience* **33**, 3228–3239, doi: 10.1523/JNEUROSCI.4299-12.2013 (2013).
- Sachse, S., Rappert, A. & Galizia, C. G. The spatial representation of chemical structures in the antennal lobe of honeybees: steps towards the olfactory code. *The European journal of neuroscience* **11**, 3970–3982 (1999).
- Araneda, R. C., Kini, A. D. & Firestein, S. The molecular receptive range of an odorant receptor. *Nat Neurosci* **3**, 1248–1255, doi: 10.1038/81774 (2000).
- Cherezov, V. *et al.* High-Resolution Crystal Structure of an Engineered Human β 2-Adrenergic G Protein–Coupled Receptor. *Science* **318**, 1258–1265, doi: 10.1126/science.1150577 (2007).

11. Palczewski, K. *et al.* Crystal structure of rhodopsin: A G protein-coupled receptor. *Science* **289**, 739–745 (2000).
12. Kobilka, B. K. *et al.* Chimeric alpha 2-,beta 2-adrenergic receptors: delineation of domains involved in effector coupling and ligand binding specificity. *Science* **240**, 1310–1316 (1988).
13. Hussain, A., Saraiva, L. R. & Korsching, S. I. Positive Darwinian selection and the birth of an olfactory receptor clade in teleosts. *Proc Natl Acad Sci USA* **106**, 4313–4318, doi: 10.1073/pnas.0803229106 (2009).
14. Hussain, A. The Olfactory Nervous System Of Terrestrial And Aquatic Vertebrates. *Nature precedings* hdl:10101/npre.2011.6642.1 (2011).
15. Warne, T. *et al.* Structure of a beta1-adrenergic G-protein-coupled receptor. *Nature* **454**, 486–491, doi: 10.1038/nature07101 (2008).
16. Kirchberg, K. *et al.* Conformational dynamics of helix 8 in the GPCR rhodopsin controls arrestin activation in the desensitization process. *Proc Natl Acad Sci USA* **108**, 18690–18695, doi: 10.1073/pnas.1015461108 (2011).
17. Rosenbaum, D. M., Rasmussen, S. G. & Kobilka, B. K. The structure and function of G-protein-coupled receptors. *Nature* **459**, 356–363, doi: 10.1038/nature08144 (2009).
18. Wheatley, M. *et al.* Lifting the lid on GPCRs: the role of extracellular loops. *Br J Pharmacol* **165**, 1688–1703, doi: 10.1111/j.1476-5381.2011.01629.x (2012).
19. Rovati, G. E., Capra, V. & Neubig, R. R. The highly conserved DRY motif of class A G protein-coupled receptors: beyond the ground state. *Mol Pharmacol* **71**, 959–964, doi: 10.1124/mol.106.029470 (2007).
20. Yang, J., Roy, A. & Zhang, Y. Protein-ligand binding site recognition using complementary binding-specific substructure comparison and sequence profile alignment. *Bioinformatics* **29**, 2588–2595, doi: 10.1093/bioinformatics/btt447 (2013).
21. Yang, J., Roy, A. & Zhang, Y. BioLiP: a semi-manually curated database for biologically relevant ligand-protein interactions. *Nucleic acids research* **41**, D1096–1103, doi: 10.1093/nar/gks966 (2013).
22. Huang, E. S. Construction of a sequence motif characteristic of aminergic G protein-coupled receptors. *Protein science: a publication of the Protein Society* **12**, 1360–1367, doi: 10.1110/ps.0305603 (2003).
23. Blundell, T., Barlow, D., Borkakoti, N. & Thornton, J. Solvent-induced distortions and the curvature of alpha-helices. *Nature* **306**, 281–283 (1983).
24. Rosenbaum, D. M. *et al.* GPCR engineering yields high-resolution structural insights into beta2-adrenergic receptor function. *Science* **318**, 1266–1273, doi: 10.1126/science.1150609 (2007).
25. Surgand, J. S., Rodrigo, J., Kellenberger, E. & Rognan, D. A chemogenomic analysis of the transmembrane binding cavity of human G-protein-coupled receptors. *Proteins* **62**, 509–538, doi: 10.1002/prot.20768 (2006).
26. Rowland, R. S. & Taylor, R. Intermolecular Nonbonded Contact Distances in Organic Crystal Structures: Comparison with Distances Expected from van der Waals Radii. *The Journal of Physical Chemistry* **100**, 7384–7391, doi: 10.1021/jp953141+ (1996).
27. Barlow, D. J. & Thornton, J. M. Ion-pairs in proteins. *J Mol Biol* **168**, 867–885 (1983).
28. Hall, S. E., Floriano, W. B., Vaidehi, N. & Goddard, W. A., 3rd. Predicted 3-D structures for mouse I7 and rat I7 olfactory receptors and comparison of predicted odor recognition profiles with experiment. *Chemical senses* **29**, 595–616, doi: 10.1093/chemse/bjh063 (2004).
29. Krautwurst, D., Yau, K. W. & Reed, R. R. Identification of ligands for olfactory receptors by functional expression of a receptor library. *Cell* **95**, 917–926 (1998).
30. Li, J., Haddad, R., Chen, S., Santos, V. & Luetje, C. W. A broadly tuned mouse odorant receptor that detects nitrotoluenes. *Journal of neurochemistry* **121**, 881–890, doi: 10.1111/j.1471-4159.2012.07740.x (2012).
31. Li, Q. *et al.* Non-classical amine recognition evolved in a large clade of olfactory receptors. *Elife* **4**, doi: 10.7554/eLife.10441 (2015).
32. Katritch, V., Cherezov, V. & Stevens, R. C. Structure-function of the G protein-coupled receptor superfamily. *Annu Rev Pharmacol Toxicol* **53**, 531–556, doi: 10.1146/annurev-pharmtox-032112-135923 (2013).
33. Katada, S., Hirokawa, T., Oka, Y., Suwa, M. & Touhara, K. Structural basis for a broad but selective ligand spectrum of a mouse olfactory receptor: mapping the odorant-binding site. *The Journal of neuroscience: the official journal of the Society for Neuroscience* **25**, 1806–1815, doi: 10.1523/jneurosci.4723-04.2005 (2005).
34. Kato, A., Katada, S. & Touhara, K. Amino acids involved in conformational dynamics and G protein coupling of an odorant receptor: targeting gain-of-function mutation. *Journal of neurochemistry* **107**, 1261–1270, doi: 10.1111/j.1471-4159.2008.05693.x (2008).
35. Wachten, S., Schlenstedt, J., Gauss, R. & Baumann, A. Molecular identification and functional characterization of an adenylyl cyclase from the honeybee. *Journal of neurochemistry* **96**, 1580–1590, doi: 10.1111/j.1471-4159.2006.03666.x (2006).
36. Ludwig, J., Margalit, T., Eismann, E., Lancet, D. & Kaupp, U. B. Primary structure of cAMP-gated channel from bovine olfactory epithelium. *FEBS Lett* **270**, 24–29 (1990).
37. Balfanz, S. *et al.* Functional characterization of transmembrane adenylyl cyclases from the honeybee brain. *Insect biochemistry and molecular biology* **42**, 435–445, doi: 10.1016/j.ibmb.2012.02.005 (2012).
38. Chen, C. & Okayama, H. High-efficiency transformation of mammalian cells by plasmid DNA. *Mol Cell Biol* **7**, 2745–2752 (1987).
39. Zhang, J., Yang, J., Jang, R. & Zhang, Y. GPCR-I-TASSER: A Hybrid Approach to G Protein-Coupled Receptor Structure Modeling and the Application to the Human Genome. *Structure* **23**, 1538–1549, doi: 10.1016/j.str.2015.06.007 (2015).
40. Ge, L. *et al.* Differential proteomic analysis of the anti-depressive effects of oleamide in a rat chronic mild stress model of depression. *Pharmacol Biochem Behav* **131**, 77–86, doi: 10.1016/j.pbb.2015.01.017 (2015).
41. Pettersen, E. F. *et al.* UCSF Chimera—a visualization system for exploratory research and analysis. *Journal of computational chemistry* **25**, 1605–1612, doi: 10.1002/jcc.20084 (2004).
42. Xu, D. & Zhang, Y. Improving the physical realism and structural accuracy of protein models by a two-step atomic-level energy minimization. *Biophys J* **101**, 2525–2534, doi: 10.1016/j.bpj.2011.10.024 (2011).
43. Lovell, S. C. *et al.* Structure validation by Calpha geometry: phi,psi and Cbeta deviation. *Proteins* **50**, 437–450, doi: 10.1002/prot.10286 (2003).
44. Trott, O. & Olson, A. J. AutoDock Vina: improving the speed and accuracy of docking with a new scoring function, efficient optimization, and multithreading. *Journal of computational chemistry* **31**, 455–461, doi: 10.1002/jcc.21334 (2010).
45. Morris, G. M. *et al.* AutoDock4 and AutoDockTools4: Automated docking with selective receptor flexibility. *Journal of computational chemistry* **30**, 2785–2791, doi: 10.1002/jcc.21256 (2009).
46. Schrödinger, L. L. C. The PyMOL Molecular Graphics System. *Version 1.8* (2015).

Acknowledgements

We thank Lena Sachs, who was involved in an early stage of the project. We gratefully acknowledge financial support from the German Science foundation (grants KO 1046/7-1 and RTG 1960 to S.I.K.), and the International Graduate Schools IGSDHD (K.S., G.A.) and IGS-GFG (A.H.).

Author Contributions

The experiments were conceived by S.I.K. and designed by K.S., G.A., S.I.K. and A.B. Experiments were performed by S.B., K.S., G.A. and A.H. Illustrations were drafted by K.S., S.B. and S.I.K. Data analysis was done by K.S. and S.B. K.S., A.B. and S.I.K. wrote the paper.

Additional Information

Supplementary information accompanies this paper at <http://www.nature.com/srep>

Competing financial interests: The authors declare no competing financial interests.

How to cite this article: Sharma, K. *et al.* Elimination of a ligand gating site generates a supersensitive olfactory receptor. *Sci. Rep.* **6**, 28359; doi: 10.1038/srep28359 (2016).



This work is licensed under a Creative Commons Attribution 4.0 International License. The images or other third party material in this article are included in the article's Creative Commons license, unless indicated otherwise in the credit line; if the material is not included under the Creative Commons license, users will need to obtain permission from the license holder to reproduce the material. To view a copy of this license, visit <http://creativecommons.org/licenses/by/4.0/>

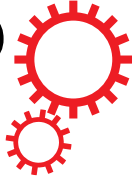
.2. Publication 2

Kanika Sharma, Sabine Balfanz, Arnd Baumann and Sigrun I. Korsching "**Full rescue of an inactive olfactory receptor mutant by elimination of an allosteric ligand-gating site.**" *Sci Rep* **8**, 9631

doi: 10.1038/s41598-018-27790-7

<https://www.nature.com/articles/s41598-018-27790-7>

SCIENTIFIC REPORTS



OPEN

Full rescue of an inactive olfactory receptor mutant by elimination of an allosteric ligand-gating site

Kanika Sharma¹, Sabine Balfanz², Arnd Baumann¹  & Sigrun Korsching¹

Ligand-gating has recently been proposed as a novel mechanism to regulate olfactory receptor sensitivity. TAAR13c, the zebrafish olfactory receptor activated by the death-associated odor cadaverine, appears to possess an allosteric binding site for cadaverine, which was assumed to block progress of the ligand towards the internal orthosteric binding-and-activation site. Here we have challenged the suggested gating mechanism by modeling the entry tunnel for the ligand as well as the ligand path inside the receptor. We report an entry tunnel, whose opening is blocked by occupation of the external binding site by cadaverine, confirming the hypothesized gating mechanism. A multistep docking algorithm suggested a plausible path for cadaverine from the allosteric to the orthosteric binding-and-activation site. Furthermore we have combined a gain-of-function gating site mutation and a loss-of-function internal binding site mutation in one recombinant receptor. This receptor had almost wildtype ligand affinities, consistent with modeling results that showed localized effects for each mutation. A novel mutation of the suggested gating site resulted in increased receptor ligand affinity. In summary both the experimental and the modeling results provide further evidence for the proposed gating mechanism, which surprisingly exhibits pronounced similarity to processes described for some metabotropic neurotransmitter receptors.

Gating of ion channels constitutes a central feature of ionotropic neurotransmitter receptors, also dubbed ligand-gated ion channels (LGIC)^{1–3}. Ligands like acetylcholine, glutamate, GABA or glycine usually bind far away from the channel domain. Upon binding ligand-induced conformational changes result in opening of the channel pore (Fig. 1a)^{4–6} and allow ions to traverse the channel. Allosteric effects on receptor activation are well known for metabotropic receptors as well: receptor-ligand interaction far away from the binding-and-activation site (the orthosteric site) can control receptor activity, e.g. by locking the receptor in an inactive conformation⁷.

However, an alternative mechanism exists, in which an LGIC ligand binds inside the channel pore, thus blocking the channel (Fig. 1b). Metabotropic receptors (GTP-binding-protein coupled receptors, GPCRs) lack a channel pore, but exhibit a related feature⁸. The ligand binding-and-activation site of class A GPCRs⁹ is usually located in a cavity formed by the transmembrane domains of the receptor (Fig. 1c). Therefore a ligand, starting at the extracellular face of the receptor, has to traverse an entry tunnel to gain access to its final binding-and-activation site. This geometry potentially enables ligands to block the entry tunnel thereby regulating GPCR signaling (Fig. 1d). Although a few publications have addressed this possibility, an allosteric modulatory site located above the orthosteric binding-and-activation site has only been described for muscarinic acetylcholine receptors (mAChR)^{10,11} the occupied state, this site might be properly positioned to obstruct the ligand entry tunnel.

Usually, allosteric and orthosteric binding sites are occupied by different ligands. For mAChRs, however, a weak binding of acetylcholine and other agonists to an allosteric binding site has been deduced from complex binding studies¹². In this sense an allosteric ligand binding site positioned above the orthosteric binding-and-activation site would be well suited to regulate ligand access to the latter.

While a recent molecular dynamics simulation of the β_2 adrenergic receptor (β_2 AR) has not addressed the case of ligand-gating, a transient arrest of alprenolol has been observed at a weak binding site in an outer ‘vestibule’ of the protein, before the ligand traverses to its final binding-and-activation site¹³. Pausing at a weak binding site will result in a slower ligand on-rate at the binding-and-activation site and eventually result in a lower apparent affinity. An allosteric ligand binding site thus opens a fascinating possibility for receptor evolution to

¹Institute of Genetics, Biocenter, University at Cologne, Zùlpicherstrasse 47a, 50674, Cologne, Germany. ²Institute of Complex Systems (ICS-4), Research Center Jùlich, 52428, Jùlich, Germany. Correspondence and requests for materials should be addressed to K.S. (email: ksharma997@gmail.com) or S.K. (email: sigrun.korsching@uni-koeln.de)

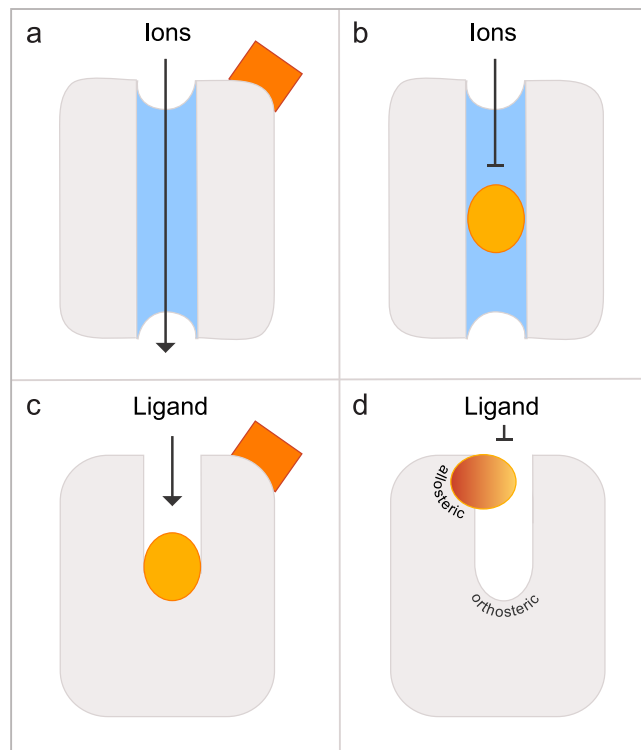


Figure 1. Schematic illustration of allosteric and orthosteric sites in ligand-gated ion channels and GPCRs. (a) Binding of an allosteric ligand (reddish) to the extracellular binding site of a ligand-gated ion channel induces a conformational change causing opening of the ion-conducting pore. (b) Binding of an antagonist (dark yellow) in the pore blocks the channel and can lead to its deactivation. (c) An orthosteric binding site is located inside a cavity formed by transmembrane domains in class A GPCRs. Binding of a ligand (reddish) to an allosteric site topographically distinct from the orthosteric site eventually can modulate binding of the orthosteric ligand (dark yellow). (d) Allosteric binding sites in some GPCRs are located externally and almost above the orthosteric binding-and-activation site. Binding of a ligand (bicolor) to this site could block ligand access to the internal binding-and-activation site.

fine-tune the affinity of GPCRs according to the respective functional requirements without affecting the intricate binding-and-activation machinery.

The vast majority of GPCRs are members of the chemosensory receptor family (olfactory and taste receptors)¹⁴, and the large majority of these are assigned to the class A clade of GPCRs⁹. Recently the possible existence of such allosteric ligand-gating mechanisms in chemosensation has been considered for a member of the trace amine associated receptor (TAAR) family^{15–18} of olfactory receptors from zebrafish, TAAR13c. The binding-and-activation site was shown its position to be located about one third into the cavity formed by the transmembrane domains, an expected position for a ligand binding-and-activation site in class A GPCRs. Additionally, a weaker binding site in an outer vestibule was described, which appeared to be properly located to block access of cadaverine, the native ligand of TAAR13c, to the internal binding-and-activation site¹⁹. Destruction of this outer binding site resulted in a supersensitive mutant¹⁹ leading us to suggest that this site controls ligand entry to the binding-and-activating site of the receptor. This is a novel mechanism for chemosensory receptors, and to the best of our knowledge has not been examined in these terms in any GPCR. Thus we sought independent proof and stringently tested our hypothesis both with additional mutations and with more specialized modeling approaches.

We report here that a novel mutation of the potential gating site (D279R) shows significantly enhanced affinity compared to the wildtype receptor, consistent with the suggested gating function. In an attempt to understand the potential interaction between the binding-and-activation site and the gating site we generated a double mutant (D112E/D279N), which fully rescued the severe loss in binding ability of the binding-and-activation site mutant (D112E) to wildtype levels, consistent with the individual mutations sequentially affecting the overall affinity of the receptor. Furthermore, two independent modeling approaches confirmed the existence of the predicted allosteric ligand-gating site in a vestibule at the extracellular face of TAAR13c. Our findings suggest that a ligand-binding external vestibule may be a much more widespread regulatory feature of class A GPCRs than previously assumed. If so, future attempts at structure-based rational drug design in class A GPCRs may be well advised to focus on modifications of this external niche. Even where such an external vestibule is not present, modeling-guided mutations may be used to introduce novel allosteric binding sites bordering the entry tunnel for receptor ligands.

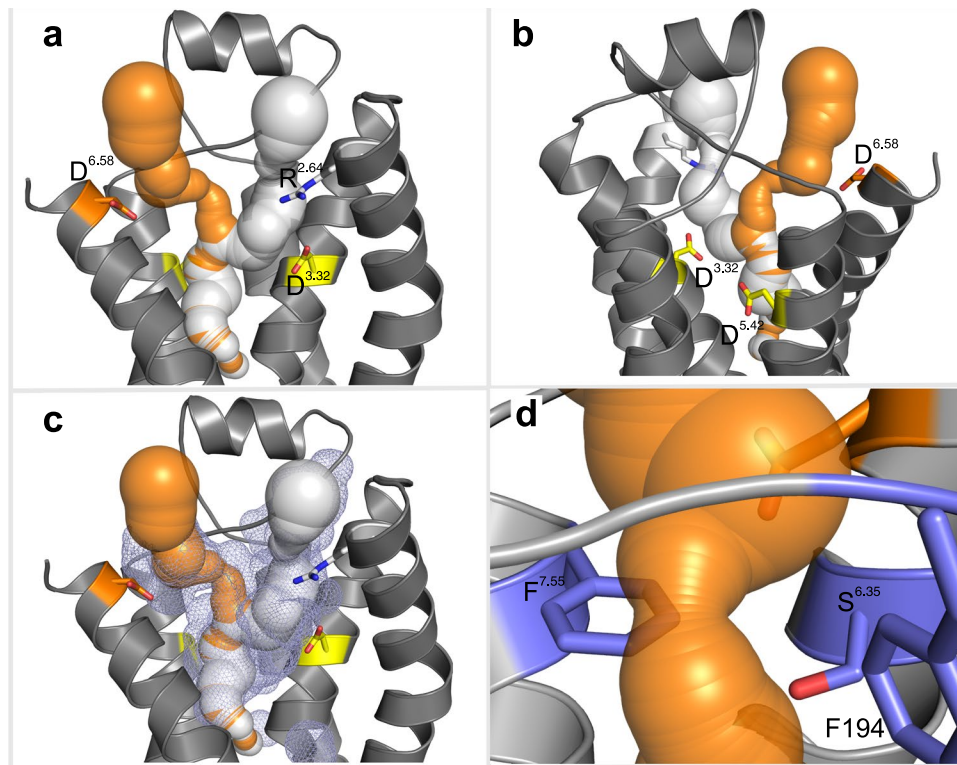


Figure 2. Prediction of ligand access tunnels in TAAR13c by MOLE2.0 shows presence of a bottleneck. **(a)** Ligand access tunnels predicted by MOLE2.0 were imposed on a cartoon representation of the TAAR13c structure, leading towards the internal ligand binding-and-activation site. The negatively charged aspartic acid residue D279^{6.58} in TM6 lines a tunnel (orange) through which cadaverine passes on its way to the internal binding site. The positively charged arginine residue R92^{2.64} in TM2 impedes ligand entry via an alternative tunnel (white). **(b)** View of panel (a) from the back; residues D112^{3.32} and D202^{5.42} (yellow) in TM3 and TM5 are part of the ligand binding site. **(c)** Both ligand access tunnels are located inside the central cavity (blue mesh). **(d)** Zoom-in on the bottleneck of the tunnel shown in (b) with a radius of 1.53 Å. Residues F194, F291^{7.55}, and S276^{6.35} (blue) are shown facing the bottleneck.

Results

Previous studies have identified zebrafish TAAR13c as the highly sensitive and specific receptor for cadaverine¹⁷. The docking of cadaverine to the binding-and-activation site of TAAR13c was shown to engage two aspartates, D112^{3.32} in transmembrane region (TM) 3 and D202^{5.42} in TM5 which form salt bridges with the two positively charged amino groups of cadaverine^{19,20}. Some mutations of TAAR13c had unexpectedly resulted in the generation of supersensitive mutants, and the loss of a gating site (D279N) impeding ligand entry to the receptor's binding-and-activating site has been hypothesized as a possible explanation¹⁹. The proposed gating site appeared to serve as a ligand-binding site on its own and in its occupied form seemed to block ligand entry. Since this amounts to a highly unusual mechanism for chemosensory receptors, we challenged the hypothesis here in several ways. Firstly, we employed two advanced modeling approaches to identify the tunnel allowing ligand passage to the binding-and-activation site of TAAR13c. These algorithms were more robust and versatile than general-purpose molecular visualization programs used previously to assess binding pockets of receptor proteins. Secondly, to gain independent support for our hypothesis we introduced additional mutations into TAAR13c. The mutant receptors were constitutively expressed in cell lines and examined pharmacologically. Furthermore, ligand-interaction of these receptor mutants was modelled and compared to the wildtype receptor.

The predicted ligand-gating site lines the entry tunnel for cadaverine in TAAR13c. Previously we had predicted¹⁹ the existence of a ligand-gating site near the extracellular surface of the TAAR13c receptor, using PyMol²¹, a general purpose molecular visualization tool. Aiming to independently test this prediction, here we employed MOLE2.0²², a more advanced and robust approach compared to PyMol. With MOLE2.0 the cavities and potential tunnels allowing the ligand to enter the receptor, contact the gating site, and traverse towards its final binding site were identified. Two tunnels were predicted in the upper third of TAAR13c TM domains (Fig. 2a). Both are buried inside the protein cavity (Fig. 2c) and lead towards the internal ligand binding-and-activation site (Fig. 2b). One of the tunnels in TAAR13c is 26.0 Å long and situated between TM 2, 3, and 7. At its entrance, it is lined by a positively charged arginine residue, R92^{2.64} (Fig. 2a). The presence of this positive charge might disfavor this path for the positively charged cadaverine to enter the receptor and to reach the ligand binding-and-activation site. The second tunnel is shorter (20.6 Å) and located between TM 3, 5, 6 and 7. It is lined by the previously identified ligand gating residue, D279^{6.58} at its entrance (Fig. 2a). This negative

Wt/Mutant	Bottleneck diameter in Å	TomoDock distance of Cad-NH ₂ with	
		112	202
TAAR13c	3.06	3.1	3.0
D279R	2.06	3.2	3.0
D112E/D279N	2.16	9.0	3.1
D279N	2.14	3.0	3.3
D112E	2.12	9.0	3.1
D279E	2.12	—	—
D279A	2.14	—	—

Table 1. Bottleneck diameter and contact distances for cadaverine amino groups with D112^{3,32} and D202^{5,42} for mutant and wildtype TAAR13c predicted by TomoDock.

charge around the entrance probably serves as an attractant for cadaverine, thus making this path more favorable to reach the ligand binding-and-activation site.

Cadaverine has to traverse a bottleneck after passing the gating site. The tunnel predicted by MOLE2.0 for the cadaverine path features a pronounced constriction (Fig. 2d), which is mainly formed by three residues: F194 in ECL2, F291^{7,55}, and S276^{6,35}. The arrangement of these three residues creates a ‘bottleneck’ of 3.06 Å in diameter, which is by far the narrowest part along the entire path. Similar bottlenecks have also been observed in opsin as well as in several ion channels^{23,24}.

Docking simulations (described below) for cadaverine never showed a binding interaction for the constriction site. Thus, cadaverine moves from the extracellular region to the internal binding-and-activation site without pausing at the constriction. Since cadaverine is a straight chain diamine with a cross section diameter of 3 Å, its molecular properties should allow it to squeeze through the bottleneck, especially when considering the rotatable single carbon-bonds in the backbone. We also observed the constriction in the TAAR13c mutants described below and those studied previously (Table 1). Interestingly, in all mutants, including the super-sensitive ones¹⁹, the constriction is even more pronounced than in the wildtype receptor (Table 1), further consistent with no deleterious influence on the affinity of TAAR13c.

Multistep docking algorithm suggests cadaverine lingering at the gating site before its progress to the internal binding-and-gating site. In order to study interactions of cadaverine as it moves along its path inside the receptor, we used the TomoDock algorithm²⁵. The path towards the binding-and-activation site of TAAR13c is arbitrarily divided into a number of segments. Each segment is treated individually for the docking step thereby allowing the detection of local optima for ligand position and interaction with the receptor. For each segment we defined a cubic search space that moves from the top of the tunnel to the bottom in steps of 1 Å length. The starting point of the docking simulation is the very beginning of the tunnel flanked by the gating site (D279^{6,58}) at its bottom and then the position of segments gradually progresses towards the internal ligand binding-and-activation site of the receptor (Fig. 3a). The final step encompasses the key interacting residues of the internal binding-and-activation site, D112^{3,32} and D202^{5,42} (Fig. 3a). TomoDock assigns a low numerical score to ligand orientations which allow an interaction with the receptor. Consequently, for each step along the migration path of cadaverine we chose the cadaverine orientation with the lowest score.

At the first step of docking, cadaverine is located at the rim of the tunnel entry surface, which constitutes an “external niche”. Inside this niche, cadaverine engages with S199^{5,39} in TM5 and Y193 to form a hydrogen bond, as well as F194 and E175 in ECL2 to stabilize the backbone (Supplementary Table 2). In the second step, as cadaverine moves further inside from the cavity mouth (Fig. 3e), the contact with E175 is lost while the others are retained. In step 3, cadaverine moves towards the gating site residue, D279^{6,58}, which resides near the external end of TM6, resulting in an interaction between the carboxyl group of D279^{6,58} and an amino group of cadaverine (Fig. 3f). This results in the occupation of the hypothesized gating site. In the next step, there isn’t much change in the position of cadaverine (Fig. 3g). Thus, cadaverine appears to pause at the gating site in the external niche, before it slips through the bottleneck between ECL2, ECL3 and TM5–7 (Fig. 3g). In the next step (step 5) cadaverine has passed the constriction, approaching D112^{3,32} in TM3 (one of the two aspartate ‘anchors’ of the internal binding-and-activation site) to form a salt bridge (Fig. 3h). In steps 6 to 7, cadaverine stays around D112^{3,32} by adopting various orientations (Fig. 3h). A common interaction in steps 5–7 is a salt bridge with D112^{3,32} and a polar interaction with neighboring residue Y299^{7,43} in TM7. Deep inside the binding site, cadaverine changes its orientation slightly in step 8 and 9 (Fig. 3i,j). Finally in step 10, for the first time cadaverine makes a contact with D202^{5,42} in TM5 to attain the most favorable binding position with two salt bridges (Fig. 3j). One amino group of cadaverine forms a salt bridge with D112^{3,32} with a distance of 3.1 Å. The other amino group forms a salt bridge with D202^{5,42} with a distance of 3.0 Å (Fig. 3d) in the final docked position. The results obtained from this docking simulation are in close agreement with our previous data¹⁹ (Table 1). Taken together, the stepwise docking algorithm employed here provides a plausible path for cadaverine to traverse the receptor from the gating site to the internal binding-and-activation site. Furthermore, the close similarity to earlier predicting confirms the shape and location of both external gating and internal binding-and-activation site.

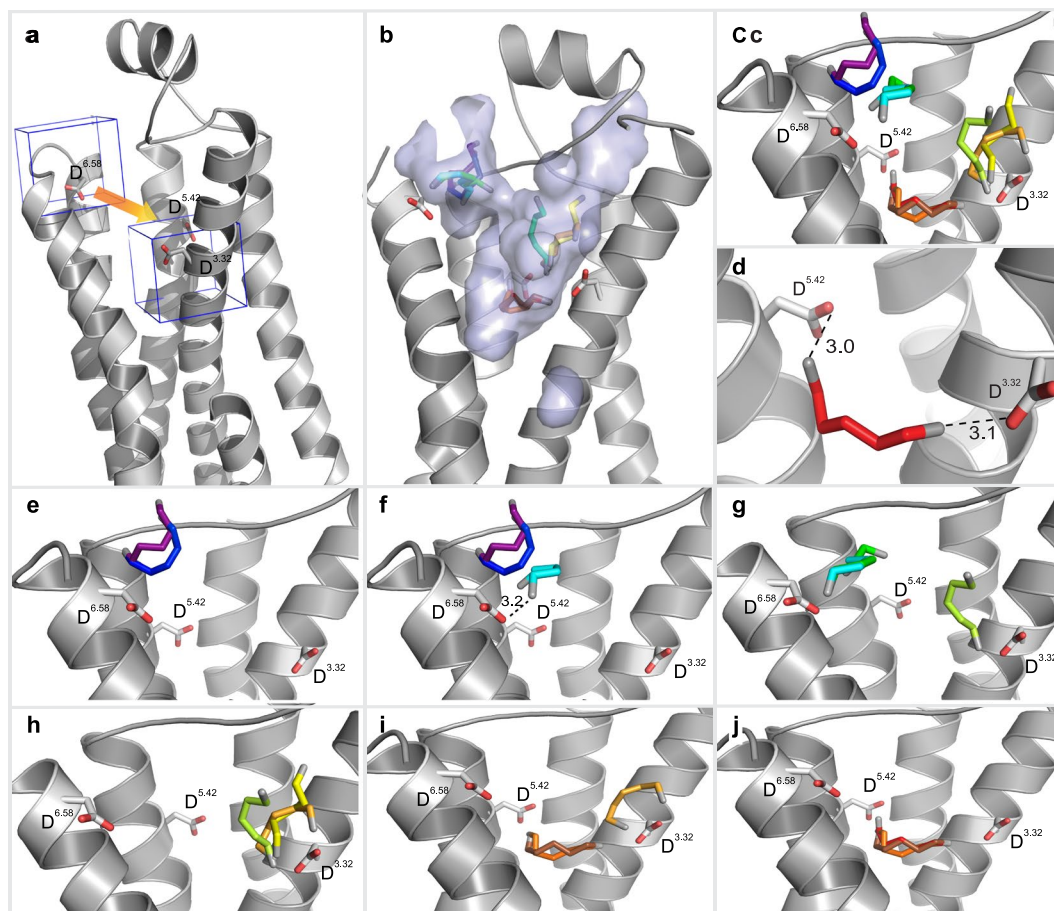


Figure 3. Binding path of cadaverine predicted by TomoDock exhibiting different cadaverine poses. **(a)** A cube (in blue line) encompassing gating site residue D279^{6.58} in TM 6 shows the first search space for TomoDock. The last search space is visualized by the second cube containing D112^{3.32} and D202^{5.42}. Intervening search spaces are intercalated at 1 Å steps along the orange arrow. **(b)** Surface view of the largest cavity in TAAR13c. Predicted cadaverine binding positions inside this cavity range from the extracellular protein surface to the internal ligand binding-and-activation site and are shown as sticks in rainbow colors (magenta to red). **(c)** Zoom-in on panel (b) without displaying the cavity to enable a clearer view on the intermediate binding positions of cadaverine along its path. **(d)** Final binding position of cadaverine with the main interacting residues (D112^{3.32}, D202^{5.42}) and the distances in Å from the carboxyl groups of these residues to the amino groups of cadaverine. Salt bridges are visualized as black dashed lines. **(e)** Progressive docking showing the first two steps of different orientations of cadaverine entering the cavity. Progress in ligand entry is shown in rainbow colors. **(f)** Step 3 of cadaverine (cyan) interacting with D279^{6.58} in TM6. **(g)** Step 4 of the cadaverine (dark green) path. In step 5 (light green) cadaverine leaves its previous position and slides to approach aspartate D112^{3.32} of the binding site. Step 1 and 2 are hidden for clarity. **(h)** Steps 6 and 7 (yellow and orange) show cadaverine exploring the D112^{3.32} area without any major interactions. Step 1–4 are hidden for clarity. **(i)** In step 8 and 9 (orange and brown) cadaverine is approaching the binding site. Cadaverine turns in order to establish binding to D112^{3.32} and D202^{5.42}. Steps 1–7 are hidden for clarity. **(j)** Final step of docking (red) showing cadaverine inside the binding site with its main interacting residues, aspartate D112^{3.32} and D202^{5.42}.

Abolishing the gating site by introducing a ligand-repellent charge results in significantly increased receptor affinity. In order to further explore the function of the gating site residue, we substituted the negatively charged D279^{6.58} in TM6 for a positively charged arginine residue, creating a D279R mutant (Fig. 4b). The major differences in this mutant are the loss of the salt bridge with D279, i.e. the destruction of the gating site, which should facilitate the entry of cadaverine into TAAR13c, and, on the other hand, the introduction of a ligand-repellent charge, which should hinder the approach of cadaverine towards the external niche. Experimentally, we observed that the apparent affinity of the mutant is 5.2 times higher than for the wild-type receptor (Fig. 5a and Supplementary Table 1), but significantly below the previously reported supersensitive mutant D279E¹⁹. This result is consistent with the assumption that the loss of the gating site overrides ligand repulsion by the positively charged arginine residue in the D279R mutant. Similar results were observed for mutant TAAR13c receptors, when putrescine was applied as a ligand (Fig. 5a).

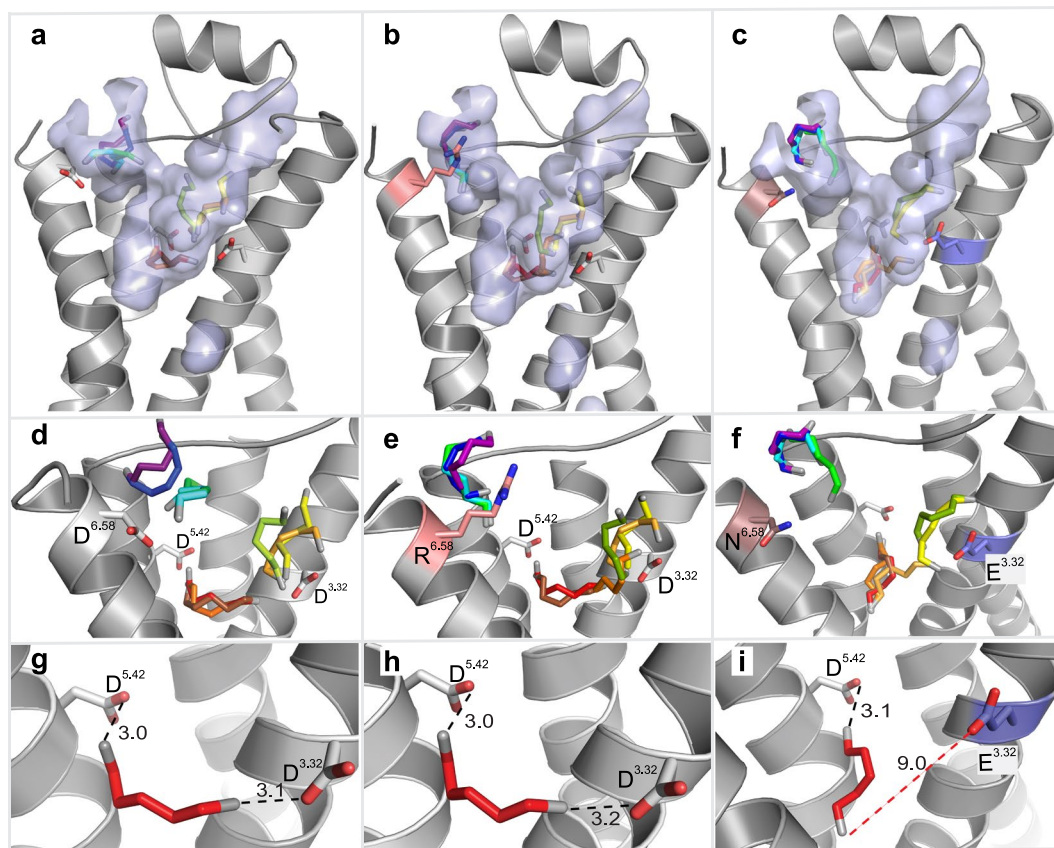


Figure 4. Binding path analyses of TAAR13c mutants indicate effects limited to the gating-site. Panels (a,d and g) show the wildtype and are taken from Fig. 3(b–d). (b) Surface view of the largest cavity in the D279R mutant. The mutated residue, R279^{6.58} is shown in pink. Successive progress in ligand entry is shown in rainbow colors. (c) Surface view of the largest cavity in the double mutant D112E/D279N. Mutated residues, E112^{3.32} and N279^{6.58} are shown in brown and blue, respectively. Progress in ligand entry is shown in rainbow colors. Panels d–f are zoom in on panels a–c without cavity showing the various orientations of cadaverine at different time points in rainbow color. (e) The introduced arginine residue R279 is shown in salmon. (f) The introduced asparagine and glutamate residues are shown in brown and blue respectively. Panels g–i show final binding position of cadaverine inside binding site with final binding position of cadaverine. The distances between the carboxyl groups of the aspartate(s) and the amino group(s) of cadaverine are given in Å. Salt bridges are visualized as black dashed lines. (h) Wildtype-like docking of D279R mutant. (i) Cadaverine in the binding site of the D112E/D279N mutant. The distance of E112^{3.32} from cadaverine is 9.5 Å (red dashed line) and thus too large to participate in ligand binding.

The D279^{6.58} residue is located on TM6 and close to ECL3. In many GPCRs this site appears to control receptor activity via ligand interactions^{26–30}. Future analyses will have to show, whether the influence of residue 6.58 is conserved in other olfactory receptors.

Path simulation and multistep docking show a localized effect of the gating site mutation. Next, we examined, whether the experimentally observed increase in ligand affinity of the D279R mutant could be corroborated by modeling the D279R mutant with a multistep docking procedure, using TomoDock, as described for the TAAR13c wildtype receptor. We found that in steps 1–4, cadaverine is located in the external niche close to the cavity opening (Fig. 4e). Interactions were found between cadaverine's amino groups and polar amino acid residues, Y193, S199^{5.39}, and E175 as well as the backbone carbonyl oxygen atom of F194 (Supplementary Table 2). These interactions are very similar to those observed in the wildtype receptor (see above). In other words, the external niche seems to have a very similar morphology and even retains the minor binding interactions in the mutant. Thus, the observed super sensitivity seems to originate primarily from the isolated loss of the salt bridge interaction and the ensuing reduction in binding affinity.

In step 5, cadaverine starts entering the internal binding pocket by squeezing through the constriction, which is in fact narrower than in the wildtype receptor (Table 1). Before reaching the final docked position, within the internal binding-and-activation site, cadaverine adopted several alternative orientations (Fig. 4e), all of which possessed the salt bridge between the cadaverine amino group and the carboxyl group of D112^{3.32}, before relaxing into the final docked pose. Upon reaching the internal binding-and-activation site in step 10, cadaverine orients itself to form stable salt bridges with D112^{3.32} and D202^{5.42} at a distance of 3.0 Å and 3.2 Å respectively (Fig. 4h).

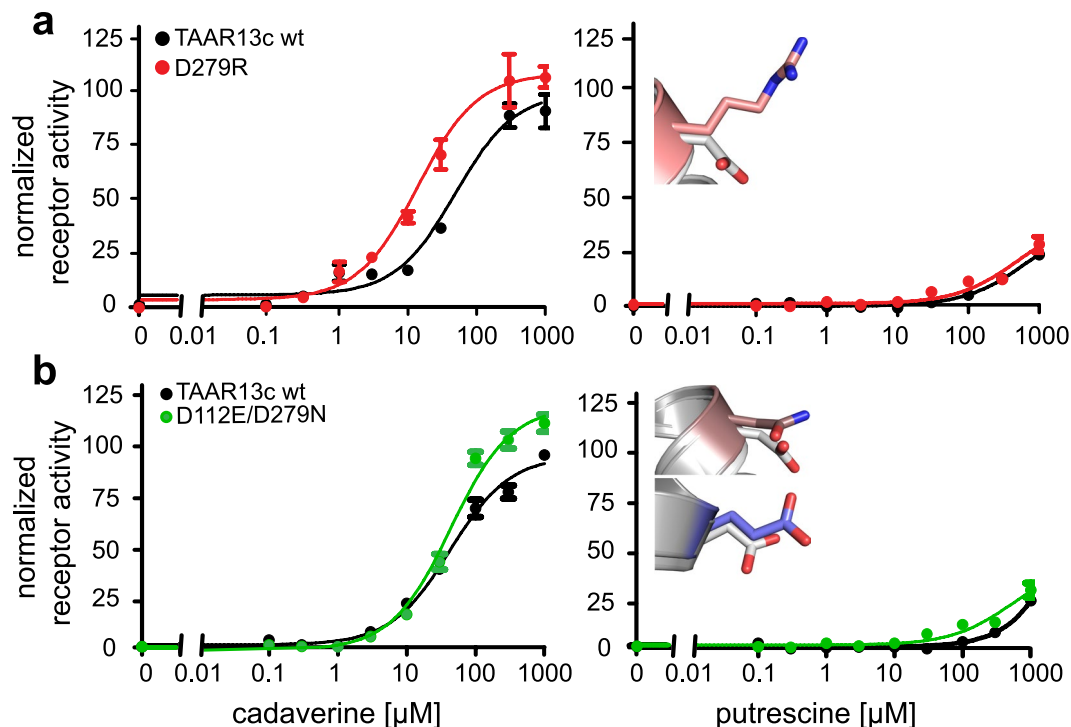


Figure 5. Concentration-response curves of TAAR13c mutants. HEK293T cells were stably transfected with TAAR13c constructs either altered by single or double point mutations. A cell line expressing TAAR13c wildtype receptors was included for control. Cadaverine and putrescine were added in the range of 0.1 μM to 1 mM. The resulting calcium increase was detected by Fluo-4 and calculated as $\Delta F/F$ and normalized to the value obtained with 10 μM NKH477, an agonist of membrane-bound adenylyl cyclases. Left column, response to cadaverine; right column, response to putrescine. Representative binding curves shown for the wildtype receptor and mutants (TAAR13c wildtype, black; D279R, red; D112E/D279N, green). Right panel, insets show mutant side chains (D279N, pale brown; D279R, pink; D112E, blue) overlaying the wildtype residue D in grey. (a) The cadaverine affinity of the D279R mutant was approximately 5fold higher compared to wildtype. (b) The double mutant D112E/D279N had a similar cadaverine affinity as the wildtype receptor with a slight increase in efficacy. For putrescine the affinities of mutant and wildtype TAAR13c receptors were also similar.

The distances are very similar to those calculated for wildtype TAAR13c (Table 1). The results suggest that the loss of the ligand gating site may have a conformational effect on the bottleneck but no or rather minute influence on the internal ligand binding-and-activation site. Constriction sites in ligand entry tunnels are not uncommon and seem to have surprisingly little influence on ease of a ligand's passage to its final binding site^{13,31}.

Taken together, we conclude that even the rather drastic exchange of a negative for a positive charge at the gating site has mostly local effects, which can be understood in terms of a balance between the loss of the external ligand-binding site and the gain of a repulsive force at the tunnel entrance.

Full rescue of an inactive TAAR13c mutant by elimination of the gating-site. The internal binding site for cadaverine is formed by two aspartate residues, D112^{3,32} and D202^{5,42} as the main interacting partners. In our previous docking and mutagenesis study we confirmed that both residues are essential for cadaverine binding and activation of TAAR13c. Removal of either residue resulted in total loss of observable receptor activity¹⁹. On the other hand, elimination of the external gating-site resulted in supersensitive receptors¹⁹.

In order to understand the balance between the external gating and internal binding-and-activating site, we simultaneously mutated the gating site and one residue of the internal binding site (D112E/D279N; Fig. 4c). In contrast to the inactive D112E mutant¹⁹, we observed that the double mutant (D112E/D279N) displayed a cadaverine affinity slightly less but not significantly different from the wildtype receptor (Fig. 5b and Supplementary Table 1). Similarly, putrescine activated the double mutant and the wildtype receptor comparably well (Fig. 5b), whereas no activation of the D112E mutant was detected with this ligand¹⁹.

Inspecting the docking path for the D112E/D279N mutant, cadaverine follows the same spatial route like in the wildtype TAAR13c or the D279R mutant receptors. It pauses at the external niche interacting with F194, Y193, S199^{5,39}, and E175 (Supplementary Table 2). After traversing the constriction, which is of similar size as in all other mutants (Table 1), cadaverine stays briefly close to E112^{3,32} and forms transient interactions (Fig. 4f) before it finally reaches the mutated internal binding-and-activation site (E112^{3,32}/D202^{5,42}). The carboxyl group of E112^{3,32} is displaced by 9.5 Å relative to the amino group of cadaverine, which is too far away to form a salt bridge (Fig. 4i). Thus, in the final orientation cadaverine can only form a salt bridge with D202^{5,42} at a distance of 3.2 Å but the carbon backbone of cadaverine is stabilized by (as in wildtype) L113^{3,33}, T116^{3,36}, T203^{5,43}, F272^{6,51}, and W269^{6,48} all situated within 5 Å distance and hence within the range of van der Waals interactions

(Supplementary Table 2). Thus in the mutant, the binding pocket retains most of the minor binding interactions and one of the two salt bridges. Surprisingly, this (compared to wildtype) seriously weakened binding in combination with facilitated ligand access due to gating site loss seem sufficient to activate the receptor at similar efficacy as wildtype TAAR13c. Taken together, the results suggest that the outcome of concomitant mutations of gating and internal binding sites can be understood as resulting from linear additivity of localized effects.

Discussion

Elucidating the molecular mechanism of ligand-to-receptor binding is of central importance to understand cellular signaling, not least because of its large relevance for biomedical research. However, due to the intrinsically dynamic nature of ligand-receptor interactions, little is known about the precise processes by which ligands bind to their receptors, even for GPCRs, which are among the most intensively studied groups of membrane proteins. In class A GPCRs the ligand binding-and-activation site is usually situated inside the transmembrane domain of the receptor, and the ligand has to traverse an entry tunnel to gain access to its destined location⁸. Such a geometry may also enable counteracting mechanisms similar to that of channel blockers in LGICs, where an external (allosteric) binding site for a ligand might block access of ligands to the final binding-and-activation site (orthosteric site) by physically blocking the entrance tunnel (Fig. 1). Evidence for such a mechanism indeed has been obtained for several neurotransmitter and hormone receptors of the class A GPCR group even though it has not been “discussed” in those terms^{11,32}. We have recently proposed a ligand-gating mechanism for an olfactory receptor-ligand pair, i.e. TAAR13c-cadaverine¹⁹. Since this phenomenon had not been described for any chemosensory receptor previously, we have tested our hypothesis with new mutations and modeling algorithms.

We used MOLE2.0²² to predict a tunnel paths accessed by cadaverine from the extracellular surface of TAAR13c to the internal (orthosteric) binding-and-activation site. Multistep docking was employed to visualize transient positions of cadaverine, as it moves along the tunnel. Further, to gain independent support for our hypothesis we introduced two additional mutations into TAAR13c, constitutively expressed the proteins in cell lines and investigated their effect(s) on receptor activation by cadaverine.

A generalized ligand-gating function for position 6.58 at the external end of TM6. Both in mutation analysis and in modeling an aspartate residue at the external end of TM6, position 6.58 (D279 in TAAR13c), emerged as key residue of an external niche serving as the initial binding site for cadaverine. Loss of D279^{6,58} and consequentially loss of the salt bridge to the amino group of cadaverine resulted in a supersensitive receptor, even when, as in the present case, the opposite charge was introduced (D279R) mutation. The increase in affinity of the D279R mutation is severalfold smaller than that previously observed for the D279E and D279N mutations, which is plausible if position 6.58 is ‘gating’ the access of the ligand to the internal binding-and-activation site. Thus, both quality and quantity of the affinity change provoked by the D279R mutation support the gating function of D279^{6,58} and its surrounding niche. As long as a cadaverine molecule is bound to D279^{6,58}, the passage from the extracellular surface towards the internal binding-and-activation site is blocked.

Exactly the same position, 6.58, appears to fulfil a similar function in several neurotransmitter and hormone receptors³⁰, beta adrenergic receptors¹³ and the gonadotropin releasing hormone receptor^{27,33}. In a recent modelling study on two human TAARs, 6.58 was hypothesized to serve as floodgate to remove the solvent shell from the ligand, before it reaches the internal binding site³⁴.

Only one of two entry tunnels is used in TAAR13c. Through which pathway does a ligand enter and exit the internal (orthosteric) binding-and-activation site of TAAR13c? Our results suggest that TAAR13c has two putative ligand entry tunnels. The outer opening of one of these tunnels harbors the previously identified external binding site, D279^{6,58}¹⁹. D279^{6,58} along with neighboring polar and/or charged amino acids, confers an electron-negative environment to the tunnel which is favorable to attract positively charged cadaverine (Supplementary Fig. 2). The opening of the second tunnel is bordered by a positively charged arginine residue (R92^{2,64}), which is less favorable for cadaverines’ entry. However in D279R mutation of the first tunnel introduces a very similar charge environment and still results in a considerable increase in affinity suggesting in reverse that the second tunnel is not able to provide significant ligand access due to additional restraints beyond its external positive charge.

To explain the experimentally observed super sensitivity of the D279R mutation several aspects need to be taken into account. Foremost, there is a destruction of the gating-site. Losing the ability of forming a salt bridge in the external niche should strongly reduce immobilization of cadaverine at this site and thus facilitate its entry into the tunnel. Secondly, cadaverine approaching the D279R mutated receptor could be hindered in entering the tunnel opening due to repulsive electrostatic forces. However, once cadaverine has passed the arginine residue it could even be pushed into the entry tunnel by the same electrostatic force. Additionally, the bulky side chain of arginine narrows the cavity of the external niche compared to the wildtype receptor (Supplementary Fig. 1). This could limit the exploration time for cadaverine, again speeding up its entry into the tunnel. Although these are plausible explanations, the current data unfortunately do not allow to unequivocally define the relative contribution of the individual processes.

Interestingly, beta adrenergic receptors, which share close structural similarity to olfactory receptors also possess two tunnels providing ligand access to the internal binding site³⁵. Both tunnels are lined by polar residues and thus are equipped to attract positively charged ligands. In ligand free conformation, however, only one of these tunnels seems to support ligand entry³⁶ similar to our findings reported here.

A constriction in the entry tunnel is neither rate-limiting in TAAR13c nor in other GPCRs. After entering the external niche and prior to proceeding towards the internal binding-and-activation site, cadaverine has to pass a narrow constriction in the tunnel. When comparing the diameter of this constriction in TAAR13c

wildtype to current and previously described mutants¹⁹, we found no obvious correlation with the experimentally determined changes in receptor affinities. In particular, the supersensitive mutants D279N/E/A possess a narrower constriction than the wildtype receptor (see Table 1). These observations seem to indicate that the rate limiting step for cadaverine to reach the internal binding- and activation site is not or only mildly affected by the dimension of the constriction.

A constriction like the one in TAAR13c has been described for some other class A GPCRs, and, like in our case, has not been found rate-limiting for ligand access. For opsin a 'bottleneck' structure of similar diameter (3.2 Å) has been described, but the rate at which retinal reaches the binding site is independent of the ease of passage through this constriction³¹. Also for beta adrenergic receptors it was suggested that ligands, before entering the binding pocket had to squeeze through a narrow passage but, again, this was not the rate-limiting step for receptor activation¹³.

Cadaverine pausing in the external niche may be a representative of a general mechanism regulating ligand access in GPCRs. In this study we have challenged our hypothesis of a ligand-gating mechanism in an olfactory receptor by generating novel mutations as well as calculating the ligand path in relation to the proposed gating-site using more refined modeling approaches. The experimental and theoretical results were consistent and both provided evidence for gating by an allosteric binding site lining the entry tunnel. The multi-step docking approach enabled us to visualize the path taken by cadaverine to travel from the extracellular niche to the internal binding- and activation site. During this movement cadaverine adopts various orientations in the extracellular niche before it proceeds towards the internal binding site in both wildtype and mutant receptors. Very similar results have been obtained for beta adrenergic receptors that share structural similarity with TAARs. Metastable ligand-binding sites at an extracellular vestibule cause a delay of the adrenergic ligand traversing towards and finally reaching the internal binding site^{13,35,36}. A corresponding vestibule has also been described for the interaction of the vasopressin receptor with its ligand³².

Very few GPCRs have been examined in this detail so far and, thus, regulation of ligand entry by transient lingering in an external niche or vestibule could conceivably have been overlooked in many cases. Since this mechanism has now been shown in three receptors belonging to two different subfamilies of class A GPCRs (alpha and beta subfamily) we expect that it may well be a much more wide-spread mechanism. It will be fascinating to elucidate how common this mechanism might be among class A GPCRs in general and in their largest clade, i.e. odorant receptors in particular.

Materials and Methods

Homology modeling, ligand access path prediction and docking in TAAR13c. TAAR13c homology models were generated using GPCR-I-TASSER. The crystal structures of six homologous receptors were used as templates: two β 2 and two β 1-adrenergic receptors (3sn6R and 2rh1A: 4amjA and 3zpqA, respectively), an adenosine receptor (4eiYQ) and a serotonin receptor (4iarA). The templates were selected automatically by GPCR-I-TASSER. The mutant structures were generated by Chimera³⁷ using side chain substitution in the wild-type sequence. We observed no detectable RMSD difference (<0.005) between models generated by these two methods. The receptor model was prepared for docking simulations by adding protons. Charges were assigned to ionizable side chains using the DockPrep function in Chimera³⁷. The model was then subjected to energy minimization using ModRefiner³⁸. The tunnels in TAAR13c were predicted using MOLE2.0²². Probe radius was set to 3.41 Å and the interior threshold to 1.2 keeping the path parameters default. Docking of cadaverine was performed using TomoDock²⁵. The pocket was defined by the gating-site residue leading to the internal binding- and activation site, thus defining a pocket with a depth of 16 Å with D279^{6,58} at the top and D112^{3,32} and D202^{5,42} at the bottom. In order to examine the path of cadaverine while moving towards the binding- and activation site, we defined a 18 × 18 × 18 Å cubic search space moving from above residue D279^{6,58} towards the internal binding- and activation site in steps of 1 Å. The ligand was prepared with rotatable and flexible bonds using AutoDock Tools³⁹. The resulting conformations were analyzed using PyMol⁴⁰ for visualization and for preparing the figures.

Heterologous expression of TAAR13c receptor mutants. Cell lines that constitutively expressed either the wildtype TAAR13c receptor or a mutant were generated using a previously established protocol⁴¹. We used a cell line that had been stably transfected with a gene encoding a variant of the A2-subunit of the olfactory cyclic nucleotide-gated (CNG) ion channel^{41,42}. Approximately 10 µg of the respective TAAR13c expression vectors were introduced into 4 × 10⁵ cells by a modified calcium-phosphate method⁴³. Stably transfected cells were selected in the presence of the antibiotic G418 (0.8 mg/ml). Expression of TAAR13c was monitored by Western blotting with specific anti-TAAR13c antibodies¹⁷ and anti-Rhodopsin antibodies (Sigma Aldrich, Taufkirchen, Germany).

Monitoring functional TAAR13c receptor activity. Activation of TAAR13c by cadaverine and putrescine evokes a rise in intracellular cAMP concentration that activates the CNG channel⁴¹. This subsequently causes an influx of Ca²⁺ ions through the open channel. Changes in [Ca²⁺]_i were monitored with the Ca²⁺-sensitive fluorescent dye Fluo-4. Cells were grown in 96-well plates to a density of approximately 2 × 10⁴ cells per well. Cells were loaded at room temperature with Fluo-4 AM as described previously⁴⁴. After 90 min, the loading solution was substituted for dye-free ECS (extracellular solution; 120 mM NaCl, 5 mM KCl, 2 mM MgCl₂, 2 mM CaCl₂, 10 mM HEPES, and 10 mM glucose, pH 7.4 [NaOH]) containing 100 µM IBMX. The plate was transferred into a fluorescence reader (FLUOstar Omega, BMG Labtech, Offenburg, Germany) to monitor Fluo-4 fluorescence. The excitation wavelength was 485 nm. Fluorescence emission was detected at 520 nm. A concentration series of cadaverine or putrescine (0.1 µM to 1 mM) as well as 10 µM NKH477 (adenylyl cyclase activator; positive control)

was added once Fluo-4 fluorescence had reached a stable value in each well. The fluorescence signal obtained with NKH477 was set to 100% as an internal standard. Concentration–response curves for mutant TAARs were always performed in parallel with wildtype TAAR13c, and affinity estimates were established from at least three independent experiments with quadruplicate measurements in each experiment.

Data were analyzed and displayed using Prism 5.04 software (GraphPad, San Diego, CA, USA).

Introduction of mutations into TAAR13c. Wildtype full length TAAR13c with an N-terminal extension of the first 20 amino acids of bovine rhodopsin cloned in pcDNA3.1(–) expression vector¹⁷ was used for mutagenesis. Point mutations were introduced using the QuikChange® Site-directed mutagenesis kit (Agilent Technologies, Santa Clara, CA, USA). In brief, the PCR reaction was performed using *PfuUltra* High-Fidelity DNA Polymerase with the above described plasmid as a template, along with mutagenic primers and reaction mix. Parental strands, which are methylated in contrast to the PCR products, were selectively digested with *DpnI* enzyme and the resulting product was transformed into XL-1 blue supercompetent *E. coli* cells by electroporation. Screening of colonies was done by colony PCR using wild type TAAR13c primers. Colonies positive for the desired mutation were grown under standard conditions in LB broth and the plasmids were isolated using a plasmid DNA purification kit from Zymo research (California, USA). All mutations were verified by DNA sequencing. Primers used for mutagenesis were: TAAR13cwt 5': atggattatcatcacagaagaa 3': tcaaacctgtaataatgat;

D279R 5': actctctggtgcgtccctacattaac 3': gttaatgtaggagcaccagagagt;

D112E 5': ccggtttgaactgtttctcac 3': gtgagaaacagttcaaacccg;

D279N 5': actctctggtgaatccctacattaac 3': gttaatgtaggattcaccagagagt.

References

1. Traynelis, S. F. *et al.* Glutamate receptor ion channels: structure, regulation, and function. *Pharmacol Rev* **62**, 405–496, <https://doi.org/10.1124/pr.109.002451> (2010).
2. Lummis, S. C. 5-HT(3) receptors. *J Biol Chem* **287**, 40239–40245, <https://doi.org/10.1074/jbc.R112.406496> (2012).
3. Dani, J. A. Neuronal Nicotinic Acetylcholine Receptor Structure and Function and Response to Nicotine. *Int Rev Neurobiol* **124**, 3–19, <https://doi.org/10.1016/bs.irn.2015.07.001> (2015).
4. Burgos, C. F., Yevenes, G. E. & Aguayo, L. G. Structure and Pharmacologic Modulation of Inhibitory Glycine Receptors. *Mol Pharmacol* **90**, 318–325, <https://doi.org/10.1124/mol.116.105726> (2016).
5. Michels, G. & Moss, S. J. GABA_A receptors: properties and trafficking. *Crit Rev Biochem Mol Biol* **42**, 3–14, <https://doi.org/10.1080/10409230601146219> (2007).
6. Zhang, D., Pan, Z. H., Awobuluyi, M. & Lipton, S. A. Structure and function of GABA(C) receptors: a comparison of native versus recombinant receptors. *Trends Pharmacol Sci* **22**, 121–132 (2001).
7. Gentry, P. R., Sexton, P. M. & Christopoulos, A. Novel Allosteric Modulators of G Protein-coupled Receptors. *J Biol Chem* **290**, 19478–19488, <https://doi.org/10.1074/jbc.R115.662759> (2015).
8. Lee, S. M., Booe, J. M. & Pioszak, A. A. Structural insights into ligand recognition and selectivity for class A, B, and C GPCRs. *European journal of pharmacology* **763**, 196–205, <https://doi.org/10.1016/j.ejphar.2015.05.013> (2015).
9. Fredriksson, R., Lagerström, M. C., Lundin, L.-G. & Schiöth, H. B. The G-Protein-Coupled Receptors in the Human Genome Form Five Main Families. Phylogenetic Analysis, Paralogue Groups, and Fingerprints. *Molecular Pharmacology* **63**, 1256–1272 (2003).
10. Avlani, V. A. *et al.* Critical Role for the Second Extracellular Loop in the Binding of Both Orthosteric and Allosteric G Protein-coupled Receptor Ligands. *Journal of Biological Chemistry* **282**, 25677–25686, <https://doi.org/10.1074/jbc.M702311200> (2007).
11. Kruse, A. C. *et al.* Structure and dynamics of the M3 muscarinic acetylcholine receptor. *Nature* **482**, 552–556, <https://doi.org/10.1038/nature10867> (2012).
12. Redka, Dy. S., Pisterzi, L. F. & Wells, J. W. Binding of Orthosteric Ligands to the Allosteric Site of the M2 Muscarinic Cholinergic Receptor. *Molecular Pharmacology* **74**, 834–843 (2008).
13. Dror, R. O. *et al.* Pathway and mechanism of drug binding to G-protein-coupled receptors. *Proc Natl Acad Sci USA* **108**, 13118–13123, <https://doi.org/10.1073/pnas.1104614108> (2011).
14. Nei, M., Niimura, Y. & Nozawa, M. The evolution of animal chemosensory receptor gene repertoires: roles of chance and necessity. *Nature reviews. Genetics* **9**, 951–963, <https://doi.org/10.1038/nrg2480> (2008).
15. Borowsky, B. *et al.* Trace amines: identification of a family of mammalian G protein-coupled receptors. *Proc Natl Acad Sci USA* **98**, 8966–8971, <https://doi.org/10.1073/pnas.151105198> (2001).
16. Buntzow, J. R. *et al.* Amphetamine, 3,4-methylenedioxymethamphetamine, lysergic acid diethylamide, and metabolites of the catecholamine neurotransmitters are agonists of a rat trace amine receptor. *Mol Pharmacol* **60**, 1181–1188 (2001).
17. Hussain, A. *et al.* High-affinity olfactory receptor for the death-associated odor cadaverine. *Proc Natl Acad Sci USA* **110**, 19579–19584, <https://doi.org/10.1073/pnas.1318596110> (2013).
18. Hussain, A., Saraiva, L. R. & Korsching, S. I. Positive Darwinian selection and the birth of an olfactory receptor clade in teleosts. *Proc Natl Acad Sci USA* **106**, 4313–4318, <https://doi.org/10.1073/pnas.0803229106> (2009).
19. Sharma, K. *et al.* Elimination of a ligand gating site generates a supersensitive olfactory receptor. *Sci Rep* **6**, 28359, <https://doi.org/10.1038/srep28359> (2016).
20. Li, Q. *et al.* Non-classical amine recognition evolved in a large clade of olfactory receptors. *Elife* **4**, e10441, <https://doi.org/10.7554/eLife.10441> (2015).
21. Schrodinger, L. L. C. *The PyMOL Molecular Graphics System, Version 1.8* (2015).
22. Sehnal, D. *et al.* MOLE 2.0: advanced approach for analysis of biomacromolecular channels. *Journal of Cheminformatics* **5**, 39, <https://doi.org/10.1186/1758-2946-5-39> (2013).
23. Miyazawa, A., Fujiyoshi, Y. & Unwin, N. Structure and gating mechanism of the acetylcholine receptor pore. *Nature* **423**, 949, <https://doi.org/10.1038/nature01748> (2003).
24. Hildebrand, P. W. *et al.* A ligand channel through the G protein coupled receptor opsin. *Plos One* **4**, e4382, <https://doi.org/10.1371/journal.pone.0004382> (2009).
25. Uzunova, V. V., Quareshy, M., del Genio, C. I. & Napier, R. M. Tomographic docking suggests the mechanism of auxin receptor TIR1 selectivity. *Open Biology* **6** (2016).
26. Ford, D. J., Essex, A., Spalding, T. A., Burstein, E. S. & Ellis, J. Homologous Mutations Near the Junction of the Sixth Transmembrane Domain and the Third Extracellular Loop Lead to Constitutive Activity and Enhanced Agonist Affinity at all Muscarinic Receptor Subtypes. *Journal of Pharmacology and Experimental Therapeutics* **300**, 810–817 (2002).
27. Coetsee, M., Millar, R. P., Flanagan, C. A. & Lu, Z.-L. Identification of Tyr290(6.58) of the Human Gonadotropin-Releasing Hormone (GnRH) Receptor as a Contact Residue for Both GnRH I and GnRH II: Importance for High-Affinity Binding and Receptor Activation. *Biochemistry* **47**, 10305–10313, <https://doi.org/10.1021/bi800911z> (2008).

28. Wichard, J. D. *et al.* Chemogenomic analysis of G-protein coupled receptors and their ligands deciphers locks and keys governing diverse aspects of signalling. *Plos One* **6**, e16811, <https://doi.org/10.1371/journal.pone.0016811> (2011).
29. Hulme, E. C. GPCR activation: a mutagenic spotlight on crystal structures. *Trends Pharmacol Sci* **34**, 67–84, <https://doi.org/10.1016/j.tips.2012.11.002> (2013).
30. Benredjem, B., Girard, M., Rhainds, D., St-Onge, G. & Heveker, N. Mutational Analysis of Atypical Chemokine Receptor 3 (ACKR3/CXCR7) Interaction with Its Chemokine Ligands CXCL11 and CXCL12. *J Biol Chem* **292**, 31–42, <https://doi.org/10.1074/jbc.M116.762252> (2017).
31. Piechnick, R. *et al.* Effect of channel mutations on the uptake and release of the retinal ligand in opsin. *Proc Natl Acad Sci USA* **109**, 5247–5252, <https://doi.org/10.1073/pnas.1117268109> (2012).
32. Saleh, N. *et al.* A Three-Site Mechanism for Agonist/Antagonist Selective Binding to Vasopressin Receptors. *Angewandte Chemie International Edition* **55**, 8008–8012, <https://doi.org/10.1002/anie.201602729> (2016).
33. Hovelmann, S. *et al.* Impact of aromatic residues within transmembrane helix 6 of the human gonadotropin-releasing hormone receptor upon agonist and antagonist binding. *Biochemistry* **41**, 1129–1136 (2002).
34. Izquierdo, C., Gomez-Tamayo, J. C., Nebel, J. C., Pardo, L. & Gonzalez, A. Identifying human diamine sensors for death related putrescine and cadaverine molecules. *Plos Comput Biol* **14**, e1005945, <https://doi.org/10.1371/journal.pcbi.1005945> (2018).
35. Gonzalez, A., Perez-Acle, T., Pardo, L. & Deupi, X. Molecular basis of ligand dissociation in beta-adrenergic receptors. *Plos One* **6**, e23815, <https://doi.org/10.1371/journal.pone.0023815> (2011).
36. Wang, T. & Duan, Y. Ligand Entry and Exit Pathways in the $\beta(2)$ -adrenergic Receptor. *J Mol Biol* **392**, 1102–1115, <https://doi.org/10.1016/j.jmb.2009.07.093> (2009).
37. Pettersen, E. F. *et al.* UCSF Chimera—a visualization system for exploratory research and analysis. *Journal of computational chemistry* **25**, 1605–1612, <https://doi.org/10.1002/jcc.20084> (2004).
38. Xu, D. & Zhang, Y. Improving the physical realism and structural accuracy of protein models by a two-step atomic-level energy minimization. *Biophys J* **101**, 2525–2534, <https://doi.org/10.1016/j.bpj.2011.10.024> (2011).
39. Morris, G. M. *et al.* AutoDock4 and AutoDockTools4: Automated docking with selective receptor flexibility. *Journal of computational chemistry* **30**, 2785–2791, <https://doi.org/10.1002/jcc.21256> (2009).
40. Schrodinger, L. L. C. *The AxPyMOL Molecular Graphics Plugin for Microsoft PowerPoint, Version 1.8* (2015).
41. Wachten, S., Schlenstedt, J., Gauss, R. & Baumann, A. Molecular identification and functional characterization of an adenylyl cyclase from the honeybee. *Journal of neurochemistry* **96**, 1580–1590, <https://doi.org/10.1111/j.1471-4159.2006.03666.x> (2006).
42. Ludwig, J., Margalit, T., Eismann, E., Lancet, D. & Kaupp, U. B. Primary structure of cAMP-gated channel from bovine olfactory epithelium. *FEBS Lett* **270**, 24–29 (1990).
43. Chen, C. & Okayama, H. High-efficiency transformation of mammalian cells by plasmid DNA. *Mol Cell Biol* **7**, 2745–2752 (1987).
44. Balfanz, S. *et al.* Functional characterization of transmembrane adenylyl cyclases from the honeybee brain. *Insect biochemistry and molecular biology* **42**, 435–445, <https://doi.org/10.1016/j.ibmb.2012.02.005> (2012).

Acknowledgements

We gratefully acknowledge financial support from the German Science foundation (grants KO 1046/7-1 and RTG 1960 to S.I.K.).

Author Contributions

The experiments were conceived by S.I.K. and K.S. and designed by A.B., S.B. and K.S. Experiments were performed by K.S. and S.B. Illustrations were drafted by K.S. Data analysis was done by S.B. and K.S. and K.S., A.B. and S.I.K. wrote the paper.

Additional Information

Supplementary information accompanies this paper at <https://doi.org/10.1038/s41598-018-27790-7>.

Competing Interests: The authors declare no competing interests.

Publisher's note: Springer Nature remains neutral with regard to jurisdictional claims in published maps and institutional affiliations.



Open Access This article is licensed under a Creative Commons Attribution 4.0 International License, which permits use, sharing, adaptation, distribution and reproduction in any medium or format, as long as you give appropriate credit to the original author(s) and the source, provide a link to the Creative Commons license, and indicate if changes were made. The images or other third party material in this article are included in the article's Creative Commons license, unless indicated otherwise in a credit line to the material. If material is not included in the article's Creative Commons license and your intended use is not permitted by statutory regulation or exceeds the permitted use, you will need to obtain permission directly from the copyright holder. To view a copy of this license, visit <http://creativecommons.org/licenses/by/4.0/>.

© The Author(s) 2018

4.3. Publication 3

Kanika Sharma, Adnan Syed, Sara Ferrando, Sylvie Mazan and Sigrun I. Korsching. "**The Chemosensory Receptor Repertoire of a True Shark Is Dominated by a Single Olfactory Receptor Family**" *Genome Biol. Evol.* 11(2):398–405

doi: <https://doi.org/10.1093/gbe/evz002>

<https://academic.oup.com/gbe/article/11/2/398/5288589>

The Chemosensory Receptor Repertoire of a True Shark Is Dominated by a Single Olfactory Receptor Family

Kanika Sharma^{1,†}, Adnan S. Syed^{1,†}, Sara Ferrando², Sylvie Mazan³, and Sigrun I. Korsching^{1,*}

¹Department of Biology, Institute of Genetics, Biocenter, University at Cologne, Zùlpicherstrasse 47a, 50674, Cologne, Germany

²Department of Earth, Environmental and Life Sciences (DISTAV), University of Genoa, Italy

³CNRS-UPMC-Sorbonne Universit s, UMR 7232, Banyuls sur Mer, France

[†]Shared first author.

*Corresponding author: E-mail: sigrun.korsching@uni-koeln.de.

Accepted: January 6, 2019

Abstract

Throughout the animal kingdom chemical senses are one of the primary means by which organisms make sense of their environment. To achieve perception of complex chemosensory stimuli large repertoires of olfactory and gustatory receptors are employed in bony vertebrates, which are characterized by high evolutionary dynamics in receptor repertoire size and composition. However, little is known about their evolution in earlier diverging vertebrates such as cartilaginous fish, which include sharks, skates, rays, and chimeras. Recently, the olfactory repertoire of a chimera, elephant shark, was found to be curiously reduced in odorant receptor number. Elephant sharks rely heavily on electroreception to localize prey; thus, it is unclear how representative their chemosensory receptor repertoire sizes would be for cartilaginous fishes in general. Here, we have mined the genome of a true shark, *Scyliorhinus canicula* (catshark) for olfactory and gustatory receptors, and have performed a thorough phylogenetic study to shed light on the evolution of chemosensory receptors in cartilaginous fish. We report the presence of several gustatory receptors of the TAS1R family in catshark and elephant shark, whereas TAS2R receptors are absent. The catshark olfactory repertoire is dominated by V2R receptors, with 5–8 receptors in the other three families (OR, ORA, TAAR). Species-specific expansions are mostly limited to the V2R family. Overall, the catshark chemosensory receptor repertoires are generally similar in size to those of elephant shark, if somewhat larger, showing similar evolutionary tendencies across over 400 Myr of separate evolution between catshark and elephant shark.

Key words: catshark, *Scyliorhinus canicula*, chimera, phylogeny, evolution, taste receptor.

Main Text

Catshark Possess Five of the Six Major Vertebrate Chemosensory Receptor Families

Bony vertebrates exhibit four major families of olfactory receptors (OR, TAAR, ORA, V2R) and two gustatory GPCR families, TAS1R and TAS2R (Bachmanov and Beauchamp 2007). We have performed a recursive search in the preliminary draft genome of catshark, *Scyliorhinus canicula* to delineate its complete chemosensory receptor repertoire, using representative protein sequences from all six families in several species as initial queries. Phylogenetic analysis was performed using a maximum likelihood approach, for details see Materials and Methods.

For all OR families catshark as well as elephant shark genes could be identified, with the exception of T2R receptors. Since the closely related ORA receptors were present, it is unlikely that *t2r* genes were not found for technical reasons. We conclude that T2R receptors are absent in both species, and possibly in all cartilaginous fish, for elephant shark consistent with earlier observations (Grus and Zhang 2009).

Our analysis identified between 5 and 40 receptors per chemosensory receptor family in catshark (table 1). Additionally, we found some new TAARs, ORs, V2Rs, and TAS1R gene sequences in the elephant shark genome beyond those previously published (Grus and Zhang 2009; Niimura 2009b; Venkatesh et al. 2014). In total, the catshark

Table 1

Chemosensory Receptor Repertoire Sizes

Gene Family	No. of Genes in Catshark	No. of Genes in Elephant Shark	No. of Genes in Mouse	No. of Genes in Zebrafish
OR	8 (1) ^b	7 ^a	1037 ^c	154 ^c
TAAR	5 ^b	5 ^a	15 ^d	112 ^d
ORAV1R	6 ^b	4 ^a	211 ^c	7 ^e
V2R	35 ^b	34 ^a	121 ^c	58 ^f
V2RL	5 ^b	3 ^a	0	2 ^f
TAS1R	6 ^b	4 ^a	3 ^c	4 ^g
T2R	0 ^b	0	33 ^c	4 ^c

NOTE.—Total gene numbers are given, in parentheses the number of pseudogenes.

^aAdditional genes identified (elephant shark, three TAAR, four TAS1R, one OR, two V2R, two V2RL) compared with previously published numbers (Niimura 2009b; Venkatesh et al. 2014).

^bRefer to genes newly identified here (catshark). Superscripts refer to Niimura (2009a).

^cHussain et al. (2009).

^eSaraiva and Korsching (2007).

^fAhuja et al. (2018).

^gAlioto and Ngai (2006).

chemosensory receptor repertoire encompasses 65 genes, which is slightly larger than the elephant shark repertoire with 54 genes. Both are similar to the size of the chemosensory repertoire of the sea lamprey, which has been given as 59 genes (Libants et al. 2009), but several to many times smaller than the repertoires of bony vertebrates (Niimura and Nei 2006) suggesting that gene birth events are comparatively rare in jawless and cartilaginous fish chemosensory receptor families compared with the bony fish lineage, and in particular its tetrapod branch.

The Catshark Chemosensory Receptor Repertoire Is Dominated by V2Rs

In bony fish and tetrapods ORs constitute the dominant chemosensory family (Niimura and Nei 2006). It had therefore been surprising, when only six *or* genes were reported in the elephant shark genome (Venkatesh et al. 2014), but it had been unclear, how representative this reduced repertoire was for cartilaginous fish in general and true sharks in particular. Here, we report one additional *or* gene in elephant shark and a very similar size of eight *or* genes in catshark (table 1). This is considerably less than even the sea lamprey OR repertoire, reported as 27 genes (Libants et al. 2009) and suggests that the OR family has not undergone any major radiation in cartilaginous fish.

In contrast, 40 *v2r* genes were observed in the catshark genome, slightly larger than the 37 genes we detected in the elephant shark genome (table 1). This is roughly comparable to mammalian and fish repertoire sizes (Young and Trask 2007; Ahuja et al. 2018) and more than all other chemosensory families combined. *v2r* genes have not been found in

jawless fish (Libants et al. 2009), thus the origin of the family appears to be in the most recent common ancestor (MRCA) of jawed fish.

Phylogenetic analysis shows a small subgroup of catshark and elephant shark *v2r* genes orthologous to zebrafish V2R-like OlfCa1 and OlfCb1 (fig. 1). We therefore suggest to name these genes as *v2rl*, V2R-like. The *v2rl* subgroup is most closely related to type 1 taste receptors, TAS1Rs, from which they segregate with maximal branch support (fig. 1a). We report five such genes for catshark and three for elephant shark (fig. 1b). The maximal branch support within the V2RL clade allows the deduction of two ancestral *v2rl* genes already in the MRCA of cartilaginous and bony fish. Subsequently, small gene expansions specific to the cartilaginous lineage generated the extant *v2rl* gene numbers, which are considerably larger than present in zebrafish (two genes, *olfCa1*, *olfCb1*) and mammals (one gene, *gprc6*).

The main group of V2Rs is most closely related to the calcium-sensing receptor (CaSR), from which it segregates with maximal branch support (fig. 1a). There are 35 catshark genes in this group and nearly the same number (34) of elephant shark genes (table 1). Interestingly these numbers are reached by several species-specific gene duplications generating subclades of up to 7 catshark and 12 elephant shark genes, which just happen to result in a very similar total number. In several cases, direct orthologs of catshark and elephant shark V2Rs are observed, for example, V2R2 (fig. 2).

The most basal gene, Sc-V2R1, Cm-V2R1, is orthologous to zebrafish OlfCc1 and the mammalian V2R2 subfamily (fig. 2). It may serve as coreceptor in zebrafish and mouse (Martini et al. 2001; DeMaria et al. 2013) and it will be interesting to investigate, whether such a function might also be conserved in cartilaginous fish. The second most basal gene, Sc-V2R2, Cm-V2R2, is orthologous to all remaining mouse *v2r* genes (a single clade), but appears to have been lost in zebrafish (fig. 2). The remaining catshark/elephant gene expansion is intermingled with six zebrafish clades comprising 1–19 *olfC* genes, suggesting a similar number of ancestral *v2r* genes in the MRCA of cartilaginous and bony fish, all of which appear to have been lost in tetrapods (fig. 2).

Two to Three Gustatory *tas1r* Genes Present in the MRCA of Cartilaginous and Bony Vertebrates

The gustatory *tas1r* genes are close relatives of the olfactory *v2r* genes and, like these, belong to class C GPCRs, which are characterized by a large, extracellular N-terminus and a characteristic six exon structure (Sainz et al. 2001). The mammalian taste receptor 1 (TAS1R) family is best understood. It comprises three members TAS1R1, TAS1R2, and TAS1R3 (Voigt et al. 2012), which hetero-oligomerize to TAS1R1/TAS1R3 and TAS1R2/TAS1R3, functioning as umami and sweet taste receptor, respectively (Zhao et al. 2003). Teleost fish possess the direct orthologs of TAS1R1 and TAS1R3, but

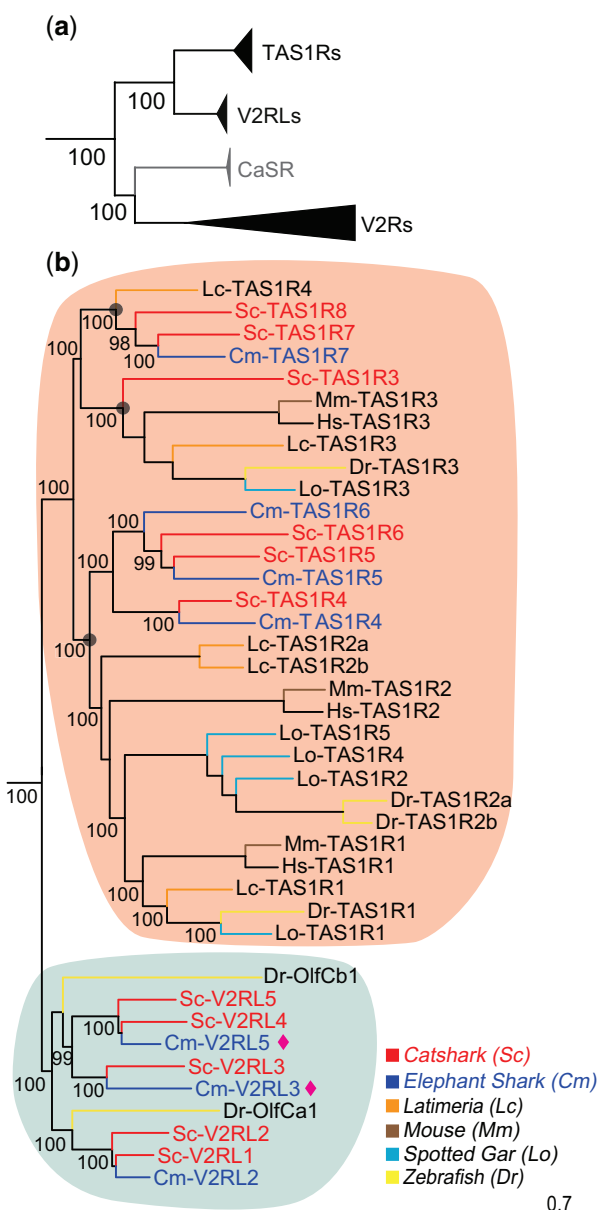


FIG. 1.—Two to three ancestral *tas1r* genes already present in the MRCA of cartilaginous and bony vertebrates. Phylogenetic tree of TAS1Rs (orange), V2RLs (grey) and V2Rs of catshark and elephant shark. CaSR and TAS1Rs as outgroups for V2Rs and V2RLs respectively. (a) All gene groups are shown in collapsed representation to emphasize the basal nodes. Note that *v2rl* genes are the sister group to TAS1Rs and CaSR represents the sister group for the main group of V2Rs. The phylogenetic tree was generated using a maximum likelihood method (PhyML-aLRT) with SPR setting for tree optimization and chi square-based aLRT for branch support (given as percentage). Note the maximal branch support for all nodes. (b) The TAS1R and V2RL node of (a) shown in detail. Branch support shown as percentage. Branches are color-coded for catshark (red) and elephant shark (blue) along with zebrafish (yellow), mouse (brown), spotted gar (cyan), and *Latimeria* (orange). Transparent grey circles denote the clades corresponding to the three predicted ancestral *tas1r* genes in the MRCA of cartilaginous and bony vertebrates. Two new *v2rl* genes were found in elephant shark (purple spades).

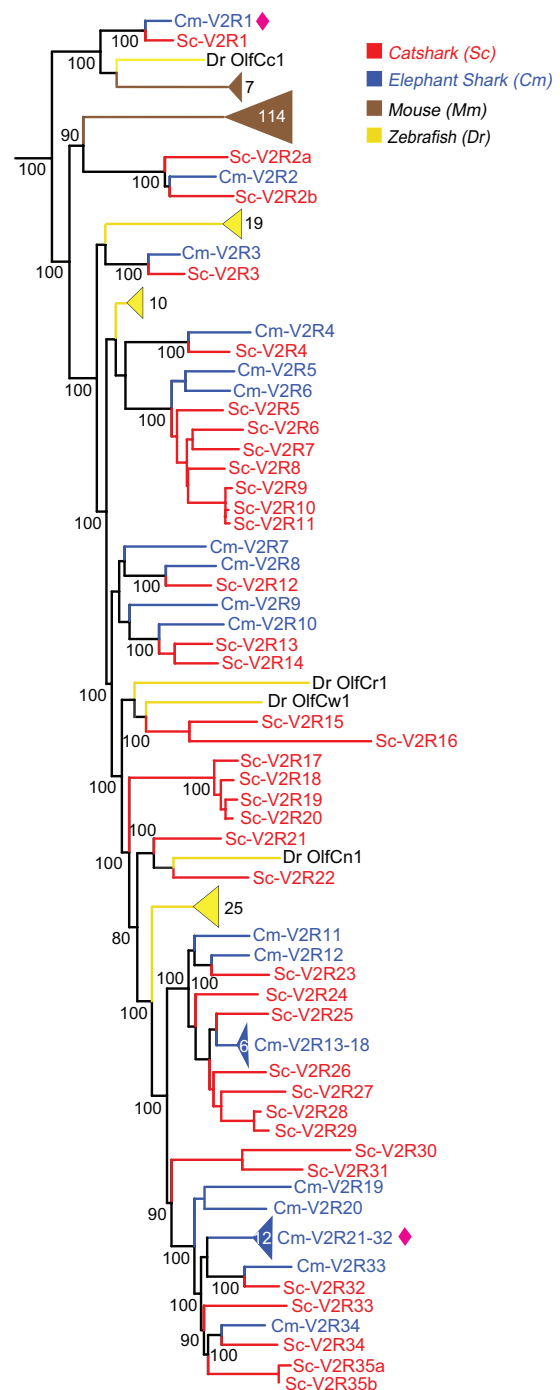


FIG. 2.—The catshark chemosensory receptor repertoire is dominated by V2Rs. Largest family of V2Rs in catshark comprising of thirty-five genes in catshark (red) were compared with thirty-four elephant shark V2Rs (blue) along with zebrafish (yellow), and mouse (brown). The most basal gene, Sc-V2R1, Cm-V2R1, is orthologous to zebrafish OlfCc1 and the mammalian V2R2 subfamily. The phylogenetic tree was generated as described in figure 1 and branch support is given as percentage. Sequences were named according to named orthologs or closest paralogs from other species otherwise according to phylogenetic relationship. Sequences are named a, b where exon 3 and exon 6 might be derived from the same gene. New genes in elephant shark are marked with purple spade.

Downloaded from https://academic.oup.com/gbe/article-abstract/11/2/398/5288589 by Universitat Koeln/Instut für Genetik user on 23 October 2019

have expanded TAS1R2 to 2–3 genes (Ishimaru et al. 2005). Interestingly, the TAS1R2/TAS1R3 hetero-oligomers of teleosts also react to amino acids, not to sugars like their mammalian counterparts (Oike et al. 2007). In *Latimeria*, one TAS1R1, two TAS1R2, and two TAS1R3 have been described (Picone et al. 2014). The evolutionary relationships of these genes are not clear so far, because the TAS1R repertoire of earlier-diverging species has not been available so far.

Here, we identified in total six *tas1r* genes in the catshark genome, and four in the elephant shark. We assume these numbers to be final for both catshark and elephant shark, because the current genomic coverage is 200× and 19.25×, respectively (Wyffels et al. 2014). All elephant shark *tas1r* genes possess orthologs in catshark. Interestingly, one of the catshark *tas1r* genes, Sc-TAS1R3, appears to have been lost in elephant shark. Furthermore, catshark TAS1R7 and TAS1R8 appear to result from a gene duplication within the true shark lineage, because elephant shark has a single gene, TAS1R7, in this subnode. All confirmed TAS1R candidates show the characteristic exon structure (data not shown), although due to the preliminary nature of the genomic assembly not all six exons could be identified in each case.

The phylogeny shown here allows some conclusions concerning the origin and relationship of mammalian and teleost TAS1R receptors. Mouse and zebrafish TAS1R3 possess a direct ortholog in catshark, Sc-TAS1R3 (fig. 1b), suggesting this gene to be already present in the MRCA of cartilaginous and bony vertebrates, whereas TAS1R1 and TAS1R2 appear to have originated in a duplication event within the bony lineage (fig. 1b). In the 420 Myr since divergence of chimeras and true sharks (Heinicke et al. 2009) the evolutionary dynamic has been very small (three gene birth event in catshark, two in elephant shark, all except one in the MRCA of true sharks and chimeras), which parallels the slow evolution of this family in bony fish and tetrapods. This is very different from the evolutionary history of the closely related V2Rs, which often exhibit species-specific repertoires (Hashiguchi and Nishida 2006). The intermingling of cartilaginous fish TAS1Rs with bony fish TAS1Rs in the phylogenetic tree (fig. 1b) allows to estimate the number of ancestral TAS1Rs in the MRCA of cartilaginous and bony vertebrates. The most parsimonious explanation of the observed tree assumes a gene loss event for bony fish in the Sc-TAS1R7, eight subclade, which results in a prediction of three ancestral *tas1r* genes in the MRCA of cartilaginous and bony vertebrates (fig. 1). The origin of the TAS1R family cannot be exactly deduced, but should have happened within the jawed lineage, since TAS1Rs were not found in lamprey (Grus and Zhang 2009).

Small Repertoires for OR, TAAR, and ORA Receptor Families in Catshark and Elephant Shark

OR genes are the largest gene family in bony vertebrates (Niimura and Nei 2006), but have only undergone very limited

gene expansion in cartilaginous fish (table 1; fig. 3). In mammals, class I and class II ORs have been distinguished, with class I orthologous to a zebrafish subfamily of five genes, and class II possessing a single zebrafish ortholog, Dr3OR5.4. Both classes exhibit a single catshark ortholog gene, Sc-OR1 and Sc-OR2, respectively (fig. 3) suggesting the origin of these two genes in the MRCA of cartilaginous and bony fish. Three more zebrafish genes or subclades are orthologous to a catshark and/or elephant shark gene, suggesting in total the presence of at least five *or* genes in the MRCA of cartilaginous and bony fish, of which elephant shark appears to have lost two genes and catshark one. Thirty-two putatively functional OR genes were identified from the sea lamprey genome (Niimura 2009b), whereas in elephant shark we identified seven ORs (Cm-OR1 and Cm-OR3–8). Previously in elephant shark *or8* and *or1* gene have been reported as real ORs but others, *or3–7* as nonORs (Niimura and Nei 2006; Venkatesh et al. 2014). Four elephant shark *or* genes have a direct ortholog in catshark, that is, for these four gene pairs not a single gene birth or death event happened in the last 420 Myr (Heinicke et al. 2009) another gene is a singleton in elephant shark (Cm-OR7), but has undergone a single duplication in catshark, resulting in Sc-OR7, Sc-OR8 (fig. 3). Overall the evolutionary dynamics of the OR family appear to be extremely limited in cartilaginous fish, in stark contrast to the very dynamic evolution in bony vertebrates.

The TAAR family is large in teleost fish, of medium size in tetrapods, and was reported as just two genes in elephant shark, based on analysis of an initial assembly (Hussain et al. 2009). We found five *taar* genes for elephant shark (Cm-Taar1a-Cm-Taar4) and report a similar size of five genes for catshark (Sc-Taar1a-Sc-Taar4), see table 1. Figure 4 shows the phylogeny of representative TAARs from zebrafish, mouse, frog, catshark, and elephant shark. This phylogeny clusters TAAR into three monophyletic groups. The most basal group *tarl3* and *tarl4* genes is clearly clustered separately from others. However, two of these genes in catshark (*tarl3* and *tarl4*) and one in elephant shark (*tarl4*), do not exhibit the characteristic TAAR motif present in TM7 (Hussain et al. 2009). Since they are a sister group to the validated *taar* genes (*taar1a–1b*), which do possess the motif, we refer to them as *taar-like* genes (*tarl*). There is a clear ortholog relationship between cartilaginous *taar1* and teleost *taar1* genes. *taar 3–4* genes of sharks are more similar to vertebrate *taar 2–4*. This could point to the retention of ancestral characteristics by *taar2–4*.

The V1R/ORa gene family also shows opposing evolutionary characteristics in tetrapods versus teleosts. Here, the tetrapod families can be very large, but the teleost family is highly conserved, with 6–7 genes in many species (Zapilko and Korsching 2016). We identified six *ora* genes in catshark, and confirmed four ORAs for elephant shark (table 1). This conforms to the general tendency for catshark receptor repertoires to be somewhat larger than those of elephant shark.

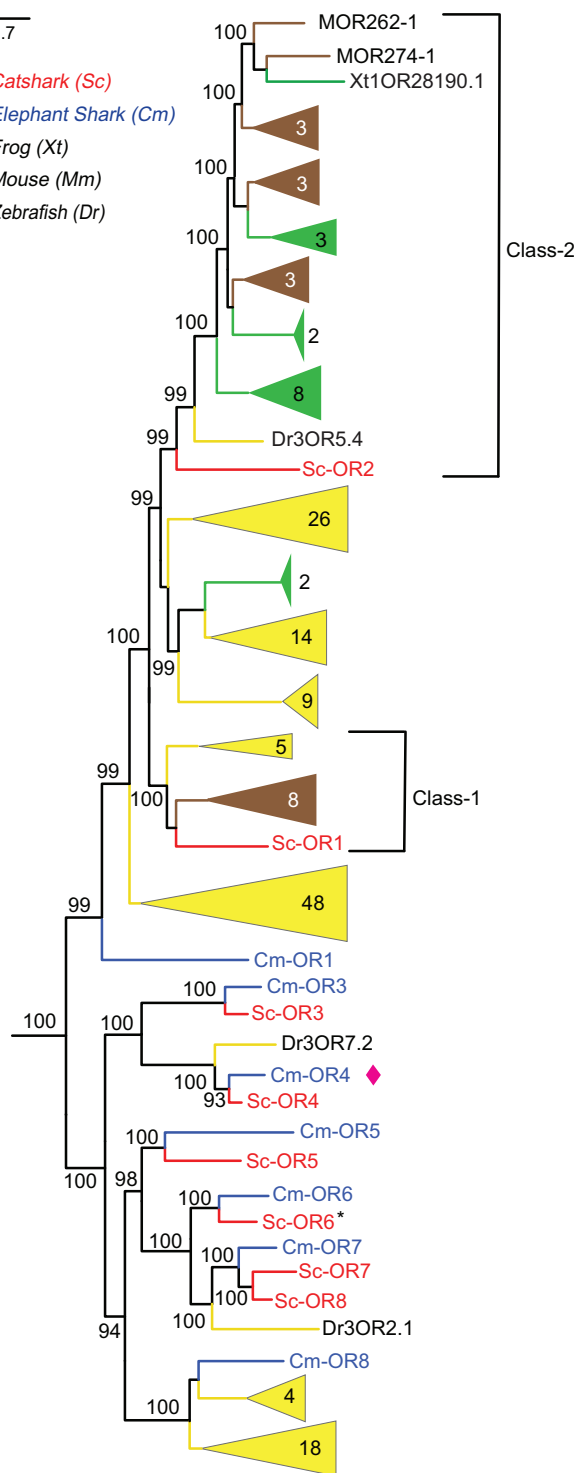


FIG. 3.—Sharks possess a small odorant receptor repertoire. Eight or genes of catshark (red), were compared with elephant shark (blue), frog (green), zebrafish (yellow), and mouse (brown). Phylogenetic tree was generated as described in figure 1 and branch support is given as percentage. Potential pseudogenes indicated by asterisk or genes are named by class to which they belong, eight genes are labelled one to eight. One new or gene found in elephant shark marked with purple spade.

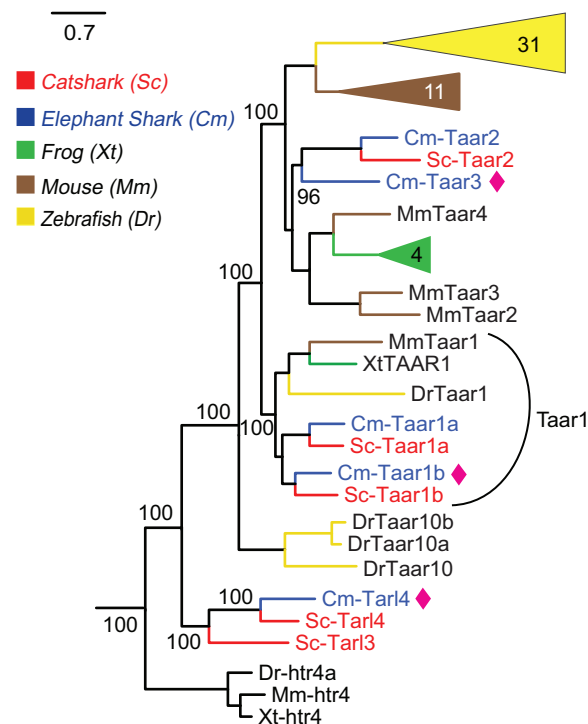


FIG. 4.—The TAAR repertoire of catshark and elephant shark consists of five genes each. Phylogenetic tree of five taar genes of both catshark (red) and elephant shark (blue), frog, zebrafish, and mouse (species and color code as given in fig. 2). The phylogenetic tree was generated as described in figure 1 and branch support is given as percentage. TAARs are named according to class and orthologs they are located with. Aminergic receptors are used as outgroup, only the closest outgroup (*htr4*) is shown.

Nevertheless, catshark has lost one of the genes present in elephant shark, ORA1, consistent with both gene birth and gene death events sculpting the ORA repertoire in catshark. Interestingly, this is the gene giving rise to all of tetrapod ORAs (fig. 5). The remaining three elephant shark genes possess direct orthologs in catshark, whose different terminal branch lengths suggest individually different evolutionary rates for these three genes (fig. 5). All of these genes are lost in tetrapods, with the exception of a single *Xenopus* gene, ORA15. Furthermore, we identified three additional *ora* genes in catshark that cluster with teleost *ora5* and *ora6*. The absence of such genes in lamprey (Grus and Zhang 2009) and elephant shark (Venkatesh et al. 2014), confirmed here, had raised doubts as to the evolutionary origin of ORA5-6 compared with ORA1-4, whose orthologs are present in elephant shark. Now it can be concluded that the ancestral gene of the ORA5/6 clade was already present in the MRCA of cartilaginous fish and bony fish.

Taken together, all three families (OR, TAAR, ORA) show only minor gene birth and death events in a shark and a chimera species, in stark contrast to the evolutionary dynamics of these families in bony vertebrates. Thus, in sharks these three

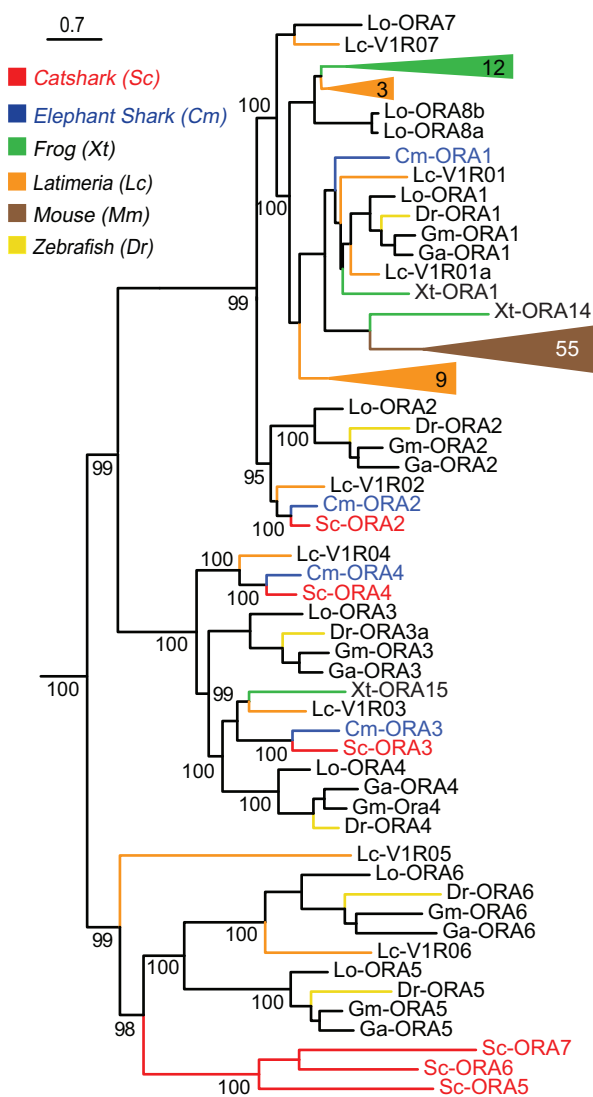


Fig. 5.—The catshark ORA repertoire shows an ancient origin of the ORA5/6 subclade. Six *ora* genes from catshark (red) and four from elephant shark (blue) were used along with the followings: frog, zebrafish, Latimeria, and mouse (species and color code as given in fig. 2). The phylogenetic tree was generated as described in figure 1 and branch support is given as percentage. Catshark ORAs were named according to the orthologs from two to seven. TAS2Rs were used as outgroup (not shown here).

receptor families seem to play a much reduced role in olfaction as compared with bony vertebrates. In contrast, the shark V2R family exhibits extensive gene birth events very similar to the evolutionary characteristics of V2Rs in bony vertebrates, consistent with the hypothesis that odor detection in both true sharks and chimeras depends heavily on the V2R family of ORs. Although no shark V2Rs have been deorphanized so far, they may well comprise amino acid receptors like their teleost counterparts (Specia et al. 1999; Oike et al. 2007). Thus, one may expect odor detection via V2Rs to help in food localization. The large evolutionary divergence of

420 Myr notwithstanding, both catshark and elephant shark are benthic predators of small invertebrates (Cox and Francis 1997; Valls et al. 2011), consistent with an important role of V2Rs in prey detection.

The olfactory organ of elephant shark has not been described so far, and together with the known specialization in electroreception of this species (Didier 1995; Lisney 2010) this raised doubts how representative the OR repertoire of this species might be. Catshark, on the other hand, exhibit a complex olfactory organ (Theisen et al. 1986) and do not appear as specialized for electroreception as elephant shark. The overall similarity of the chemosensory repertoires of catshark and elephant shark we describe here suggests now that the elephant shark repertoire is no outlier. The slightly larger chemosensory receptor repertoire of catshark is consistent with a somewhat larger dependence on olfaction for catshark.

Materials and Methods

In order to delineate the olfactory and gustatory genes, scaffolds (sf., see supplementary data set S1, Supplementary Material online) from the draft of the catshark genome (to be published elsewhere) and recent elephant shark genome (Venkatesh et al. 2014) were obtained by genome-wide searches using TblastN with the representative TAS1R, TAS2R, OR, TAAR, ORA, and V2R sequences from mouse, frog, elephant shark, *Latimeria* and zebrafish as queries, and recursively in follow-up searches. For TAS1R phylogeny we additionally searched for spotted gar sequences. Homology regions above 200 amino acid length were considered further. Splicing predictions were made by comparing related protein sequences to genomic DNA sequences with the online-tool GeneWise (Birney et al. 2004). Sequence data used in this article are included in supplementary file (data set S2), Supplementary Material online. Sequences were aligned with MAFFT 7 (Katoh and Standley 2013) an online version of the multiple alignment tool MAFFT (Katoh et al. 2002) using the E-INS-I strategy with the default parameters. Clustal Omega (Sievers et al. 2011) was also used for alignment. The multiple sequence alignment was edited using Gap Strip Squeeze to remove regions with gaps in over 90% of sequences (<https://www.hiv.lanl.gov/content/sequence/GAPSTREEZE/gap.html>, last accessed January 22, 2019).

The phylogenetic trees were calculated using a Maximum likelihood algorithm, PhyML-aLRT with SPR setting for tree optimization and chi square-based aLRT (Guindon et al. 2010) for branch support on Phylemon server available online (Sanchez et al. 2011). Branch support above 80% was considered significant. TAS1R, CasR, nonOR rhodopsin-like GPCR genes, htr, and T2Rs of zebrafish, mouse, xenopus, human and *latimeria* served as outgroups for V2RL, V2R, OR, TAAR, and ORA, respectively. Treefiles for figure 1a, figure 2 (Treefile 1); figure 1b (Treefile 2); figure 3 (Treefile 3); figure 4 (Treefile 4); figure 5 (Treefile 5) are given in supplementary file (data

Downloaded from https://academic.oup.com/gbe/article-abstract/11/2/398/5288589 by Universitat Koeln/Instut für Genetik user on 23 October 2019

set S3), **Supplementary Material** online. Trees were drawn using FigTree (<http://tree.bio.ed.ac.uk/software/figtree/>, last accessed January 22, 2019). Newly predicted genes were named according to previously named orthologs or closest paralogs from other species, starting with more basal genes. Gene with one or more stop codons was labelled as pseudogene. One or gene may either represent pseudogenes or databank inaccuracies due to the preliminary assembly (fig. 2, **supplementary data** set 1, **Supplementary Material** online). Fifteen genes are full or nearly full length (above 700 aa), three are partial (between 550 and 700 aa), fifteen and nine sequences were restricted to one of the large exons (exon 3 and exon 6, respectively). In those cases, where exon 3 and exon 6 might be derived from the same gene, we distinguished with a letter, for example, Sc-V2R2a and Sc-V2R2b.

Supplementary Material

Supplementary data are available at *Genome Biology and Evolution* online.

Acknowledgments

We thank the Genoscope-Centre National de Séquençage (Evry, France) for sequencing the catshark draft genome used in this work, H el ene Mayeur (UMR 7232, Observatoire Océanologique, Banyuls sur Mer, France) and Jean-Marc Aury (Genoscope) for assembling these data. This work was supported by the German Science foundation (grant KO 1046/7-1 to S.I.K.).

Author Contributions

The experiments were conceived by S.F., S.M., and S.I.K., designed and performed by K.S. and A.S.S. Illustrations were drafted by K.S. and S.I.K. Data analysis was done by K.S., A.S.S., and K.S., S.F. and S.I.K. wrote the paper.

Literature Cited

- Ahuja G, et al. 2018. Overlapping but distinct topology for zebrafish V2R-like olfactory receptors reminiscent of odorant receptor spatial expression zones. *BMC Genomics* 19:383.
- Alioto TS, Ngai J. 2006. The repertoire of olfactory C family G protein-coupled receptors in zebrafish: candidate chemosensory receptors for amino acids. *BMC Genomics* 7:309.
- Bachmanov AA, Beauchamp GK. 2007. Taste receptor genes. *Annu Rev Nutr.* 27:389–414.
- Birney E, Clamp M, Durbin R. 2004. GeneWise and genomewise. *Genome Res.* 14(5):988–995.
- Cox GJ, Francis M. 1997. *Sharks and rays of New Zealand*. New Zealand: Canterbury University Press.
- DeMaria S, et al. 2013. Role of a ubiquitously expressed receptor in the vertebrate olfactory system. *J Neurosci.* 33(38):15235–15247.
- Didier DA. 1995. *Phylogenetic systematics of extant chimaeroid fishes (Holocephali, Chimaeroidei)*. New York, NY: American Museum Novitates; no. 3119.
- Grus WE, Zhang J. 2009. Origin of the genetic components of the vomeronasal system in the common ancestor of all extant vertebrates. *Mol Biol Evol.* 26(2):407–419.
- Guindon S, et al. 2010. New algorithms and methods to estimate maximum-likelihood phylogenies: assessing the performance of PhyML 3.0. *Syst Biol.* 59(3):307–321.
- Hashiguchi Y, Nishida M. 2006. Evolution and origin of vomeronasal-type odorant receptor gene repertoire in fishes. *BMC Evol Biol.* 6:76.
- Heinicke M, Naylor G, Hedges S. 2009. Cartilaginous fishes (Chondrichthyes). *Timetree Life.* 9:320–327.
- Hussain A, Saraiva LR, Korsching SI. 2009. Positive Darwinian selection and the birth of an olfactory receptor clade in teleosts. *Proc Natl Acad Sci U S A.* 106(11):4313–4318.
- Ishimaru Y, et al. 2005. Two families of candidate taste receptors in fishes. *Mech Dev.* 122(12):1310–1321.
- Katoh K, Misawa K, Kuma K, Miyata T. 2002. MAFFT: a novel method for rapid multiple sequence alignment based on fast Fourier transform. *Nucleic Acids Res.* 30(14):3059–3066.
- Katoh K, Standley DM. 2013. MAFFT multiple sequence alignment software version 7: improvements in performance and usability. *Mol Biol Evol.* 30(4):772–780.
- Libants S, et al. 2009. The sea lamprey *Petromyzon marinus* genome reveals the early origin of several chemosensory receptor families in the vertebrate lineage. *BMC Evol Biol.* 9:180.
- Lisney TJ. (Lisney2010 co-authors). 2010. A review of the sensory biology of chimaeroid fishes (Chondrichthyes; Holocephali). *Rev Fish Biol Fish.* 20(4):571–590.
- Martini S, Silvotti L, Shirazi A, Ryba NJ, Tirindelli R. 2001. Co-expression of putative pheromone receptors in the sensory neurons of the vomeronasal organ. *J Neurosci.* 21(3):843–848.
- Niimura Y. 2009a. Evolutionary dynamics of olfactory receptor genes in chordates: interaction between environments and genomic contents. *Hum Genomics.* 4(2):107–118.
- Niimura Y. 2009b. On the origin and evolution of vertebrate olfactory receptor genes: comparative genome analysis among 23 chordate species. *Genome Biol Evol.* 1:34–44.
- Niimura Y, Nei M. 2006. Evolutionary dynamics of olfactory and other chemosensory receptor genes in vertebrates. *J Hum Genet.* 51(6):505–517.
- Oike H, et al. 2007. Characterization of ligands for fish taste receptors. *J Neurosci.* 27(21):5584–5592.
- Picone B, et al. 2014. Taste and odorant receptors of the coelacanth – a gene repertoire in transition. *J Exp Zool B Mol Dev Evol.* 322(6):403–414.
- Sainz E, Korley JN, Battey JF, Sullivan SL. 2001. Identification of a novel member of the T1R family of putative taste receptors. *J Neurochem.* 77(3):896–903.
- Sanchez R, et al. 2011. Phylemon 2.0: a suite of web-tools for molecular evolution, phylogenetics, phylogenomics and hypotheses testing. *Nucleic Acids Res.* 39(Web Server issue):W470–W474.
- Saraiva LR, Korsching SI. 2007. A novel olfactory receptor gene family in teleost fish. *Genome Res.* 17(10):1448–1457.
- Sievers F, et al. 2011. Fast, scalable generation of high-quality protein multiple sequence alignments using Clustal Omega. *Mol Syst Biol.* 7:539.
- Specia DJ, et al. 1999. Functional identification of a goldfish odorant receptor. *Neuron* 23(3):487–498.
- Theisen B, Zeiske E, Breucker H. 1986. Functional morphology of the olfactory organs in the spiny dogfish (*Squalus acanthias* L.) and the small-spotted catshark (*Scyliorhinus canicula* (L.)). *Acta Zool.* 67(2):73–86.

- Valls M, Quetglas A, Ordines F, Moranta J. 2011. Feeding ecology of demersal elasmobranchs from the shelf and slope off the Balearic Sea (Western Mediterranean). *Sci Mar*. 75:7.
- Venkatesh B, et al. 2014. Elephant shark genome provides unique insights into gnathostome evolution. *Nature* 505(7482):174–179.
- Voigt A, et al. 2012. Genetic labeling of Tas1r1 and Tas2r131 taste receptor cells in mice. *Chem Senses*. 37(9):897–911.
- Wyffels J, et al. 2014. SkateBase, an elasmobranch genome project and collection of molecular resources for chondrichthyan fishes. *F1000Res*. 3:191.
- Young JM, Trask BJ. 2007. V2R gene families degenerated in primates, dog and cow, but expanded in opossum. *Trends Genet*. 23(5):212–215.
- Zapilko V, Korsching SI. 2016. Tetrapod V1R-like ora genes in an early-diverging ray-finned fish species: the canonical six ora gene repertoire of teleost fish resulted from gene loss in a larger ancestral repertoire. *BMC Genomics* 17:83.
- Zhao GQ, et al. 2003. The receptors for mammalian sweet and umami taste. *Cell* 115(3):255–266.

Associate editor: Martin Embley

4.4. Manuscript in preparation

Kanika Sharma, Gaurav Ahuja, and Sigrun I. Korsching “**Spatial topology of zebrafish TAAR expressing neurons is broadly overlapping but distinct.**”
(manuscript in preparation)

Spatial topology of zebrafish TAAR expressing neurons is broadly overlapping but distinct

Kanika Sharma¹, Gaurav Ahuja^{1,2}, and Sigrun I. Korsching¹

Corresponding author: S.I. Korsching

¹ Institute of Genetics, Biocenter, University at Cologne, Zùlpicherstrasse 47a, 50674 Cologne, Germany

² Present address: Center for Molecular Medicine Cologne (ZMMK), Robert-Koch-Str. 21, 50931 Cologne, Germany

4.4.1 Abstract

Zonal expression of olfactory receptors is a common phenomenon across species as seen by restricted spatial pattern of olfactory receptor (OR) gene expression in peripheral sense organs. In zebrafish, the OR expression pattern occurs as fuzzy concentric zones with preferred diameters for different ORs. A recent study showed non-random distributions for V2R-related *OlfC* genes which are intercalated into expression zones of ORs. However nothing is known for the largest olfactory family in teleost, TAAR genes. Here we wished to investigate, whether the principle of spatial segregation observed for OR and *OlfC* receptors also extends to TAAR genes.

4.4.2 Background

The first step in the neuronal encoding of olfactory input is the mapping of an olfactory stimuli onto the sensory surface of the olfactory epithelium. The analysis of the spatial distribution allows to infer features of information processing in the olfactory epithelium. Restricted zonal expression of *ors* gene expression in peripheral sense organs of mammals is a common phenomenon across species. (Vassar, Ngai et al. 1993). In zebrafish the expression patterns of *or* is reminiscent of zones occurring as concentric domains with preferred diameters for various ORs (Weth, Nadler et al. 1996). A recent publication from Korsching lab showed that in zebrafish, V2R-related *OlfC* genes also follow the same logic of expression as *ors* with intermingled expression zones. There is a non-random distribution of the labeled neurons for all *OlfC* genes with a broad overlap in spite of distinct zones. Presence of distinctly different expression zones for individual receptor genes constitutes a general feature amongst teleost and tetrapod V2R/*OlfC* and *or* gene families.

The *taar* family is the largest gene family in zebrafish; over 100 genes (Hussain, Saraiva et al. 2009) which is about 5 times the number of genes in the largest mammalian family, and double that in stickleback (Hashiguchi and Nishida 2007). In this study, we analysed 5 representative genes from all the three classes of zebrafish TAARs expressing cells. We examine whether the principle of spatial segregation observed for *ors* and V2R-related *OlfC* genes also extends to the *taar* family.

4.4.3 Results and discussion

In order to analyse the spatial distribution of *taar*-expressing neurons, we selected five representative genes from all the three phylogenetic classes of *taars* (Hussain, Saraiva et al. 2009) and performed in situ hybridization on the complete series of horizontal cryostat sections from adult zebrafish OE. Probes were generated with cross-reactivity amongst the family members (see Material & Methods). We analyzed the spatial pattern of *taar*-expressing cells in two dimensions (height within the epithelial layer and horizontal distance from the center of the olfactory organ). We report a broad but non-random distribution of *taar* expressing cells (Figure 3). Frequency of expression of TAAR19I was observed to be most wide (Figure 3 i,j). For other genes, frequency of the labelled cells ranged between 200 to 420 per OE which is due to cross-reactivity.

Thus, the *taar* expression zones seem to be intercalated with those of the *OlfC* and odorant receptor zones.

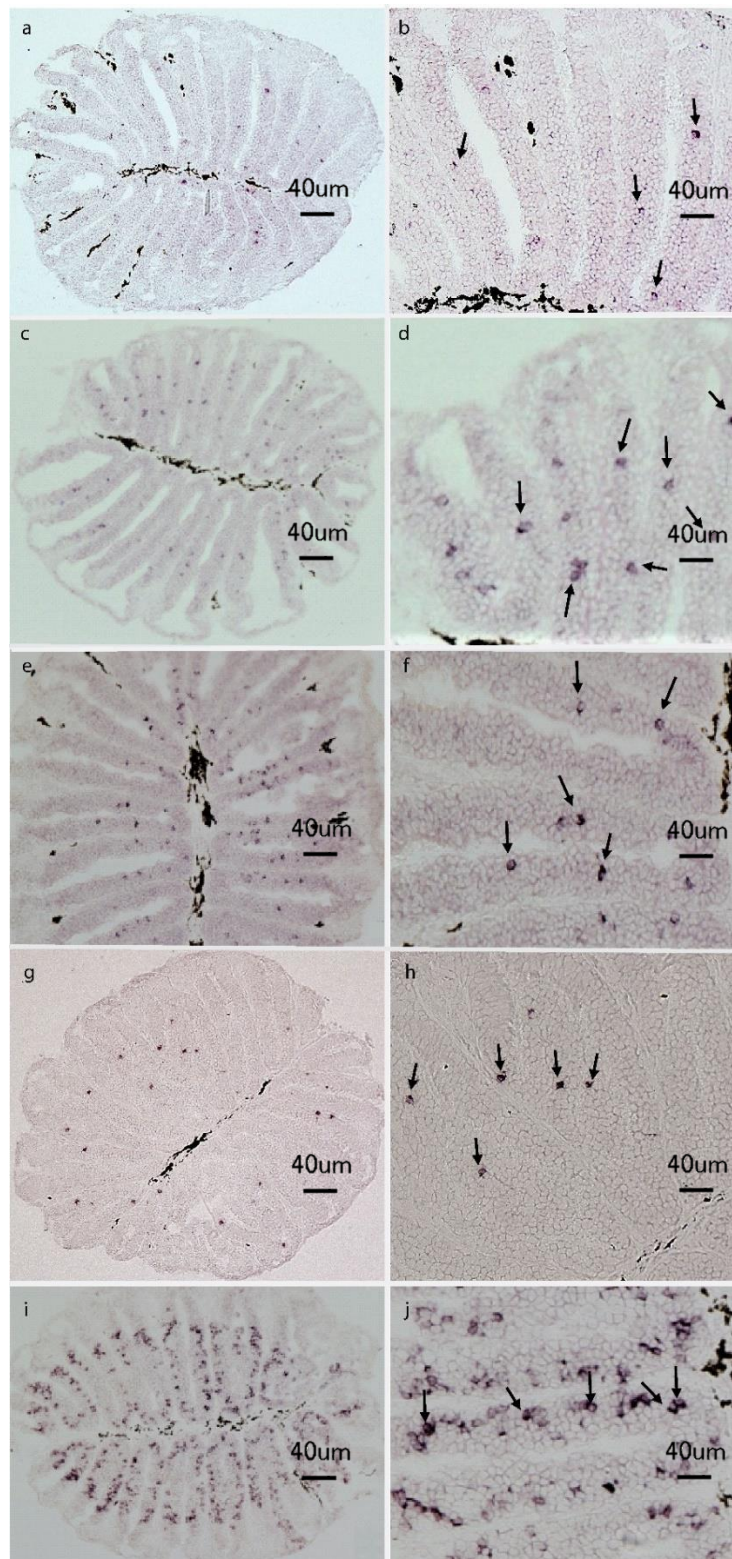


Figure 3. *taar* genes are expressed in small subsets of scattered olfactory sensory neurons.

Horizontal tissue sections of fresh-frozen OE labelled with digoxigenin antisense specific RNA probes of (a) (b) TAAR10; (c) (d) TAAR12f; (e) (f) TAAR13c; (g) (h) TAAR15a; (i) (j) TAAR19l. Left: 10x magnification. Right: 20x magnification. Arrows show the position of labelled TAAR

receptor cells. The median raphe contains melanophores that are visible as elongated dark stains. (Scale bar = 40 μ M). For orientation compare Fig 2.

4.4.3.1 Relative Radius

We quantified the radius coordinate as relative radius ($r_{rel} = r_{soma\ center}/length\ of\ the\ lamella$; 0, innermost; 1, outermost). The horizontal distance of the labelled cell from the center of the lamella has been shown to be characteristically different for several *or* and *olfc* genes (Weth, Nadler et al. 1996, Ahuja, Reichel et al. 2018). TAAR13c-expressing cells are found closest to the centre of epithelium in comparison to all other *taar* genes (Figure 4). Indeed, the KS test (Table 1) shows the TAAR13c distribution to be significantly different from those for other TAARs (Figure 4). In contrast, TAAR10 - expressing cells occupy the farthest expression zone from the centre epithelium. The distributions for TAAR10 and TAAR19I-labeled receptor cells are very similar to each other, also the distribution for TAAR15a shows high similarity to that of TAAR10 (Figure 4b). As expected, the KS test shows no significant difference within each of these pairs (Table1).

	13c	19I	10	15a	12f
13c					
19I	<0.001				
10	<0.001	0.062			
15a	<0.001	<0.001	0.107		
12f	<0.001	<0.001	<0.001	<0.001	

Table1. KS test result for relative radius values of all different analysed epithelium in case of TAARs10, 12f, 13c, 15a, and 19I. P-values < 0.01 are considered significant

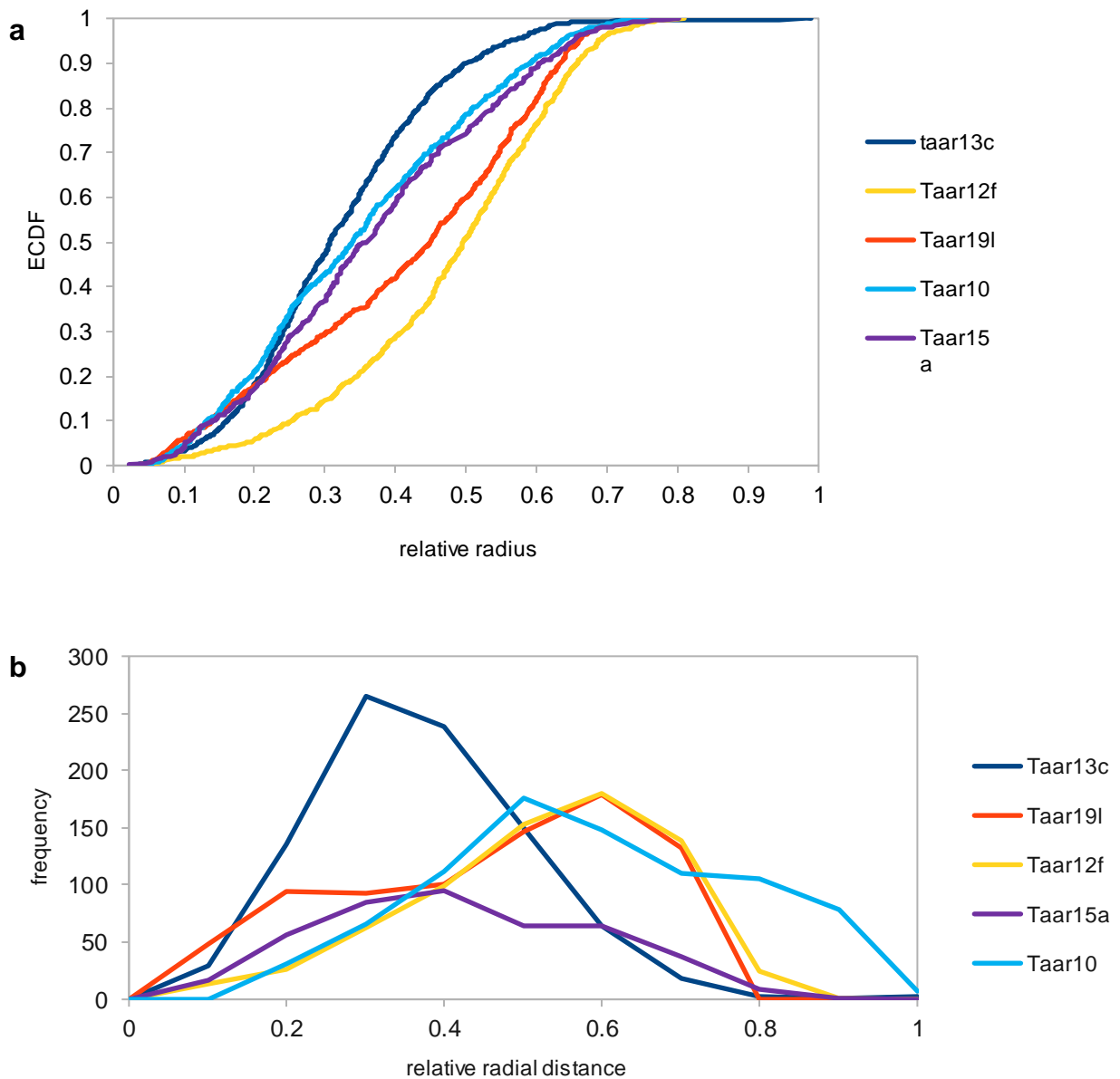


Figure 4. Quantitative assessment of the radial distribution of five TAAR receptor neurons in the OE of zebrafish.

The distribution of radial positions of taar-expressing cells was quantified using the same set of sections, for which laminar height was determined, except the very first sections, where the sensory surface does not yet extend toward the median raphe. The radial position within the section was normalized to maximal radius, i.e. length of the lamella containing each labeled cell a. The resulting distributions of relative radius (from 0, innermost to 1, outermost) are shown unbinning empirical cumulative distribution function (ECDF) b. shown binned (histogram)

4.4.3.2 Relative Height

Relative height of labelled TAAR receptor cells was also measured as a parameter of the spatial expression pattern of these receptor genes. We quantified the laminar height (height of the neuronal soma within the epithelial layer) as relative height ($h_{rel} = h_{soma\ center} / \text{thickness of sensory layer}$; 0, basal; 1, apical) for all of the five genes. We observed that there is a broad but distinct expression zones for *taars*. TAAR15a-labeled cells are expressed closest to the base. In contrast to TAAR15a, TAAR13c labelled cells are expressed more apically than the other TAAR cells (Figure 5b). P-values < 0.01 are considered significant (Table 2). Height distribution of TAAR15a is highly similar to TAAR12f (Table 2).

	13c	19l	10	15a	12f
13c					
19l	<0.001				
10	<0.001	<0.001			
15a	<0.001	<0.001	<0.001		
12f	<0.001	<0.001	<0.001	0.037	

Table2. KS test result for relative height values of all different analysed epithelium in case of TAARs10, 12f, 13c, 15a, and 19l. P-values < 0.01 are considered significant.

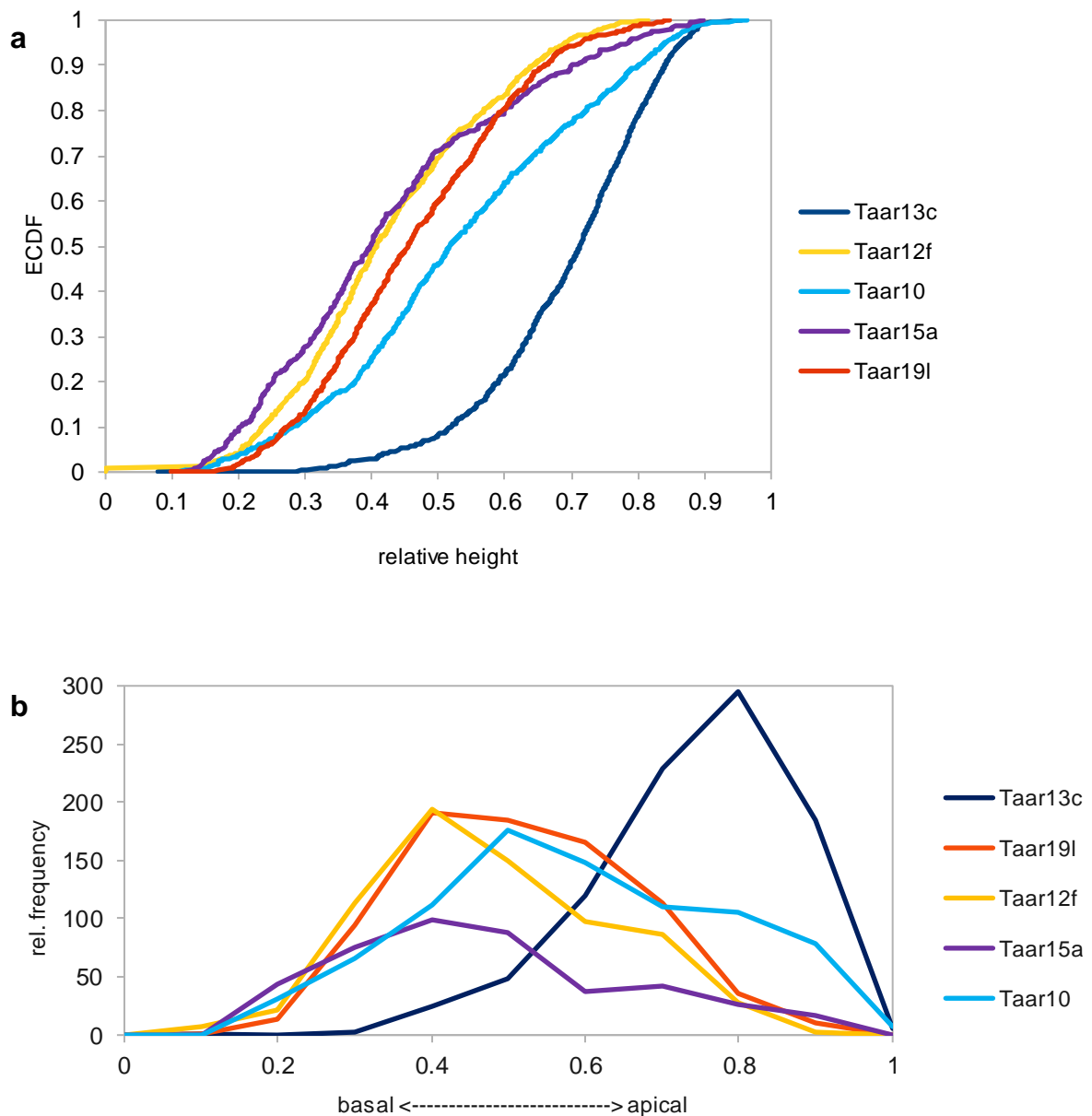


Figure 5. Quantitative assessment of laminar height distributions for five TAAR receptor neurons expressing five taar receptor cells in OE of zebrafish

Complete series of sections from three to five olfactory epithelia were evaluated for each of the five taar genes. Height within the lamina was normalized to maximal laminal thickness. The resulting distributions of relative laminar height (from 0, most basal to 1, most apical, i.e. bordering to the lumen) are shown a. unbinned empirical cumulative distribution function (ECDF) b. binned histogram. The color code for the taar genes is the same as in Fig. 4 to facilitate comparisons between different positional parameters.

4.4.4 Materials and Methods

Animal handling and probe generation

Zebrafish used (Ab/Tü genetic background) were raised in the local fish facility. Adult wild type zebrafish (8–11 months old) were anesthetized and decapitated. Olfactory epithelia were dissected out, embedded in TissueTek O.C.T. compound (Tissue-Tek; Sakura Finetek USA), and frozen at -20°C . Ten micrometer-thick horizontal cryosections were thaw-mounted onto Superfrost Plus slide glasses (Fisher Scientific, Pittsburgh, PA).

Digoxigenin (DIG)-labeled probes for seven V2R-related *OlfC* genes were generated as described (Saraiva and Korsching 2007). Templates for probes were amplified from genomic DNA, with T3 promoter site (TATTAACCCTCACTAAAGGGAA) attached to the 5' end of the primers. In situ probes were generated for the following genes: *taar10*, *taar12f*, *taar13c*, *taar15b*, and *taar19l* using the following primer pairs: *taar10* Fwd: 5' ATGGACCTAAGCAATTCA 3'; Rev.: 5' TACCATCGCAAATCCAACAA 3'; *taar12f* Fwd: 5' ATGAAGCCTTCAAATGAGAC 3'; Rev.: 5' GTCACAAATGGCCCAGTACC 3'; *taar13c* Fwd: 5' ATGGATTTATCATCACAAG 3; Rev: 5' AACTGACCACAAGGCATTGAA 3'; *taar15a* Fwd: 5' ATGGAATTTCAAGAGC 3'; Rev: 5' TGGTGCAATAAATGTA ACTATTAAGTC 3'; *taar19l* Fwd: 5' ATGAAAGGACAGAAAGGAGAAC 3'; Rev: 5' ACACACGTCTGTTCTGTTTGAAGGTG 3'.

In situ hybridization

Ten micrometer-thick horizontal cryosections were thaw-mounted onto Superfrost Plus slide glasses (Thermo). Pre-treatment of sections, probe hybridization, and stringent washing were performed as described (Weth, Nadler et al. 1996), except omitting Proteinase K digestion. After stringent washing at 65°C , sections were blocked in 1% blocking reagent (Roche) in PBS for 1 h. The slides were then incubated at 37°C for 2 h with sheep anti-DIG Fab fragments conjugated with alkaline phosphatase (Roche), dilution 1:500 in blocking solution. After washing 3 times in PBS, hybridized probes were visualized by enzymatic reaction with NBT-BCIP (Roche). After evaluating the success of the staining, slides were washed 2 times in PBS for 5 mins each, mounted with VectaMount (Vector Laboratories, Burlingame, CA, USA) and photographed with a wide field microscope (Keyence BZ-9000).

Measurement and analysis of spatial coordinates

The distribution of receptor neurons labelled with a DIG-labelled probe was assessed in complete series of sections of olfactory epithelium. The olfactory organ of adult zebrafish consists of an oval shaped rosette that comprises several lamellae surrounding a non-sensory midline raphe. The position of each labelled cell was quantified for radial distance from the centre of the lamella and laminar height within the lamella. All parameters are normalized to allow comparison between different epithelia. Relative radial position within the lamella is calculated as R/R_0 , where R represents the distance between starting point of R_0 (centre of epithelium) and centre

of labelled cell with R_0 is the length of the lamella containing the labelled cell. Relative laminar height within the lamella is calculated as H/H_0 . H_0 is the height of the lamella at the position of the labelled cell, while H represents the shortest distance between basal border of the lamella and the centre of the labelled cell. Spatial coordinates were measured in arbitrary units and normalized as described (Ahuja, Bozorg Nia et al. 2014). For example, apical-to-basal position within a lamella (laminar height) was measured as the shortest distance between centre of the cell and basal border of the epithelial layer, and normalized to the thickness of the epithelial layer at the position of the cell. Thus the range of values is between 0 (most basal) and 1 (most apical). Unbinned distributions were represented as the corresponding empirical cumulative distribution function (ECDF) (Wilk and Gnanadesikan 1968). In this presentation, data points are sorted by their parameter value (x axis), with their ordinal number (normalized) as y axis. Each data point results in a curve point, thus no information about the distribution is lost in the representation as ECDF, in contrast to the usual histogram representation. To estimate, whether two spatial distributions were significantly different, we have performed Kolmogorov-Smirnov tests on the unbinned distributions using http://www.physics.csbsju.edu/stats/KS-test.n.plot_form.html. The Kolmogorov-Smirnov test makes no assumptions about the nature of the distributions investigated, which is essential since the skewness of many distributions showed that these are not Gaussian. Due to the sensitive nature of the test on large distributions ($n > 100$) we selected $p < 0.01$ as cut-off criterion for significant difference, cf (Syed, Sansone et al. 2013).

5. Discussion

Evolution of olfactory receptors: from phylogeny to function

The olfactory system is essential for the most basic matters of concern, such as food sources, social interaction, oviposition sites or predator avoidance. How does this system work amongst varied number of living species? The ability of the olfactory system to detect a diverse array of odors is mediated by the distinct receptors encoded by several gene families. The size and the diversity of the olfactory receptor families is considered as basis for the discriminative ability of the olfactory system. The relevance of different olfactory receptor families changes during the evolution of species. In species representing various levels of vertebrate evolution, varying number of olfactory receptor genes have been identified, for example, the largest number of functional ORs in vertebrates with ~2000 ORs is found in African elephants (Niimura, Matsui et al. 2014) and a relatively smaller number in zebrafish (150 genes) (Alioto and Ngai 2005). In contrast the largest TAAR gene repertoire in zebrafish has 112 genes (Hussain, Saraiva et al. 2009), whereas the smallest repertoire, in chicken, has only 3 intact genes (Hashiguchi and Nishida 2007).

In order to thoroughly understand the sense of smell requires a multipronged approach from the evolutionary identification of olfactory receptor repertoires, their localization in neurons, and the interaction of the ligands with these receptors. In my thesis I have worked at all three levels.

Among the three lineages of vertebrates (cyclostomes, cartilaginous fishes and bony vertebrates), bony vertebrates are the largest and most diverse group of vertebrates and since cartilaginous fishes are the sister group of bony vertebrates, they constitute a critical outgroup for understanding the evolution and diversity of bony vertebrates. Vertebrates exhibit four major families of olfactory receptors (OR, TAAR, V1R, V2R) and two gustatory GPCR families, T1R and T2R (Bachmanov and Beauchamp 2007). Here we have mined the genome of a true shark, catshark for olfactory and gustatory receptors, we have completed the elephant shark chemoreceptor repertoire and have performed a thorough phylogenetic study to shed light on the evolution of chemosensory receptors in cartilaginous fish. We report the presence of several gustatory receptors of the T1R family in catshark and elephant shark, while T2R receptors are absent. It is possible that the origin of the T1R family could have happened within the jawed lineage, since T1Rs were not found in lamprey (Grus & Zhang, 2009).

The catshark olfactory repertoire is dominated by V2R receptors with 40 genes, slightly larger than elephant shark with 37 genes, which is roughly comparable to mammalian and fish repertoire sizes (Ahuja et al., 2018; Young & Trask, 2007). Olfactory receptor (OR) genes, which are the largest gene family in bony vertebrates (Niimura & Nei, 2006), have undergone very limited gene expansion in cartilaginous fish. Surprisingly, in catshark there are only eight ORs identified and seven in elephant shark. TAAR family is large in teleost fish, of medium size in tetrapods, and was reported as just 5

genes in elephant shark and a similar size of 5 genes for catshark. V1R.ORA gene family in cartilaginous fish is four to six genes, which is similar to teleosts.

Taken together, all three families (OR, TAAR, V1R) show only minor gene birth and death events in a shark and a chimera species, in stark contrast to the evolutionary dynamics of these families in bony vertebrates. Thus, in sharks these three receptor families seem to play a much reduced role in olfaction as compared to bony vertebrates. In contrast, the shark V2R family exhibits extensive gene birth events very similar to the evolutionary characteristics of V2Rs in bony vertebrates; consistent with the hypothesis that odor detection in sharks depends heavily on the V2R family of olfactory receptors. This suggests that gene birth events are not generally rare in cartilaginous fish chemosensory receptor families compared to the bony fish lineage.

Common organisation principles serving crucial aspects of olfactory function is suggested by the similarity of functional architecture of the olfactory system across phyla from insects to mammals. Usually, from a large and diverse repertoire the OSNs express only one or a specific combination of a few chemoreceptors (Li, Ishii et al. 2004, Goldman, Van der Goes van Naters et al. 2005, Monahan and Lomvardas 2015) and the axons of these OSNs expressing the same olfactory OR converge onto the same glomerulus in the vertebrate OB or insect antennal lobe.

An equally interesting concept is the spatial organization of olfactory gene expression patterns in olfactory organs. OSNs expressing the same receptor are not evenly scattered across the surface of the OE but are restricted to distinct zones. Pattern of expression of the OR has been described for *Drosophila* (Fishilevich and Vosshall 2005), frog (Freitag, Krieger et al. 1995), salamander (Marchand, Yang et al. 2004), rodents (Ressler, Sullivan et al. 1993, Vassar, Ngai et al. 1993), and zebrafish (Weth, Nadler et al. 1996). Physiological and developmental roles have been proposed for the significance of OR spatial pattern but the function remains elusive. ORs are located in the OE according to their ligand profiles and the likelihood of the interaction of a ligand with a receptor based on local airflow and physicochemical properties of the ligand (Schoenfeld and Cleland 2006). It is also suggested that the pattern of expression of ORs might be crucial for glomeruli formation in the OB and a zone-to-zone correlation between the positions of glomeruli and the OE (Vassalli, Rothman et al. 2002) (Miyamichi, Serizawa et al. 2005). Spatial segregation of expression of olfactory receptor genes expression within a family seems to be a conserved feature in the tetrapod lineage (Ressler, Sullivan et al. 1993, Vassar, Ngai et al. 1993, Miyamichi, Serizawa et al. 2005). Recently, our lab published the expression zones for the V2R-related *OlfC* genes in zebrafish OE and found a non-random distribution of labeled neurons for all the *OlfC* genes analysed (Ahuja, Reichel et al. 2018).

Since fish possess only one olfactory organ, in which all their olfactory receptor families are expressed, it was interesting to find out, how the expression of TAAR olfactory receptor family, is integrated into the spatial pattern of OR-expressing and *OlfC*-expressing neurons. We have examined five different *taar* genes, chosen as representative by their position in the phylogenetic tree (Hussain, Saraiva et al. 2009). We have performed a thorough quantitative analysis in two dimensions, radial

distance (central to peripheral), and the laminar height (basal to apical), to establish the spatial pattern of *taar* gene expression.

We show that there are distinctly different, if broadly overlapping expression zones that can be distinguished for zebrafish TAARs. The spread of radial distributions for zebrafish *taar* genes appears to be wide where the radial patterns for *TAAR10* and *TAAR19l* are significantly different and the radial pattern for *TAAR15a* could be distinguished from *TAAR19l*. Also, the distribution of *TAAR10* and *TAAR15a* is significantly different from each other. We also observed that *TAAR13c* is present apical to all other TAARs and *TAAR15a* is most basal. Hence, there are different expression zones for *taar* genes.

The interaction of odors with their respective receptors presents one of the most complex ligand/receptor binding problems in biology due to the sheer quantity of potential odor molecules facing a limited albeit huge number of different olfactory receptors. Ligands have been reported for many olfactory receptors but only in very few cases we know the molecular understanding of the binding interaction between an odorant and its receptor. Due to many challenges in attempts to crystallize olfactory receptors so far none have been produced, and thus prediction of olfactory receptor structures has relied on *in-silico* studies. The trace amine associated receptor (TAAR) family is the only olfactory receptor family, which is much larger in teleost fish in comparison to tetrapods (Hashiguchi and Nishida 2007, Hussain, Saraiva et al. 2009, Tessarolo, Tabesh et al. 2014). This suggests a possible essential role for TAARs in fish. Recently, the Korsching lab deorphanized an olfactory receptor, *TAAR13c*, as a specific receptor for the death-associated odor cadaverine (Hussain, Saraiva et al. 2013). This receptor is a member of the TAAR family of olfactory receptors, and is activated by the death-associated odor cadaverine in the micromolar range, and, much less efficiently, by the closely related diamine putrescine.

In this study, we used modeling and docking to predict binding interactions of this receptor linked to robust innate avoidance behaviour (Hussain, Saraiva et al. 2013). Due to unavailability of a crystal structure, *TAAR13c* structure was built using homology and *ab initio* modelling techniques using established templates such as the beta-adrenergic receptor (β -AR) and rhodopsin which was then energy-minimized for a more stable structure. We modelled the cadaverine/*TAAR13c* interaction to uncover residues participating in ligand binding and receptor activation. To support our modelling study we exchanged the predicted binding residues by site-directed mutagenesis, and measured the activity of the mutant receptors.

Furthermore, we employed MOLE2.0 (Sehna, Svobodová Vařeková et al. 2013), a more advanced and robust approach to predict the cavities and potential tunnels allowing the ligand to enter the receptor, contact the gating site, and traverse towards its final binding site were identified. Two tunnels were predicted in the upper third of *TAAR13c*, one lined by positive charge and another lined by previously identified ligand gating residue, Asp279^{6,58} at its entrance which possible acts as an attractant for cadaverine. In beta adrenergic receptors, which share close structural similarity to olfactory receptors two tunnels are present which provide ligand access

to the internal binding site (Gonzalez, Perez-Acle et al. 2011). However only one of these tunnels seems to support ligand entry (Wang and Duan 2009) similar to our findings.

Next, we used a multistep docking approach called TomoDock to elucidate the path taken by cadaverine to reach the binding site. The stepwise docking algorithm employed here provides a plausible path for cadaverine to traverse the receptor from the gating site to the internal binding-and-activation site. The path suggested that during this movement cadaverine adopts various orientations in the extracellular niche before it proceeds towards the internal binding site in both wildtype and mutant receptors with a small pause in the external niche to form a single salt bridge with amino group of cadaverine and Asp279^{6.58}. Furthermore, the close similarity to earlier predicting confirms the shape and location of both external gating and internal binding-and-activation site. Very similar results have been seen for beta adrenergic receptors that share structural similarity with TAARs where external ligand-binding sites cause a delay of the adrenergic ligand traversing towards and finally reaching the internal binding site (Dror, Pan et al. 2011, Gonzalez, Perez-Acle et al. 2011)(Dror PNAS 2011). We identified Asp112^{3.32} and Asp202^{5.42}, as essential sites of a binding site for cadaverine and putrescine in the upper third of the TM region (internal binding site). The results suggested docking of one amino group of cadaverine (protonated at physiological pH) via a salt bridge with Asp112^{3.32} at a distance of 2.7 Å and the second protonated amino group of cadaverine was docked 3.2 Å away from Asp202^{5.42} to form another salt bridge. We then reaffirmed these predictions by generating mutants of the two aspartates to alanine, glutamate and asparagine which covers a broad approach by including conservative changes to confidently state that the observed loss of receptor activation is caused by drastic aspartate to alanine exchange in the binding pocket and not due to general conformational changes.

Interestingly, a second binding site was predicted at the external surface of TAAR13c, right above the internal binding site. Mutation of the pivotal element Asp279^{6.58}, resulted in a supersensitive receptor, displaying an increase in apparent affinity (EC₅₀) for cadaverine and putrescine of up to two orders of magnitude. This external binding site does not activate, rather impairs receptor activation. Externally for TAAR13c there are only two conceivable access points to the internal binding site. One of these points is positively charged, Arg92^{2.64} making it unlikely to allow passage of positively charged diamine compounds into the receptor's internal binding pocket. The second access point is negatively charged and therefore is more suitable to allow access of the ligand to the internal binding site. This access point, when blocked by external binding of cadaverine acts as a gate and closes the access of cadaverine to internal binding site for receptor activation. When the ligand is dissociated from this gate, it is open for access to internal binding site. Elimination of the external binding site by mutating Asp279^{6.58} destroys the gate and ligand access to the internal binding site is no longer. Thus, generating a supersensitive receptor.

In order to further explore the gating site residue functionality, we substituted the negatively charged Asp279^{6.58} for a positively charged arginine residue, creating a D279R mutant. Experimentally, we observed that the apparent affinity of D279R

mutant was 5.2 times higher than wildtype receptor. We then checked the stepwise docking of cadaverine in the mutant and found that the interacting residues and the binding orientations was similar to the wildtype TAAR13c suggesting that the loss of the ligand gating site has mostly local effects, which can be explained in terms of a balance between the loss of the external ligand-binding site and the tunnel entrance gain of a repulsive force.

To fully understand the balance between the external gating and internal binding site, we simultaneously mutated one residue of the internal binding site and the gating site (D112E/D279N). In contrast to the fully inactive D112E mutant, the double mutant showed an affinity slightly less but not significantly different from the wildtype receptor and retains one of the salt bridges with cadaverine. Therefore the binding pocket of the mutant retains most of the minor binding interactions. Interestingly, this seriously weakened binding in combination with loss of gating site to facilitate ligand access seems sufficient to activate the receptor at similar efficacy as wildtype TAAR13c. Taken together, the results suggest that the outcome of simultaneous mutations of gating and internal binding sites can be understood as resulting from linear additivity of localized effects.

The occurrence of a ligand-binding external vestibule might be a much more widespread regulatory feature of class A GPCRs than previously assumed (Redka, Pisterzi et al. 2008) (Dror, Pan et al. 2011). If so, in future it might be interesting to uncover how widespread this feature is in class A GPCRs. The affinity of olfactory receptors is constantly tuned to physiologically relevant odor concentrations during evolution. Presence of an external allosteric binding site might amount to down-tuning the affinity, indirectly *via* a ligand-regulated gating mechanism such as described for TAAR13c. This phenomenon constitutes a novel mechanism in olfactory receptor function.

6. References

- Ahuja, G., S. Bozorg Nia, V. Zapilko, V. Shiriagin, D. Kowatschew, Y. Oka and S. I. Korsching (2014). "Kappe neurons, a novel population of olfactory sensory neurons." *Sci Rep* **4**: 4037.
- Ahuja, G., I. Ivandic, M. Salturk, Y. Oka, W. Nadler and S. I. Korsching (2013). "Zebrafish crypt neurons project to a single, identified mediodorsal glomerulus." *Sci Rep* **3**: 2063.
- Ahuja, G. and S. Korsching (2014). "Zebrafish olfactory receptor ORA1 recognizes a putative reproductive pheromone." *Commun Integr Biol* **7**(5).
- Ahuja, G., V. Reichel, D. Kowatschew, A. S. Syed, A. K. Kotagiri, Y. Oka, F. Weth and S. I. Korsching (2018). "Overlapping but distinct topology for zebrafish V2R-like olfactory receptors reminiscent of odorant receptor spatial expression zones." *BMC Genomics* **19**(1): 383.
- Alioto, T. S. and J. Ngai (2005). "The odorant receptor repertoire of teleost fish." *BMC Genomics* **6**: 173.
- Alioto, T. S. and J. Ngai (2006). "The repertoire of olfactory C family G protein-coupled receptors in zebrafish: candidate chemosensory receptors for amino acids." *BMC Genomics* **7**: 309.
- Bachmanov, A. A. and G. K. Beauchamp (2007). "Taste receptor genes." *Annu Rev Nutr* **27**: 389-414.
- Barth, A. L., J. C. Dugas and J. Ngai (1997). "Noncoordinate expression of odorant receptor genes tightly linked in the zebrafish genome." *Neuron* **19**(2): 359-369.
- Behrens, M., O. Frank, H. Rawel, G. Ahuja, C. Potting, T. Hofmann, W. Meyerhof and S. Korsching (2014). "ORA1, a zebrafish olfactory receptor ancestral to all mammalian V1R genes, recognizes 4-hydroxyphenylacetic acid, a putative reproductive pheromone." *J Biol Chem* **289**(28): 19778-19788.
- Benton, R., S. Sachse, S. W. Michnick and L. B. Vosshall (2006). "Atypical membrane topology and heteromeric function of Drosophila odorant receptors in vivo." *PLoS Biol* **4**(2): e20.
- Braubach, O. R., A. Fine and R. P. Croll (2012). "Distribution and functional organization of glomeruli in the olfactory bulbs of zebrafish (*Danio rerio*)." *J Comp Neurol* **520**(11): 2317-2339, Spc2311.
- Buck, L. and R. Axel (1991). "A novel multigene family may encode odorant receptors: a molecular basis for odor recognition." *Cell* **65**(1): 175-187.
- Buck, L. B. (2000). "The molecular architecture of odor and pheromone sensing in mammals." *Cell* **100**(6): 611-618.
- Buck, L. B. (2004). "Olfactory receptors and odor coding in mammals." *Nutr Rev* **62**(11 Pt 2): S184-188; discussion S224-141.
- Carey, A. F., G. Wang, C. Y. Su, L. J. Zwiebel and J. R. Carlson (2010). "Odorant reception in the malaria mosquito *Anopheles gambiae*." *Nature* **464**(7285): 66-71.
- Cherezov, V., D. M. Rosenbaum, M. A. Hanson, S. G. Rasmussen, F. S. Thian, T. S. Kobilka, H. J. Choi, P. Kuhn, W. I. Weis, B. K. Kobilka and R. C. Stevens (2007). "High-resolution crystal structure of an engineered human beta2-adrenergic G protein-coupled receptor." *Science* **318**(5854): 1258-1265.
- Dewan, A., R. Pacifico, R. Zhan, D. Rinberg and T. Bozza (2013). "Non-redundant coding of aversive odours in the main olfactory pathway." *Nature* **497**(7450): 486-489.
- Dorries, K. M., E. Adkins-Regan and B. P. Halpern (1997). "Sensitivity and behavioral responses to the pheromone androstenone are not mediated by the vomeronasal organ in domestic pigs." *Brain Behav Evol* **49**(1): 53-62.
- Dror, R. O., A. C. Pan, D. H. Arlow, D. W. Borhani, P. Maragakis, Y. Shan, H. Xu and D. E. Shaw (2011). "Pathway and mechanism of drug binding to G-protein-coupled receptors." *Proc Natl Acad Sci U S A* **108**(32): 13118-13123.
- Dulac, C. (2000). "Sensory coding of pheromone signals in mammals." *Curr Opin Neurobiol* **10**(4): 511-518.
- Dulac, C. and R. Axel (1995). "A novel family of genes encoding putative pheromone receptors in mammals." *Cell* **83**(2): 195-206.
- Ferrero, D. M., J. K. Lemon, D. Fluegge, S. L. Pashkovski, W. J. Korzan, S. R. Datta, M. Spehr, M. Fendt and S. D. Liberles (2011). "Detection and avoidance of a carnivore odor by prey." *Proc Natl Acad Sci U S A* **108**(27): 11235-11240.

Ferrero, D. M., D. Wacker, M. A. Roque, M. W. Baldwin, R. C. Stevens and S. D. Liberles (2012). "Agonists for 13 trace amine-associated receptors provide insight into the molecular basis of odor selectivity." *ACS Chem Biol* **7**(7): 1184-1189.

Fishilevich, E. and L. B. Vosshall (2005). "Genetic and functional subdivision of the *Drosophila* antennal lobe." *Curr Biol* **15**(17): 1548-1553.

Fleischer, J., H. Breer and J. Strotmann (2009). "Mammalian olfactory receptors." *Front Cell Neurosci* **3**: 9.

Fleischer, J., K. Schwarzenbacher, S. Besser, N. Hass and H. Breer (2006). "Olfactory receptors and signalling elements in the Grueneberg ganglion." *J Neurochem* **98**(2): 543-554.

Fredriksson, R., M. C. Lagerstrom, L. G. Lundin and H. B. Schiöth (2003). "The G-protein-coupled receptors in the human genome form five main families. Phylogenetic analysis, paralogon groups, and fingerprints." *Mol Pharmacol* **63**(6): 1256-1272.

Freitag, J., J. Krieger, J. Strotmann and H. Breer (1995). "Two classes of olfactory receptors in *Xenopus laevis*." *Neuron* **15**(6): 1383-1392.

Friedrich, R. W. and S. I. Korsching (1997). "Combinatorial and chemotopic odorant coding in the zebrafish olfactory bulb visualized by optical imaging." *Neuron* **18**(5): 737-752.

Fulle, H. J., R. Vassar, D. C. Foster, R. B. Yang, R. Axel and D. L. Garbers (1995). "A receptor guanylyl cyclase expressed specifically in olfactory sensory neurons." *Proc Natl Acad Sci U S A* **92**(8): 3571-3575.

Gadenne, C., R. B. Barrozo and S. Anton (2016). "Plasticity in Insect Olfaction: To Smell or Not to Smell?" *Annu Rev Entomol* **61**: 317-333.

Germana, A., G. Montalbano, R. Laura, E. Ciriaco, M. E. del Valle and J. A. Vega (2004). "S100 protein-like immunoreactivity in the crypt olfactory neurons of the adult zebrafish." *Neurosci Lett* **371**(2-3): 196-198.

Gliem, S., A. S. Syed, A. Sansone, E. Kludt, E. Tantalaki, T. Hassenklover, S. I. Korsching and I. Manzini (2013). "Bimodal processing of olfactory information in an amphibian nose: odor responses segregate into a medial and a lateral stream." *Cell Mol Life Sci* **70**(11): 1965-1984.

Glusman, G., I. Yanai, I. Rubin and D. Lancet (2001). "The complete human olfactory subgenome." *Genome Res* **11**(5): 685-702.

Goldman, A. L., W. Van der Goes van Naters, D. Lessing, C. G. Warr and J. R. Carlson (2005). "Coexpression of two functional odor receptors in one neuron." *Neuron* **45**(5): 661-666.

Gonzalez, A., T. Perez-Acle, L. Pardo and X. Deupi (2011). "Molecular basis of ligand dissociation in beta-adrenergic receptors." *PLoS One* **6**(9): e23815.

Grus, W. E. and J. Zhang (2009). "Origin of the genetic components of the vomeronasal system in the common ancestor of all extant vertebrates." *Mol Biol Evol* **26**(2): 407-419.

Hanchate, N. K., K. Kondoh, Z. Lu, D. Kuang, X. Ye, X. Qiu, L. Pachter, C. Trapnell and L. B. Buck (2015). "Single-cell transcriptomics reveals receptor transformations during olfactory neurogenesis." *Science* **350**(6265): 1251-1255.

Hansen, A. and B. S. Zielinski (2005). "Diversity in the olfactory epithelium of bonyfishes: development, lamellar arrangement, sensory neuron cell types and transduction components." *J Neurocytol* **34**(3-5): 183-208.

Hansson, B. S. and M. C. Stensmyr (2011). "Evolution of insect olfaction." *Neuron* **72**(5): 698-711.

Hasen, N. S. and S. C. Gammie (2009). "Trpc2 gene impacts on maternal aggression, accessory olfactory bulb anatomy and brain activity." *Genes Brain Behav* **8**(7): 639-649.

Hashiguchi, Y. and M. Nishida (2007). "Evolution of trace amine associated receptor (TAAR) gene family in vertebrates: lineage-specific expansions and degradations of a second class of vertebrate chemosensory receptors expressed in the olfactory epithelium." *Mol Biol Evol* **24**(9): 2099-2107.

Henin, J., B. Maigret, M. Tarek, C. Escrieut, D. Fourmy and C. Chipot (2006). "Probing a model of a GPCR/ligand complex in an explicit membrane environment: the human cholecystikinin-1 receptor." *Biophys J* **90**(4): 1232-1240.

Herrada, G. and C. Dulac (1997). "A novel family of putative pheromone receptors in mammals with a topographically organized and sexually dimorphic distribution." *Cell* **90**(4): 763-773.

Huber, T., S. Menon and T. P. Sakmar (2008). "Structural basis for ligand binding and specificity in adrenergic receptors: implications for GPCR-targeted drug discovery." Biochemistry **47**(42): 11013-11023.

Hudson, R. and H. Distel (1986). "Pheromonal release of suckling in rabbits does not depend on the vomeronasal organ." Physiol Behav **37**(1): 123-128.

Hussain, A., L. R. Saraiva, D. M. Ferrero, G. Ahuja, V. S. Krishna, S. D. Liberles and S. I. Korsching (2013). "High-affinity olfactory receptor for the death-associated odor cadaverine." Proc Natl Acad Sci U S A **110**(48): 19579-19584.

Hussain, A., L. R. Saraiva and S. I. Korsching (2009). "Positive Darwinian selection and the birth of an olfactory receptor clade in teleosts." Proc Natl Acad Sci U S A **106**(11): 4313-4318.

Karlson, P. and M. Luscher (1959). "Pheromones: a new term for a class of biologically active substances." Nature **183**(4653): 55-56.

Kato, A. and K. Touhara (2009). "Mammalian olfactory receptors: pharmacology, G protein coupling and desensitization." Cell Mol Life Sci **66**(23): 3743-3753.

Keller, M., Q. Douhard, M. J. Baum and J. Bakker (2006). "Destruction of the main olfactory epithelium reduces female sexual behavior and olfactory investigation in female mice." Chem Senses **31**(4): 315-323.

Korsching, S. (2009). "The molecular evolution of teleost olfactory receptor gene families." Results Probl Cell Differ **47**: 37-55.

Larsson, M. C., A. I. Domingos, W. D. Jones, M. E. Chiappe, H. Amrein and L. B. Vosshall (2004). "Or83b encodes a broadly expressed odorant receptor essential for Drosophila olfaction." Neuron **43**(5): 703-714.

Leal, W. S. (2013). "Odorant reception in insects: roles of receptors, binding proteins, and degrading enzymes." Annu Rev Entomol **58**: 373-391.

Leinders-Zufall, T., P. Brennan, P. Widmayer, P. C. S. A. Maul-Pavicic, M. Jager, X. H. Li, H. Breer, F. Zufall and T. Boehm (2004). "MHC class I peptides as chemosensory signals in the vomeronasal organ." Science **306**(5698): 1033-1037.

Leinders-Zufall, T., T. Ishii, P. Chamero, P. Hendrix, L. Oboti, A. Schmid, S. Kircher, M. Pyrski, S. Akiyoshi, M. Khan, E. Vaes, F. Zufall and P. Mombaerts (2014). "A family of nonclassical class I MHC genes contributes to ultrasensitive chemodetection by mouse vomeronasal sensory neurons." J Neurosci **34**(15): 5121-5133.

Lemaitre, V., P. Yeagle and A. Watts (2005). "Molecular dynamics simulations of retinal in rhodopsin: from the dark-adapted state towards lumirhodopsin." Biochemistry **44**(38): 12667-12680.

Li, J., T. Ishii, P. Feinstein and P. Mombaerts (2004). "Odorant receptor gene choice is reset by nuclear transfer from mouse olfactory sensory neurons." Nature **428**(6981): 393-399.

Li, Q., Y. Tachie-Baffour, Z. Liu, M. W. Baldwin, A. C. Kruse and S. D. Liberles (2015). "Non-classical amine recognition evolved in a large clade of olfactory receptors." Elife **4**: e10441.

Liberles, S. D. and L. B. Buck (2006). "A second class of chemosensory receptors in the olfactory epithelium." Nature **442**(7103): 645-650.

Lindemann, L., M. Ebeling, N. A. Kratochwil, J. R. Bunzow, D. K. Grandy and M. C. Hoener (2005). "Trace amine-associated receptors form structurally and functionally distinct subfamilies of novel G protein-coupled receptors." Genomics **85**(3): 372-385.

Lundin, C., L. Kall, S. A. Kreher, K. Kapp, E. L. Sonnhammer, J. R. Carlson, G. Heijne and I. Nilsson (2007). "Membrane topology of the Drosophila OR83b odorant receptor." FEBS Lett **581**(29): 5601-5604.

Luu, P., F. Acher, H. O. Bertrand, J. Fan and J. Ngai (2004). "Molecular determinants of ligand selectivity in a vertebrate odorant receptor." J Neurosci **24**(45): 10128-10137.

Malnic, B., J. Hirono, T. Sato and L. B. Buck (1999). "Combinatorial receptor codes for odors." Cell **96**(5): 713-723.

Marchand, J. E., X. Yang, D. Chikaraishi, J. Krieger, H. Breer and J. S. Kauer (2004). "Olfactory receptor gene expression in tiger salamander olfactory epithelium." J Comp Neurol **474**(3): 453-467.

Matsunami, H. and L. B. Buck (1997). "A multigene family encoding a diverse array of putative pheromone receptors in mammals." Cell **90**(4): 775-784.

Miyamichi, K., S. Serizawa, H. M. Kimura and H. Sakano (2005). "Continuous and overlapping expression domains of odorant receptor genes in the olfactory epithelium determine the dorsal/ventral positioning of glomeruli in the olfactory bulb." *J Neurosci* **25**(14): 3586-3592.

Mombaerts, P. (2004). "Genes and ligands for odorant, vomeronasal and taste receptors." *Nat Rev Neurosci* **5**(4): 263-278.

Mombaerts, P., F. Wang, C. Dulac, S. K. Chao, A. Nemes, M. Mendelsohn, J. Edmondson and R. Axel (1996). "Visualizing an olfactory sensory map." *Cell* **87**(4): 675-686.

Monahan, K. and S. Lomvardas (2015). "Monoallelic expression of olfactory receptors." *Annu Rev Cell Dev Biol* **31**: 721-740.

Niesen, M. J., S. Bhattacharya and N. Vaidehi (2011). "The role of conformational ensembles in ligand recognition in G-protein coupled receptors." *J Am Chem Soc* **133**(33): 13197-13204.

Niimura, Y., A. Matsui and K. Touhara (2014). "Extreme expansion of the olfactory receptor gene repertoire in African elephants and evolutionary dynamics of orthologous gene groups in 13 placental mammals." *Genome Res* **24**(9): 1485-1496.

Niimura, Y., A. Matsui and K. Touhara (2018). "Acceleration of Olfactory Receptor Gene Loss in Primate Evolution: Possible Link to Anatomical Change in Sensory Systems and Dietary Transition." *Mol Biol Evol* **35**(6): 1437-1450.

Niimura, Y. and M. Nei (2003). "Evolution of olfactory receptor genes in the human genome." *Proc Natl Acad Sci U S A* **100**(21): 12235-12240.

Niimura, Y. and M. Nei (2005). "Evolutionary dynamics of olfactory receptor genes in fishes and tetrapods." *Proc Natl Acad Sci U S A* **102**(17): 6039-6044.

Niimura, Y. and M. Nei (2007). "Extensive gains and losses of olfactory receptor genes in mammalian evolution." *PLoS One* **2**(8): e708.

Oka, Y., L. R. Saraiva and S. I. Korsching (2012). "Crypt neurons express a single V1R-related ora gene." *Chem Senses* **37**(3): 219-227.

Olender, T., T. Fuchs, C. Linhart, R. Shamir, M. Adams, F. Kalush, M. Khen and D. Lancet (2004). "The canine olfactory subgenome." *Genomics* **83**(3): 361-372.

Pacifico, R., A. Dewan, D. Cawley, C. Guo and T. Bozza (2012). "An olfactory subsystem that mediates high-sensitivity detection of volatile amines." *Cell Rep* **2**(1): 76-88.

Palczewski, K., T. Kumasaka, T. Hori, C. A. Behnke, H. Motoshima, B. A. Fox, I. Le Trong, D. C. Teller, T. Okada, R. E. Stenkamp, M. Yamamoto and M. Miyano (2000). "Crystal structure of rhodopsin: A G protein-coupled receptor." *Science* **289**(5480): 739-745.

Pfister, P. and I. Rodriguez (2005). "Olfactory expression of a single and highly variable V1r pheromone receptor-like gene in fish species." *Proc Natl Acad Sci U S A* **102**(15): 5489-5494.

Pin, J. P., T. Galvez and L. Prezeau (2003). "Evolution, structure, and activation mechanism of family 3/C G-protein-coupled receptors." *Pharmacol Ther* **98**(3): 325-354.

Redka, D. S., L. F. Pisterzi and J. W. Wells (2008). "Binding of orthosteric ligands to the allosteric site of the M(2) muscarinic cholinergic receptor." *Mol Pharmacol* **74**(3): 834-843.

Ressler, K. J., S. L. Sullivan and L. B. Buck (1993). "A zonal organization of odorant receptor gene expression in the olfactory epithelium." *Cell* **73**(3): 597-609.

Riviere, S., L. Challet, D. Fluegge, M. Spehr and I. Rodriguez (2009). "Formyl peptide receptor-like proteins are a novel family of vomeronasal chemosensors." *Nature* **459**(7246): 574-577.

Saraiva, L. R. and S. I. Korsching (2007). "A novel olfactory receptor gene family in teleost fish." *Genome Res* **17**(10): 1448-1457.

Sato, Y., N. Miyasaka and Y. Yoshihara (2005). "Mutually exclusive glomerular innervation by two distinct types of olfactory sensory neurons revealed in transgenic zebrafish." *J Neurosci* **25**(20): 4889-4897.

Sato, Y., N. Miyasaka and Y. Yoshihara (2007). "Hierarchical regulation of odorant receptor gene choice and subsequent axonal projection of olfactory sensory neurons in zebrafish." *J Neurosci* **27**(7): 1606-1615.

Schoenfeld, T. A. and T. A. Cleland (2006). "Anatomical contributions to odorant sampling and representation in rodents: zoning in on sniffing behavior." *Chem Senses* **31**(2): 131-144.

Sehnal, D., R. Svobodová Vařeková, K. Berka, L. Pravda, V. Navrátilová, P. Banáš, C.-M. Ionescu, M. Otyepka and J. Koča (2013). "MOLE 2.0: advanced approach for analysis of biomacromolecular channels." *Journal of Cheminformatics* **5**(1): 39.

Serizawa, S., T. Ishii, H. Nakatani, A. Tsuboi, F. Nagawa, M. Asano, K. Sudo, J. Sakagami, H. Sakano, T. Ijiri, Y. Matsuda, M. Suzuki, T. Yamamori, Y. Iwakura and H. Sakano (2000). "Mutually exclusive expression of odorant receptor transgenes." *Nat Neurosci* **3**(7): 687-693.

Serizawa, S., K. Miyamichi and H. Sakano (2004). "One neuron-one receptor rule in the mouse olfactory system." *Trends Genet* **20**(12): 648-653.

Shi, L. and J. A. Javitch (2002). "The binding site of aminergic G protein-coupled receptors: the transmembrane segments and second extracellular loop." *Annu Rev Pharmacol Toxicol* **42**: 437-467.

Shi, P. and J. Zhang (2009). "Extraordinary diversity of chemosensory receptor gene repertoires among vertebrates." *Results Probl Cell Differ* **47**: 1-23.

Strotmann, J., I. Wanner, T. Helfrich, A. Beck, C. Meinken, S. Kubick and H. Breer (1994). "Olfactory neurones expressing distinct odorant receptor subtypes are spatially segregated in the nasal neuroepithelium." *Cell Tissue Res* **276**(3): 429-438.

Suh, E., J. Bohbot and L. J. Zwiebel (2014). "Peripheral olfactory signaling in insects." *Curr Opin Insect Sci* **6**: 86-92.

Syed, A. S., A. Sansone, T. Hassenklover, I. Manzini and S. I. Korsching (2017). "Coordinated shift of olfactory amino acid responses and V2R expression to an amphibian water nose during metamorphosis." *Cell Mol Life Sci* **74**(9): 1711-1719.

Syed, A. S., A. Sansone, W. Nadler, I. Manzini and S. I. Korsching (2013). "Ancestral amphibian v2rs are expressed in the main olfactory epithelium." *Proc Natl Acad Sci U S A* **110**(19): 7714-7719.

Takahashi, L. K. (2014). "Olfactory systems and neural circuits that modulate predator odor fear." *Front Behav Neurosci* **8**: 72.

Takeuchi, H. and H. Sakano (2014). "Neural map formation in the mouse olfactory system." *Cell Mol Life Sci* **71**(16): 3049-3057.

Tessarolo, J. A., M. J. Tabesh, M. Nesbitt and W. S. Davidson (2014). "Genomic organization and evolution of the trace amine-associated receptor (TAAR) repertoire in Atlantic salmon (*Salmo salar*)." *G3 (Bethesda)* **4**(6): 1135-1141.

Traynelis, S. F., L. P. Wollmuth, C. J. McBain, F. S. Menniti, K. M. Vance, K. K. Ogden, K. B. Hansen, H. Yuan, S. J. Myers and R. Dingledine (2010). "Glutamate receptor ion channels: structure, regulation, and function." *Pharmacol Rev* **62**(3): 405-496.

Tsitoura, P., E. Andronopoulou, D. Tsikou, A. Agalou, M. P. Papakonstantinou, G. A. Kotzia, V. Labropoulou, L. Swevers, Z. Georgoussi and K. Iatrou (2010). "Expression and membrane topology of *Anopheles gambiae* odorant receptors in lepidopteran insect cells." *PLoS One* **5**(11): e15428.

Vassalli, A., A. Rothman, P. Feinstein, M. Zapotocky and P. Mombaerts (2002). "Minigenes impart odorant receptor-specific axon guidance in the olfactory bulb." *Neuron* **35**(4): 681-696.

Vassar, R., J. Ngai and R. Axel (1993). "Spatial segregation of odorant receptor expression in the mammalian olfactory epithelium." *Cell* **74**(2): 309-318.

Vosshall, L. B. and B. S. Hansson (2011). "A unified nomenclature system for the insect olfactory coreceptor." *Chem Senses* **36**(6): 497-498.

Wang, T. and Y. Duan (2009). "Ligand Entry and Exit Pathways in the $\beta(2)$ -adrenergic Receptor." *J Mol Biol* **392**(4): 1102-1115.

Weth, F., W. Nadler and S. Korsching (1996). "Nested expression domains for odorant receptors in zebrafish olfactory epithelium." *Proc Natl Acad Sci U S A* **93**(23): 13321-13326.

Wicher, D. (2015). "Olfactory signaling in insects." *Prog Mol Biol Transl Sci* **130**: 37-54.

Wilk, M. B. and R. Gnanadesikan (1968). "Probability plotting methods for the analysis of data." *Biometrika* **55**(1): 1-17.

Young, J. M., C. Friedman, E. M. Williams, J. A. Ross, L. Tonnes-Priddy and B. J. Trask (2002). "Different evolutionary processes shaped the mouse and human olfactory receptor gene families." *Hum Mol Genet* **11**(5): 535-546.

Young, J. M. and B. J. Trask (2002). "The sense of smell: genomics of vertebrate odorant receptors." Hum Mol Genet **11**(10): 1153-1160.

Zapilko, V. and S. I. Korsching (2016). "Tetrapod V1R-like ora genes in an early-diverging ray-finned fish species: the canonical six ora gene repertoire of teleost fish resulted from gene loss in a larger ancestral repertoire." BMC Genomics **17**: 83.

Zhang, Y., Y. Y. Sham, R. Rajamani, J. Gao and P. S. Portoghese (2005). "Homology modeling and molecular dynamics simulations of the mu opioid receptor in a membrane-aqueous system." Chembiochem **6**(5): 853-859.

Zou, Z. and L. B. Buck (2006). "Combinatorial effects of odorant mixes in olfactory cortex." Science **311**(5766): 1477-1481.

7. Summary

Olfaction or the sense of smell is phylogenetically ancient, and mediates many vital functions such as detection of prey, predator evasion, kin recognition, and reproduction. With the sheer quantity of potential odor molecules facing a limited though huge number of different olfactory receptors, interaction of the odors with their cognate receptors creates one of the most complex ligand/receptor binding problems in biology. Due to unavailability of crystal structures for any olfactory receptor, the prediction of olfactory receptor structures relies on homology modeling studies using established templates such as the beta-adrenergic receptor (β -AR) and rhodopsin, in case of TAARs; further supported by site-directed mutagenesis and subsequent functional analysis of mutant receptors.

In this study, we have used a unique combination of computational bioinformatics coupled with molecular biology to unravel the structure and the ligand interaction of a zebrafish olfactory receptor specific for aliphatic diamines, TAAR13c with its preferred ligand, cadaverine. We modelled an entry tunnel for cadaverine and identified the residues participating in binding and activation of the receptor. Using a multistep docking algorithm we suggested a plausible path for cadaverine from the external to the internal binding-and-activation site. We then generated a series of mutation in the binding site which led to loss in the receptor activity, hence confirmed our predictions.

During the course of the study, we observed an unexpected binding site for cadaverine lining the access point at the external surface of TAAR13c. Elimination of the pivotal element of this external binding site resulted in a supersensitive receptor. Modeling study suggested this site to act as a gate, limiting access of the ligand to the internal binding and activation site, thereby downregulating the affinity of the native wildtype receptor. Elimination of this site destroys the gate and ligand access is no longer impeded, thus generating a supersensitive receptor. This constitutes a novel mechanism to fine-tune physiological sensitivity to socially relevant odors.

We also analysed the spatial pattern of *taar*-expressing cells for five representative receptors in two dimensions, for height within the epithelial layer and horizontal distance from the centre of the olfactory organ. We report non-random, distinct, if broadly overlapping distributions for all five *taar* genes, similar to the spatial topology observed for odorant receptor (Weth, Nadler et al. 1996).

Next, we mined the genome of a true shark, catshark for olfactory and gustatory receptors. We also completed the elephant shark chemoreceptor repertoire and have performed a thorough phylogenetic study to shed light on the evolution of chemosensory receptors in cartilaginous fish. We report the presence of several gustatory receptors of the T1R family in catshark and elephant shark, while T2R receptors are absent. The catshark olfactory repertoire is dominated by V2R receptors, with only 5 to 8 receptors in the other three families (OR, V1R, TAAR). Overall, the catshark chemosensory receptor repertoires are generally similar in size to those of elephant shark, if somewhat larger, showing similar evolutionary tendencies across

over 400 million years of separate evolution between catshark and elephant shark.

8. APPENDIX

OE:	Olfactory epithelium
OSN:	Olfactory sensory neuron
GPCR:	G protein-coupled receptor
MOB:	Main olfactory bulb
MOE:	Main olfactory epithelium
OB:	Olfactory bulb
OSN:	Olfactory sensory neuron
OMP:	Olfactory marker protein
GC:	Guanylyl cyclase
OR:	Olfactory receptor
TAAR:	Trace Amine-Associated Receptor
FPR:	Formyl peptide receptor
V1R:	Vomer nasal receptors type 1
V2R:	Vomer nasal receptors type 2
VNO:	Vomer nasal organ
VR:	vomer nasal receptor
X.t:	<i>Xenopus tropicalis</i>
Actinopterygii:	Ray-finned fish
Sarcopterygii:	Lobe-finned fish
T2R:	Taste receptor, type 2
T1R:	Taste receptor, type 1
TRC:	Taste receptor cell

9. AUTHOR CONTRIBUTIONS

I am first author or shared first author in all the studies underlying this dissertation. My contributions are listed below for each study.

1. Sharma, K., Ahuja, G., Hussain, A., Balfanz, S., Baumann, A., Korsching, S.I. (2016). "**Elimination of a ligand gating site generates a supersensitive olfactory receptor.**" *Sci Rep* **6**, 28359

Designed Research	Performed Research	Analyzed Data	Designed Figures	Wrote Paper
Yes	Yes	Yes	Yes	Yes

2. Sharma, K., Balfanz, S., Baumann, A., Korsching, S.I. (2018). "**Full rescue of an inactive olfactory receptor mutant by elimination of an allosteric ligand-gating site.**" *Sci Rep* **8**, 9631

Designed Research	Performed Research	Analyzed Data	Designed Figures	Wrote Paper
Yes	Yes	Yes	Yes	Yes

3. Sharma, K*, Syed, A*, Ferrando, S., Mazan, S., Korsching, S.I. "**The olfactory receptor repertoire of a true shark is dominated by V2Rs.**" (submitted).

Designed Research	Performed Research	Analyzed Data	Designed Figures	Wrote Paper
Yes	Yes	Yes	Yes	Yes

* Shared 1st author.

10. ERKLÄRUNG (DECLARATION)

Ich versichere, dass ich die von mir vorgelegte Dissertation selbstständig angefertigt, die benutzten Quellen und Hilfsmittel vollständig angegeben und die Stellen in der Arbeit -einschließlich Tabellen, Karten und Abbildungen -, die anderen Werken im Wortlaut oder dem Sinn nach entnommen sind, in jedem Einzelfall als Entlehnung kenntlich gemacht habe; dass diese Dissertation noch keiner anderen Fakultät oder Universität zur Prüfung vorgelegen hat; dass sie - abgesehen von den unten angegebenen Teilpublikationen – noch nicht veröffentlicht worden ist, sowie dass ich eine solche Veröffentlichung vor Abschluss des Promotionsverfahrens nicht vornehmen werde. Die Bestimmungen dieser Promotionsordnung sind mir bekannt. Die von mir vorgelegte Dissertation ist von Prof. Dr. Sigrun. I. Korsching betreut worden.

Köln, 07/09/2018

Teilpublikationen:

1. Sharma, K., Ahuja, G., Hussain, A., Balfanz, S., Baumann, A and Korsching, S.I. (2016). "**Elimination of a ligand gating site generates a supersensitive olfactory receptor.**" *Sci Rep* **6**, 28359
2. Sharma, K., Balfanz, S., Baumann, A and Korsching, S.I. (2018). "**Full rescue of an inactive olfactory receptor mutant by elimination of an allosteric ligand-gating site.**" *Sci Rep* **8**, 9631
3. Sharma, K*, Syed, A*, Ferrando, S., Mazan, S., and Korsching, S.I. "**The olfactory receptor repertoire of a true shark is dominated by V2Rs.**" (submitted).

(* Shared 1st author.)

PERSONAL
INFORMATION

Kanika Sharma

📍 34 Gilbachstraße, 50672 Cologne, Germany
☎ (+49) 0176 80338135
✉ ksharma997@gmail.com
🌐 <https://www.linkedin.com/in/kanika-sharma-7157132a/>

Date of birth 26.03.1988 | Nationality Indian

WORK EXPERIENCE

Aug 2013 – Oct 2013

PhD rotations

Intensive lab rotations around 3 research groups in University of Cologne for selection in IGSDHD

Nov 2013 - present

PhD Researcher

“Modelling and testing an olfactory receptor for death-associated odour cadaverine: TAAR13c and its subfamily”

“Phylogenetic analysis of catshark genome provides unique insights into evolution of a true shark”

July 2011 – Aug 2013

Project Assistant

Indian Institute of Technology, Delhi

“Generation of homodimers configuration from monomeric protein subunits”

June 2011 – July 2012

Teaching Assistant

Indian Institute of Technology, Delhi

- Designed, planned, executed and controlled projects for 25 trainees
- Delivered training sessions for protein structure analysis
- Documented the final reports

EDUCATION

Aug 2013 – present

Doctor of Philosophy, Neuroscience

Feb 2009 – May 2011

Masters in Bioinformatics

TRAINING AND SKILLS

Technical Skills

- Programming
 - Adobe Illustrator, Dream Viewer, Bash, Python, Perl, MS Office
- Bioinformatics
 - RNASeq, NGS, Phylogenetics, Drug designing, Molecular docking, Homology modelling, Biological databases, GenScan, Molecular visualization, Transcriptomics
- Biology
 - Molecular Biology, PCR, NGS, RNA/DNA prep/analysis, In-situ, Immunohistochemistry, Cloning, Cell Culture, Mutations

Interpersonal skills

- People oriented, strong work ethic and goal-oriented
- Exemplary presentation skills.
- Multitasking skills by analysing data from collaborative groups
- Excellent writing and editing skills
- Ability to translate complex text into easily readable form
- Creative thinker and persuasive writer on social media

Communication skills

- Experienced in successful management of international groups
- Confident, articulate, and professional speaking experience
- Adaptable to different work cultures and environments
- Active listener
- Natural communicator, managed over 100 international guests on social platforms
- Keen on asking open-ended questions to stimulate dialogue

Language skills

- English (Native)
- Hindi (Native)
- German (A2)

Scientific Workshop

Cologne Excellent women in Science (CEWIS) Organizer

- Content writing for conference brochure
- Lead for opening and closing speech
- Team leader for social media campaigns and sponsor planning
- Developed strategies for efficient organization and execution of plans
- Independently seized sponsor for the conference by networking and conversation from previous conference
- Team lead for writing scripts for social media campaigns for creating interest and awareness
- Wrote invitations to scientists
- Negotiated for possible recruitment of participants

Courses

- Career Mentoring and Management

- Effective (Gender related) communication in Scientific World
- Presenting Professionally

Publications

2018

- Sharma, K., S. Balfanz, A. Baumann and S. I. Korsching (2018). "Full rescue of an inactive olfactory receptor mutant by elimination of an allosteric ligand-gating site", Sci Rep. (in press).

2016

- Sharma, K., G. Ahuja, A. Hussain, S. Balfanz, A. Baumann and S. I. Korsching (2016). "Elimination of a ligand gating site generates a supersensitive olfactory receptor." Sci Rep 6: 28359.

Presentations/

Conferences

- 17th International Symposium of Olfaction and Taste (ISOT2016), Japan
- XXVIth meeting of the European Chemoreception Research Organization (ECRO2017), Greece
- 2th Göttingen Meeting of the German Neuroscience Society (GNS), Germany
- XXVth meeting of the European Chemoreception Research Organization (ECRO2017), Turkey
- 6th Crossroads in Biology (CiB2015), Germany
- Cologne Neuroscience Meeting (2014), Germany

Honours and awards

- Best poster award at ECRO2017
- iPAK Travel Grant (2017) for attending conference